Royal Netherlands Meteorological Institute
Ministry of Infrastructure and Water Management

TROPOMI ATBD of the Aerosol Layer Height

TROPOMI

sentinel-5p

document number	:	S5P-KNMI-L2-0006-RP
authors	:	M. de Graaf, J.F. de Haan and A.F.J. Sanders
CI identification	:	CI-7430-ATBD_Aerosol_Layer_Height
issue	:	1.1.0
date	:	2019-09-30
status	:	Released

Document approval record

	digital signature
Prepared:	Martin de Graaf Digitally signed by Martin de Graaf Date: 2019.09.26 15:32:46 +02'00'
Checked:	
Approved PM:	
Approved PI:	

Document change record

issue	date	item	comments
0.0.1	2012-09-10	All	Initial version.
0.0.2	2012-09-25	All	Updated with feed from KNMI Level-2 team.
0.1.0	2012-09-27	-	Released for first review by Level-2 Working Group.
0.1.1	2012-11-16	All	Updated with feedback from aerosol science verification team. Document number changed from S5P-KNMI-L2-0115-RP to S5P-KNMI-L2-0006-RP.
0.2.0	2012-11-16	-	Released for first review by ESA.
0.2.1	2013-06-04	All	Section Absorbing Aerosol Index moved to separate ATBD (S5P-KNMI-L2-0008-RP). Added error analysis. Completed and revised other sections.
0.3.0	2013-06-04	-	Released for Level-2 Working Group.
0.3.1	2013-06-21	All 10	Updated with feedback from aerosol science verification team (no major changes). Added application to GOSAT spectra (Section 10).
0.5.0	2013-06-21	-	Released for external science review.
0.5.1	2013-11-29	 6.4.1 9.9	Updated with feedback from external science reviewers. Clarified text on ignoring polarization in Section 6.4.1. Added paragraph on fluorescence to Section 8.9. Minor other clarifications throughout the text.
0.9.0	2013-11-29	-	Released for external science review.
0.9.1	2014-04-15	4 10 4.7,11	Section Instrument (Section 4) moved to separate ATBD (S5P-KNMI-L2-0010-RP). Revised and completed Section 10; section renamed to Application to GOME-2 spectra. Updated Section 4.7 and Section 11.
0.10.0	2014-04-15	-	Released for Critical Design Review.
0.10.1	2014-09-30	7 5.3.3	Revised Section 7 Added paragraph to Section 5.3.3. Several minor clarifications throughout the text.
0.11.0	2014-09-30	-	Released for review by ESA.
0.11.1	2015-09-04	7 6.2,7.3.3	Updated pixel selection with description of VIIRS cloud mask. Added remark on alternative surface albedo climatologies. Several minor changes throughout the text.
0.13.0	2015-09-04	-	Limited release to S5P Validation Team.
0.13.1	2016-01-29	4.2,4.5-6, 5.3,5.5, 6.2 11	Updated sections on algorithm heritage, algorithm overview, development risks, the atmospheric model, the instrument model and the state vector composition. Main changes: surface albedo removed from state vector, reduction of fit window to 758–762 nm, interpretation of Aerosol Layer Height parameter, other conclusions from recent GOME-2 and SCIAMACHY case studies included in the ATBD. Updated conclusion and outlook. Several minor changes throughout the text.

issue	date	item	comments
1.0.0	2016-01-29	-	Public release.
1.0.1	2019-06-24	5	Update forward model with neural network estimate of O2-A band reflectances. First validation and verifcation.
1.1.0	2019-09-30	-	Public release.

Contents

Document approval record **2**
Document change record **3**
List of Tables **6**
List of Figures **7**
1 Introduction **11**
1.1 Identification 11
1.2 Purpose and objective 11
1.3 Document overview 11
1.4 Acknowledgements 11
2 Applicable and reference documents **12**
2.1 Applicable documents 12
2.2 Reference documents 12
2.3 Electronic references 13
3 Terms, definitions and abbreviated terms **14**
3.1 Terms and definitions 14
3.2 Acronyms and Abbreviations 14
3.3 Symbols 15
4 Introduction to Aerosol Layer Height product **17**
4.1 Product description 17
4.2 Heritage 18
4.3 Product requirements 19
4.4 Overview of the retrieval algorithm 19
4.5 Development risks 20
4.6 Foreseen update approach 21
4.7 Terminology 21
5 Algorithm description **23**
5.1 Spatial data selection 23
5.1.1 Cloud mask 23
5.1.2 Snow or ice covered pixels 23
5.1.3 Sunglint 24
5.1.4 Pixels containing aerosol 24
5.1.5 Pixel selection scheme 24
5.2 Forward model 25
5.2.1 Overview 25
5.2.2 Radiative transfer model 25
5.2.3 The Neural Network forward model 26
5.2.4 NN configuration and training 27
6 Algorithm description: Retrieval method **31**
6.1 Optimal Estimation 31
6.2 State vector elements and *a priori* information 32
6.2.1 Height variable 32
6.2.2 Profile parameterization 33
6.3 Convergence of retrieval and uniqueness of solution 33
7 Feasibility **35**
7.1 Estimated Computational Effort 35
7.2 Timeliness 36
7.3 Input data for the Aerosol Layer Height algorithm 37
7.3.1 TROPOMI Level-1b 37
7.3.2 Dynamic input 37
7.3.3 Static input 39
7.4 Robustness against instrumental errors 39
7.5 Data product description 40

8 Error analysis **41**
8.1 Performance of the neural network forward model 41
8.2 Default settings for the error analysis 42
8.3 Baseline precision of Aerosol Layer Height 43
8.4 Required knowledge of aerosol type 47
8.4.1 Single scattering albedo 47
8.4.2 Phase function 49
8.4.3 Conclusion 51
8.5 Role of a priori knowledge of the surface albedo 51
8.6 Fitting surface albedo to compensate errors in single scattering albedo 54
8.7 Effect of uncertainty in a priori meteorological data 56
8.7.1 Temperature profile 56
8.7.2 Surface pressure 57
8.7.3 Conclusion 59
8.8 Aerosol pressure biases due to cloud contamination 59
8.9 Alternative profile parameterization: aerosol layer with variable pressure thickness 60
8.10 Interference of chlorophyll fluorescence 61
8.11 Instrumental errors 63
8.11.1 Stray light 63
8.11.2 Wavelength calibration 63
9 Application to GOME-2 spectra **65**
9.1 Introduction 65
9.2 GOME-2 pixel selection 65
9.3 Retrieval experiments 66
9.3.1 General setup 66
9.3.2 Varying aerosol layer's assumed geometric thickness 67
9.3.3 Increasing oxygen absorption cross section by 3% 67
9.3.4 Fitting a temperature offset 68
9.3.5 Residuals 68
9.4 Comparison with lidar observations 70
9.5 Retrieval simulation: boundary layer aerosol 70
9.6 Conclusion 73
10 Validation **74**
10.1 Validation with lidar measurements 74
10.1.1 First validation with Caliop 74
10.2 Intercomparison of passive satellite retrievals 74
10.3 Dedicated validation campaigns 75
11 Conclusion and outlook **76**
12 References **77**

List of Tables

1 Scene-dependent input model parameters for the NN model. 27
2 State vector elements and typical a priori values and errors for the Aerosol Layer Height retrieval algorithm. In the current implementation, the state vector contains the parameters printed in bold. For an explanation, see text. 32
3 Statistics of the NN AER_LH processing of 1 August 2018 measurements. 36
4 TROPOMI Level-1b input data. 37
5 Dynamic input data for off-line processing and reprocessing. 38
6 Dynamic input data for near real-time processing. 38
7 Static input data. 39
8 Level-2 output data. 40
9 Surface types and corresponding albedos considered in the error analysis 43

10 Correlation coefficients between errors in fit parameters for an aerosol layer with optical thickness of 0.5 at 800 hPa over sea / ocean and vegetated land. The solar zenith angle is 60° and the viewing direction is nadir. The height variable is altitude (in km) instead of pressure (in hPa). 46
11 True values, a priori values and a priori errors used in the retrieval simulations of Figure 12 investigating the sensitivity of retrieval to the assumed single scattering albedo. 47
12 Optical properties at the O_2 A band for the three aerosol models used in the retrieval simulations of Figure 16 (based on [14]). Properties for the Dust model are based on T-matrix calculations, which are kindly provided by Oleg Dubovik and co-workers; for the other two models we performed Mie calculations. 49
13 True values, a priori values and a priori errors used in the retrieval simulations of Figure 16 investigating the sensitivity of retrieval to the assumed phase function. 50
14 *A* priori error in the surface albedo for the three types of retrieval investigating the effect of an error in climatological surface albedo values. 53
15 True values, a priori values and a priori errors used in the retrieval simulations of Figure 18 investigating the sensitivity of retrieval to the assumed phase function. 54
16 Retrieved aerosol pressures for a number of atmospheric scenarios when an offset of 1 K is applied to the mid-latitude summer temperature profile in the simulation. 57
17 Retrieved aerosol pressures for a number of atmospheric scenarios when the true surface pressure is 1011 hPa while the surface pressure assumed in retrieval is 1013 hPa. 58
18 True values, a priori values and a priori errors used in the retrieval simulations of Figure 14 investigating the sensitivity of retrieval to the assumed single scattering albedo. 62
19 Pressure biases and retrieved optical thicknesses in case of additive offsets applied to the radiance and irradiance spectrum. The aerosol layer has an optical thickness of 0.5 and is at 700 hPa over sea / ocean or vegetated land. Stray light offsets are constant with wavelength and they are defined as percentages of the (ir)radiance at 758 nm. 63
20 Pressure biases and retrieved optical thicknesses in case the width of the radiance and irradiance slit functions in the simulation differs from the width of the slit functions assumed in the retrieval. The aerosol layer has an optical thickness of 0.5 and is at 700 hPa over sea / ocean or vegetated land. The FWHM of the radiance and irradiance slit functions in retrieval is 0.5 nm. 64
21 Parameter values for the various sets of fit parameters in the retrieval experiments of Figure 33. 72
22 Correlation matrix (r^2) for the posteriori error when all three parameters are fitted (green line in Figure 33). 72

List of Figures

1 Simulated reflectance spectra of the O_2 A band at a spectral resolution (FWHM) of 0.5 nm for a scene containing a representative aerosol layer. The aerosol layer is between 950 and 850 hPa (green line) or between 540 and 475 hPa (blue line). The 1-σ measurement errors on reflectance are smaller than the width of the plotting lines: anticipated signal-to-noise ratios for these spectra (based on [63]) are about 645 in the continuum and 302 and 207 in the deepest part of the O_2 A band assuming pure shot noise. The solar zenith angle is 25° and the viewing direction is nadir. The aerosol optical thickness τ_0 at 550 nm is 1.0, the Ångström coefficient α is 2.0, the single scattering albedo is 1.0, and the phase function is a Henyey-Greenstein function with asymmetry parameter g of 0.7. Spectra were simulated with a temperature profile corresponding to the mid-latitude summer (MLS) atmosphere, a surface pressure of 1013 hPa and a constant ground surface albedo of 0.025. 17
2 Schematic depiction of the atmosphere and typical TROPOMI satellite configuration for retrieval of Aerosol Layer Height. The Rayleigh scattering optical thickness at the O_2 A band is ~0.02 18
3 Flow chart for the Aerosol Layer Height retrieval algorithm. 20
4 Example of the Sun-normalised radiance spectrum in the Oxygen-A band as computed by the RTM and by the NN model. The top panel shows the spectra after convolution with the S5P slit function, the middle panel shows a comparison between the high resolution spectra, and the bottom show the difference between the LBL and NN spectra, for the high resolution and convoluted spectra. 28

5 Aerosol profile parameterizations for the TROPOMI Aerosol Layer Height product. (A) The baseline profile parameterization assumes an elevated layer with a fixed pressure difference between top and bottom of the layer. The layer's mid pressure is retrieved. (B) If the aerosol optical thickness is large enough, it will perhaps be possible to simultaneously fit the top and bottom pressure. (C) An alternative parameterization that might be used, depending on the aerosol case, assumes an aerosol layer extending down to the ground. The layer's top pressure is retrieved. 33
6 χ^2 of the (simulated) measurement (first term of Eq. 5) for an aerosol layer between 980 and 800 hPa with optical thickness of 0.3 at 550 nm over vegetated land. The measurement vector **y** includes the O_2 A band, or the O_2 A and B bands. Note that the surface is much brighter in the O_2 A band. The modeled spectrum **F**(**x**) differs from the measurement with respect to optical thickness. One can clearly see multiple minima in the cost function if only the O_2 A band is taken into account. 34
7 Top panel: TROPOMI AAI on 1 August 2018 showing a large aerosol (dust) plume over the Atlantic Ocean originating from the Sahara, and several other hotspots of high AAI from smoke and dust. Bottom panel: TROPOMI AER_LH retrieval results from an initial test run of the ALH processor with NN implemented in the forward model. 35
8 Timeliness of the AER_LH processor. The upper panel shows the processing time per near-real time granule. The bottom panel shows the timeliness of the end of the processing time. 'Large' pixels refer to pixels with an integration time of 1080 ms, yielding pixel sizes of 7×7 km^2 at nadir, 'small' pixels refer to an integration time of 840 ms, yielding pixel sizes of about 7×5.6 km^2. 36
9 (top-left) Suomi/NPP VIIRS RGB on 9 Nov. 2018, overlaid with LBL ALH ; (top-right) Suomi/NPP VIIRS RGB on 9 Nov. 2018, overlaid with NN ALH; (bottom-left)Suomi/NPP VIIRS RGB on 9 Nov. 2018, overlaid with difference of NN-LBL ALH; (bottom-right) Scatterplot of NN ALH versus LBL ALH for the pixels in the left panels. 41
10 (left) Scatterplot of NN ALH versus LBL ALH on 10 Nov 2018 for the area in Fig 9; (right) Same as the left panel for 11 Nov. 2018. 42
11 Precision of retrieved aerosol mid pressure as a function of mid pressure for three values of the aerosol optical thickness. Panel A shows retrieval precision for an aerosol layer over sea / ocean; Each of the four subplots in a panel corresponds to a different observation geometry: SZA 25°, VZA 0° (top left); SZA 25°, VZA 70°, RAA 90° (top right); SZA 60°, VZA 0° (bottom left); and SZA 60°, VZA 0°, RAA 90° (bottom right). Note the different scales of the x-axis.. 44
12 Precision of retrieved aerosol mid pressure as a function of mid pressure for three values of the aerosol optical thickness. Panel A shows retrieval precision for an aerosol layer over vegetated land. Each of the four subplots in a panel corresponds to a different observation geometry: SZA 25°, VZA 0° (top left); SZA 25°, VZA 70°, RAA 90° (top right); SZA 60°, VZA 0° (bottom left); and SZA 60°, VZA 0°, RAA 90° (bottom right). Note the different scales of the x-axis. 45
13 Precision of retrieved mid pressure as a function of surface albedo for three arbitrary atmospheric states and observation geometries. 46
14 Effect of a model error in the single scattering albedo on retrieved mid pressure and aerosol optical thickness as a function of optical thickness. We assume a single scattering albedo of 0.95 in retrieval, while the true single scattering albedo is either 0.90 (solid lines) or 1.0 (dashed lines). The aerosol layer is located at 600 hPa (green lines) or 800 hPa (red lines). First row: bias in retrieved mid pressure; second row: precision of retrieved mid pressure; third row: bias in retrieved optical thickness with error bars indicating precision. Panel A (left column) shows retrieval simulations over sea / ocean; panel B (right column) shows retrieval simulations over vegetated land. The x-axis has a logarithmic scale. 48
15 Phase functions for the three aerosol models used in the retrieval simulations of Figure 16. The black line corresponds to a Henyey-Greenstein phase function with asymmetry parameter of 0.7, which is used in retrieval. 50

16 Effect of a model error in the phase function on retrieved aerosol pressure as a function of optical thickness for three values of aerosol pressure. Panel A (first row): 'Dust over ocean'; panel B (second row): 'Biomass burning over land'; panel C (third row): 'Boundary layer pollution'. For details of these scenarios, see the text and Table 13. In each panel, the left plot shows the bias in retrieved aerosol pressure and the right plot shows precision of retrieved pressure. We assume a Henyey-Greenstein phase function with asymmetry parameter of 0.7 in retrieval. Note that for the 'Boundary layer pollution' scenario, we assume an aerosol profile consisting of a single layer extending down to the ground surface. In this case, we retrieve the layer's top pressure p_{top}. The x-axis has a logarithmic scale. . . . 52

17 Reflectance spectra for two different combinations of optical thickness and surface albedo that yield the same continuum reflectance. All other parameters are the same. The aerosol layer is between 540 and 475 hPa; the single scattering albedo is 1.0; the solar zenith angle is 25° and the viewing direction is nadir. From the shape of absorption we can simultaneously fit surface albedo and aerosol optical thickness. . . . 53

18 Effect of an error in climatological albedo values on retrieved aerosol pressure as a function of the true surface albedo for three retrieval types (Table 14). Panel A (first row): aerosol layer with optical thickness of 0.5 at 500 hPa over sea / ocean; panel B (second row): aerosol layer with optical thickness of 0.5 at 800 hPa over vegetated land. In each panel, the left plot shows the bias in retrieved aerosol pressure and the right plot shows precision of retrieved pressure. The climatological surface albedo value, which is used in retrieval, is indicated by the arrow. Missing data points indicate that retrieval does not converge. . . . 55

19 Effect of a model error in the single scattering albedo on the bias in retrieved pressure as a function of the true single scattering albedo for three retrieval types (Table 14). The single scattering albedo assumed in retrieval is 0.95. Left: aerosol layer with optical thickness of 0.5 at 500 hPa over sea / ocean; right: aerosol layer with optical thickness of 0.5 at 800 hPa over vegetated land. Missing data points indicate that retrieval does not converge. . . . 56

20 Precision of retrieved aerosol pressure (left plot) and optical thickness (right plot) as a function of the a priori error in the temperature profile. The aerosol layer has optical thickness of 0.5 and is located at 500 hPa (green lines) or 800 hPa (red lines), over sea / ocean (solid lines) or vegetated land (dashed lines). Retrieval precision shows the same behavior if the optical thickness is 0.2. . . . 57

21 Precision of retrieved aerosol pressure (left plot) and optical thickness (right plot) as a function of the a priori error in the surface pressure. The aerosol layer has optical thickness of 0.5 and is located at 500 hPa (green lines) or 800 hPa (red lines), over sea / ocean (solid lines) or vegetated land (dashed lines). Retrieval precision shows the same behavior if the optical thickness is 0.2. . . . 58

22 Effect of an unscreened cloud layer on retrieved aerosol pressure for three values of the aerosol optical thickness. Left: cirrus layer between 330 and 300 hPa with cloud fraction 1.0 and varying cloud optical thicknesses; right: cumulus cloud between 910 and 890 hPa with cloud optical thickness of 10 and varying cloud fractions. The aerosol layer is at 700 hPa over sea / ocean. The profile parameterization in retrieval assumes one scattering layer. Missing data points indicate that retrieval does not converge. . . . 60

23 Precision of retrieved profile parameters as a function of the *a priori* error in the surface albedo for the baseline profile parameterization of a layer with fixed pressure thickness and the alternative implementation of a layer with variable pressure thickness. Left: aerosol layer with optical thickness of 0.5 at 500 hPa over vegetated land; right: aerosol layer with optical thickness of 0.5 at 800 hPa over sea / ocean. The baseline algorithm fits mid pressure (green solid line) and the alternative implementation fits mid pressure and pressure thickness (red dashed lines). Note the logarithmic scale of the x-axis. . . . 61

24 Accuracy (left plot) and precision (right plot) of retrieved aerosol pressure as a function of optical thickness when the vegetated land surface exhibits chlorophyll fluorescence. Solid lines correspond to a retrieval in which fluorescence is present in the simulation but not accounted for in the forward model for retrieval. Dashed lines correspond to a retrieval in which fluorescence emissions are included in the forward model and retrieved simultaneously with aerosol parameters. . . . 62

25 Sixteen GOME-2 pixels (quadrilaterals) and corresponding lidar locations (circles) used in retrieval experiments. The GOME-2 observations are of various strong aerosol events between July 2009 and July 2013. For every observation we collected lidar measurements for validation. 65
26 Convergence rate (left panel) and retrieved aerosol mid pressures (right panel) for every aerosol case in the first experiment investigating the effect of the aerosol layer's assumed pressure thickness. Assumed mid pressures are 20 hPa, 50 hPa or 100 hPa. Values for retrieved mid pressure are averages for six runs (initial values). Whiskers here indicate the max-min range of retrieval solutions; often they are barely visible. 66
27 Convergence rate (left panel) and retrieved aerosol mid pressures (right panel) for every aerosol case in the second experiment investigating the effect of an increase of the oxygen absorption cross section by 3% ('Xsec + 3%'). The baseline experiment against which results are compared ('Xsec') is the first experiment (assumed pressure thickness of 50 hPa). Values for retrieved mid pressure are averages for six runs (initial values). Whiskers indicate the max-min range of retrieval solutions. 67
28 Convergence rate (left panel) and retrieved aerosol mid pressures (right panel) for every aerosol case in the third experiment investigating the effect of including a temperature offset to the *a priori* profile in the state vector ('fit ΔT'). The baseline experiment against which results are compared ('not fit ΔT') is the second experiment. Values for retrieved mid pressure are averages for six runs (initial values). Whiskers indicate the max-min range of retrieval solutions. 68
29 Four example lidar extinction profiles (red line) with corresponding retrieved aerosol heights (green line). Blue dashed lines correspond to various characteristic heights of the lidar profile. 69
30 Residuals for every case and every run in the third experiment. Residuals are defined as the difference between measured and fitted reflectance as a percentage of the measured reflectance. 70
31 Retrieved aerosol top pressure as function of the aerosol optical thickness in the boundary layer for three values of the optical thickness of the upper (top) aerosol layer. Here the true surface albedo is 0.03. 71
32 Same as the previous figure, but for a true surface albedo of 0.20 instead of 0.03. 71
33 Residue of the fit in percent for different sets of fit parameters. The black curve shows the effect of aerosol in the boundary layer, which increases the reflectance by about 2% in the continuum and 0.4% in the deepest part of the O_2 A band. If only the surface albedo is fitted (dotted line) residues up to $\sim$0.7% occur in the O_2 A band. If the surface albedo is fitted together with the pressure of the aerosol layer (blue line) or the aerosol optical thickness (red line) we get approximately the same residue with a maximum of about 1%. If all three parameters are fitted (bright green line) the residue reduces substantially, but does not vanish. 72
34 (top) Suomi/NPP VIIRS RGB on 10 Nov. 2018, overlaid with NN ALH. The yellow line depicts the CALIPSO track overpassing that day. The yellow dashed line depict the 20 km range around the CALIPSO track; (bottom) CALIOP Total attenuated backscatter at 532 nm on 10 Nov. 2018 for the track shown by the yellow line in the top panel. 75

1 Introduction

1.1 Identification

This document, identified as S5P-KNMI-L2-0006-RP, is the Algorithm Theoretical Basis Document (ATBD) for the Tropospheric Monitoring Instrument's (TROPOMI) Aerosol Layer Height (ALH) product. It is part of a series of ATBDs describing the TROPOMI Level-2 products.

1.2 Purpose and objective

The purpose of this document is to describe the current implementation and the theoretical basis of the Aerosol Layer Height algorithm. The document is maintained during the development phase and the lifetime of the data product. Updates and new versions are foreseen if there are changes to the algorithm.

1.3 Document overview

Section 2 lists applicable and reference documents within the Sentinel-5 Precursor (S5P) / TROPOMI project as well as electronic references. Section 3 gives a list of terms, abbreviations and symbols that are specific for this document. Section 4, section 5.2 and section 6 describe the forward model and retrieval method, respectively. Section 7 discusses the operational algorithm's feasibility. Section 8 provides an extensive error analysis. Section 9 shows results of the algorithm applied to GOME-2 spectra. Section 10 presents a validation plan for the Aerosol Layer Height product. Section 11 provides a general conclusion and outlook. Finally, Section 12 lists references to peer-reviewed papers and other scientific publications.

1.4 Acknowledgements

The authors would like to thank the following persons for useful discussions: Maarten Sneep, Gijs Tilstra, Ofelia Vieitez, Piet Stammes, Arnoud Apituley and Pepijn Veefkind.

2 Applicable and reference documents

2.1 Applicable documents

[AD1] OMI Geolocation Review.
source: KNMI; **ref:** TN-OMIE-KNMI-729; **issue:** 1.0; **date:** 2004-04-05.

[AD2] Science Requirements Document for TROPOMI. Volume I: Mission and Science Objectives and Observational Requirements.
source: KNMI, SRON; **ref:** RS-TROPOMI-KNMI-017; **issue:** 2.0.0; **date:** 2008-10-30.

2.2 Reference documents

[RD1] Terms, definitions and abbreviations for TROPOMI L01b data processor.
source: KNMI; **ref:** S5P-KNMI-L01B-0004-LI; **issue:** 3.0.0; **date:** 2013-11-08.

[RD2] Terms and symbols in the TROPOMI Algorithm Team.
source: KNMI; **ref:** S5P-KNMI-L2-0049-MA; **issue:** 1.0.0; **date:** 2015-07-16.

[RD3] S5P/TROPOMI Science Verification Report.
source: IUP; **ref:** S5P-IUP-L2-ScVR-RP; **issue:** 2.1; **date:** 2015-12-22.

[RD4] TROPOMI Instrument and Performance Overview.
source: KNMI; **ref:** S5P-KNMI-L2-0010-RP; **issue:** 0.10.0; **date:** 2014-03-15.

[RD5] S5P-NPP Cloud Processor ATBD.
source: RAL Space; **ref:** S5P-NPPC-RAL-ATBD-0001; **issue:** 1.0.0; **date:** 2016-02-12.

[RD6] DISAMAR: Determining Instrument Specifications and Analyzing Methods for Atmospheric Retrieval, User Manual.
source: KNMI; **ref:** RP-TROPOMI-KNMI-104; **issue:** -; **date:** 2012-02-08.

[RD7] DISAMAR. Determining Instrument Specifications and Analyzing Methods for Atmospheric Retrieval. Algorithm description and background information.
source: KNMI; **ref:** RP-TROPOMI-KNMI-066; **issue:** 2.2.1; **date:** 2011-05-19.

[RD8] Calibration analysis report for TROPOMI UVN instrument spectral response function.
source: KNMI; **ref:** S5P-KNMI-OCAL-0124-RP; **issue:** 0.1.0; **date:** 2015-10-01.

[RD9] DISAMAR: Determining Instrument Specifications and Analyzing Methods for Atmospheric Retrieval, Algorithms and background.
source: KNMI; **ref:** RP-TROPOMI-KNMI-066; **issue:** -; **date:** 2012-01-24.

[RD10] D. P. Dee, S. M. Uppala, A. J. Simmons *et al.*; The ERA-Interim reanalysis: configuration and performance of the data assimilation system. *Quarterly Journal of the Royal Meteorological Society*; **137** (2011) (656), 553; doi:10.1002/qj.828. URL https://rmets.onlinelibrary.wiley.com/doi/abs/10.1002/qj.828.

[RD11] K. Chance and R.L. Kurucz; An improved high-resolution solar reference spectrum for earth's atmosphere measurements in the ultraviolet, visible, and near infrared. *Journal of Quantitative Spectroscopy and Radiative Transfer*; **111** (2010) (9), 1289; doi:10.1016/j.jqsrt.2010.01.036.

[RD12] Wavelength calibration for S5P L2 data processors.
source: KNMI; **ref:** S5P-KNMI-L2-0126-TN; **issue:** 1.0.0; **date:** 2015-09-11.

[RD13] DISAMAR: Determining Instrument Specifications and Analyzing Methods for Atmospheric Retrieval, Line Mixing and Collision Induced Absorption for the O2 A-band.
source: KNMI; **ref:** RP-TROPOMI-KNMI-???; **issue:** -; **date:** 2012-01-24.

[RD14] Wavelength calibration in the Sentinel 5-precursor Level 2 data processors.
source: KNMI; **ref:** S5P-KNMI-L2-0126-TN; **issue:** 1.0.0; **date:** 2015-09-11.

[RD15] Preparing elevation data for Sentinel 5 precursor.
source: KNMI; **ref:** S5P-KNMI-L2-0121-TN; **issue:** 2.0.0; **date:** 2015-09-11.

[RD16] Algorithm theoretical basis document for the TROPOMI L01b data processor.
source: KNMI; **ref:** S5P-KNMI-L01B-0009-SD; **issue:** 6.0.0; **date:** 2015-09-22.

2.3 Electronic references

[ER1] URL https://www.tensorflow.org.

[ER2] URL http://temis.nl/surface/.

[ER3] URL http://www.cfa.harvard.edu/hitran/.

[ER4] URL https://www.spec.org/cpu2006/results/res2013q1/cpu2006-20121023-24837.html.

[ER5] URL http://www.esa-aerosol-cci.org.

3 Terms, definitions and abbreviated terms

Terms, abbreviations and symbols that are used within the TROPOMI Level-2 project are described in [RD1]. and [RD2]. Terms, definitions and abbreviated terms that are specific for this document can be found below. More in [AD1]

3.1 Terms and definitions

accuracy	systematic error component
height	vertical height, either in units of hPa (pressure) or in units of km (altitude)
hyperspectral imager	imager with large number of spectral channels, often at high spectral resolution (better than about 0.5-1 nm), e.g. GOME-2
multispectral imager	imager with a number of spectral channels (typically 30-50) that are generally not contiguous and have coarser spectral resolution (2-10 nm), e.g. MODIS

3.2 Acronyms and Abbreviations

UVAI	UV Aerosol Index
AERONET	Aerosol Robotic Network
AEROPRO	Aerosol Profile Retrieval Concept Development and Validation for Sentinel-4
ALH	Aerosol Layer Height
ATBD	Algorithm Theoretical Basis Document
AVHRR	Advanced Very High Resolution Radiometer
BSA	black-sky albedo
CALIOP	Cloud-Aerosol Lidar with Orthogonal Polarisation
CALIPSO	Cloud-Aerosol Lidar and Infrared Pathfinder Satellite Observation
CIA	collision-induced absorption
CPU	central processing unit
DISAMAR	Determining Instrument Specifications and Analyzing Methods for Atmospheric Retrieval
DLR	Deutsches Zentrum für Luft- und Raumfahrt
DWD	Deutscher Wetterdienst
EarthCARE	Earth Clouds, Aerosols and Radiation Explorer
ECMWF	European Centre for Medium-Range Weather Forecasts
EARLINET	European Aerosol Research Lidar Network
ERA	ECMWF Reanalysis
FRESCO	Fast Retrieval Scheme for Clouds from the Oxygen A Band
FWHM	full width at half maximum
GALION	GAW Atmospheric Lidar Observation Network
GMES	Global Monitoring of the Environment and Security
GOME	Global Ozone Monitoring Experiment
GOSAT	Greenhouse Gases Observing Satellite
HALO	High Altitude and Long Range Research Aircraft
HG	Henyey-Greenstein
HITRAN	High Resolution Transmission
HSRL	High Spectral Resolution Lidar
IASI	Infrared Atmospheric Sounding Interferometer
IUP	Institut für Umweltphysik
JPL	Jet Propulsion Laboratory
KNMI	Koninklijk Nederlands Meteorologisch Instituut

LABOS	layer-based orders of scattering
LBL	Line-by-line
LER	Lambertian-equivalent reflectivity
LM	line mixing
MERIS	Medium Resolution Imaging Spectrometer
MetOp	Meteorological Operational Satellite
MISR	Multi-Angle Imaging Spectroradiometer
MLS	mid-latitude summer
MODIS	Moderate Resolution Imaging Spectroradiometer
MTG-S	Meteosat Third Generation - Sounder
NIR	near infrared
NN	neural network
NSIDC	National Snow & Ice Data Center
OMI	Ozone Monitoring Instrument
PMD	Polarisation Measurement Devices
POLDER	Polarization and Directionality of the Earth's Reflectance
RAA	relative azimuth angle
S5P	Sentinel-5 Precursor
S/C	spacecraft
SACURA	Semi-Analytical Cloud Retrieval Algorithm
SCIAMACHY	Scanning Imaging Absorption Spectrometer for Atmospheric Cartography
SNR	signal-to-noise ratio
Suomi-NPP	Suomi National Polar-orbiting Partnership
SWIR	shortwave infrared
SZA	solar zenith angle
TANSO-FTS	Thermal and Near Infrared Sensor for Carbon Observations Fourier-Transform Spectrometer
TROPOMI	Tropospheric Monitoring Instrument
UV	ultraviolet
UVIS	ultraviolet-visible
UVN	ultraviolet-visible-near infrared
VIIRS	Visible / Infrared Imaging Radiometer Suite
VIS	visible
VZA	viewing zenith angle

3.3 Symbols

ω_0	single scattering albedo [-]
τ_0	aerosol or cloud optical thickness [-]
α	Ångström coefficient [-]
g	asymmetry parameter [-]
p_{mid}	aerosol mid pressure [hPa]
z_{mid}	aerosol mid altitde [km]
p_{top}	aerosol top pressure [hPa]
Δp	pressure thickness [hPa]
p_{s}	surface pressure [hPa]
z_{s}	surface altitude (above reference surface) [km]
A_{s}	surface albedo [-]
F_{s}	surface (fluorescence) emission [ph. cm^{-2} s^{-1} nm^{-1} sr^{-1}]

R	Reflectance [sr^{-1}]
I	Radiance [ph. cm^{-2} s^{-1} nm^{-1} sr^{-1}]
E_0	Irradiance [ph. cm^{-2} s^{-1} nm^{-1}]

4 Introduction to Aerosol Layer Height product

4.1 Product description

The Tropospheric Monitoring Instrument features a new aerosol product that is dedicated to retrieval of the height of tropospheric aerosols. Before the launch of TROPOMI, daily global observations of aerosol height were not available on an operational basis. Aerosol profiles were provided by active sensors, particularly by ground-based lidar systems or by the space-borne Cloud-Aerosol Lidar with Orthogonal Polarisation (CALIOP), and aerosol layer height by multi-angle sensors, most notably Multi-Angle Imaging SpectrRadiometer (MISR). Active sensors have a high vertical resolution, but CALIOP and MISR observe in narrow tracks only. However, passive sensors, such as TROPOMI, can cover the entire earth in a single day.

The TROPOMI Aerosol Layer Height product focuses on retrieval of vertically localized aerosol layers in the free troposphere, such as desert dust, biomass burning aerosol, or volcanic ash plumes. The height of such layers is retrieved for cloud-free conditions. Height information for aerosols in the free troposphere is particularly important for aviation safety. Scientific applications include radiative forcing studies, long-range transport modeling and studies of cloud formation processes. Aerosol height information also helps to interpret the UV Aerosol Index (UVAI) in terms of aerosol absorption as the index is strongly height-dependent.

Retrieval of aerosol height is based on absorption by oxygen in the A band. The O_2 A band is located in the near-infrared wavelength range between about 759 and 770 nm. It is a highly structured line absorption spectrum with strongest absorption lines occurring between 760 and 761 nm. The absorption band spans a wide range of absorption optical thicknesses. At some wavelengths, photons do not reach the lower levels of the atmosphere.

Figure 1 shows simulated reflectance spectra at TROPOMI's anticipated instrument specifications (as described in [63]) for an aerosol layer at two different pressures. The difference between the two spectra

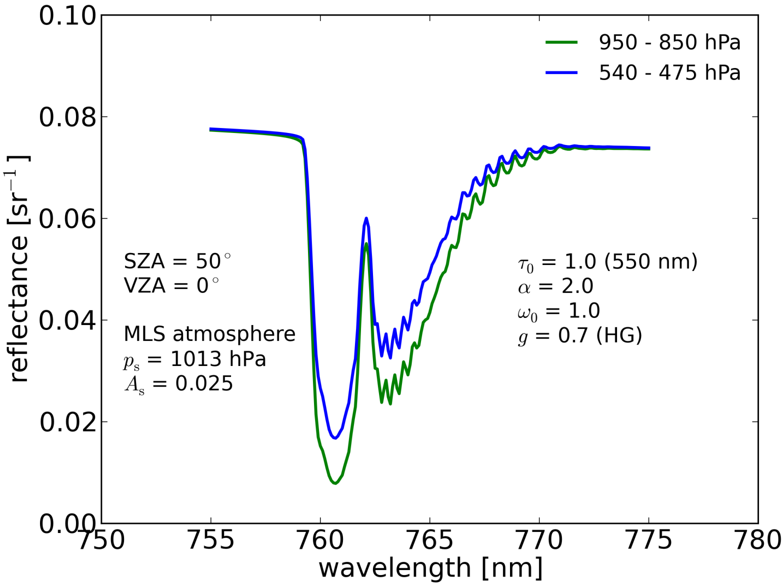

Figure 1: Simulated reflectance spectra of the O_2 A band at a spectral resolution (FWHM) of 0.5 nm for a scene containing a representative aerosol layer. The aerosol layer is between 950 and 850 hPa (green line) or between 540 and 475 hPa (blue line). The 1-σ measurement errors on reflectance are smaller than the width of the plotting lines: anticipated signal-to-noise ratios for these spectra (based on [63]) are about 645 in the continuum and 302 and 207 in the deepest part of the O_2 A band assuming pure shot noise. The solar zenith angle is 25° and the viewing direction is nadir. The aerosol optical thickness τ_0 at 550 nm is 1.0, the Ångström coefficient α is 2.0, the single scattering albedo is 1.0, and the phase function is a Henyey-Greenstein function with asymmetry parameter g of 0.7. Spectra were simulated with a temperature profile corresponding to the mid-latitude summer (MLS) atmosphere, a surface pressure of 1013 hPa and a constant ground surface albedo of 0.025.

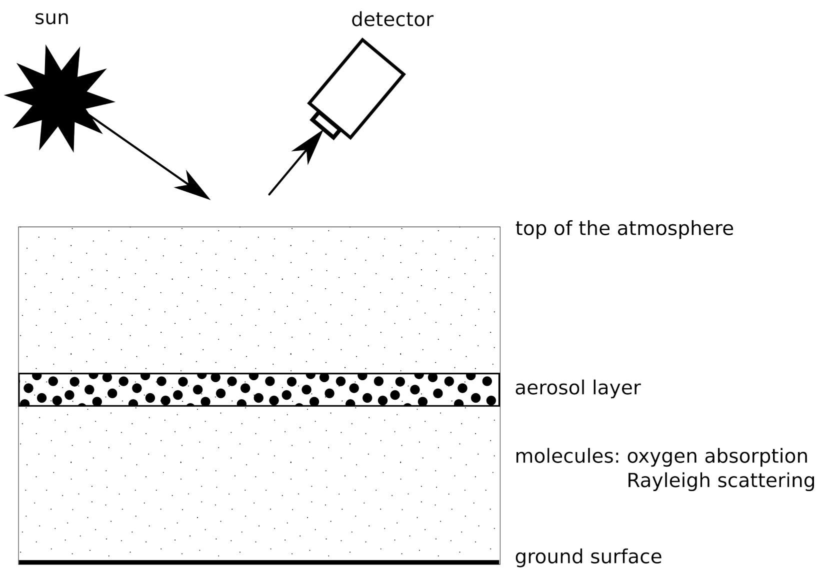

Figure 2: Schematic depiction of the atmosphere and typical TROPOMI satellite configuration for retrieval of Aerosol Layer Height. The Rayleigh scattering optical thickness at the O_2 A band is ~0.02
.

provides the aerosol pressure signal. The baseline fit window for the Aerosol Layer Height algorithm extends from 758 nm (continuum) to 770 nm. For more recent TROPOMI instrument specifications, see . A schematic depiction of the satellite configuration for observations of the O_2 A band with TROPOMI is given in Figure 2.

4.2 Heritage

TROPOMI Aerosol Layer Height is a new operational Level-2 product. Heritage products for an operational aerosol profile retrieval based on hyperspectral measurements of the oxygen A band presently do not exist. However, the Aerosol Layer Height algorithm can be applied to measurement series from the Scanning Imaging Absorption Spectrometer for Atmospheric Cartography (SCIAMACHY; [3]) and the Global Ozone Monitoring Experiment-2 (GOME-2). A first case study of ALH retrieval with GOME-2 measurements has been published as [48]. Aerosol Layer Height retrievals were performed for a number of aerosol scenes covering various aerosol types, both elevated and boundary layer aerosols and land and sea surfaces. The retrieval results were evaluated with lidar measurements. A follow-up study applied the TROPOMI ALH algorithm to desert dust outbreaks off the West African coast observed with SCIAMACHY (manuscript in preparation). Within the TROPOMI project also a scientific verification study of the prototype algorithm has been performed. An independent ALH verification algorithm from the Institute of Environmental Physics (IUP, Bremen, Germany) and the prototype ALH algorithm from KNMI were applied to the case of a volcanic ash plume near Iceland observed with GOME-2 (chapter 14 in [RD3]). Retrieval results were intercompared and evaluated with plume heights retrieved with MISR (stereoscopic retrieval). The main conclusions from these studies have been included in this ATBD as much as possible. Finally, we remark that the TROPOMI Aerosol Layer Height algorithm will serve as the ALH heritage algorithm for the future Sentinel–4 and Sentinel–5 missions [26], which make hyperspectral observations of the O_2 A band as well.

Early papers investigating the O_2 A band for aerosol retrieval are by Badayev and Malkevich (1978)[2] and Gabella et al. (1999) [2] and [19]. Corradini and Cervino (2006) [9] present a simulation study of retrieval of the extinction profile for SCIAMACHY instrument characteristics with all other parameters (e.g. aerosol and surface properties) being assumed in retrieval. Actual case studies exploiting hyperspectral O_2 A band measurements have been performed by Koppers and Murtagh (1997) [33] for GOME data, and by Kokhanovsky and Rozanov (2010) [32] and Sanghavi et al. (2012) [51] for SCIAMACHY data. Koppers and Murtagh (1997) retrieve surface albedo simultaneously with aerosol optical thickness and height distribution, while in the retrievals proposed by Kokhanovsky and Rozanov (2010) and Sanghavi et al. (2012) the surface albedo basically is a model

parameter (i.e. surface albedo not fitted). A retrieval setup similar to Kokhanovsky and Rozanov (2010) is being extended to GOME-2 case studies [36]. Sensitivity studies to consolidate instrument requirements for O_2 A band aerosol retrieval include studies by Siddans et al. (2007) [53] and Hasekamp and Siddans (2009) [22] for Sentinel–4/5, and by Hollstein et al. (2012) [24] for the Earth Explorer 8 mission Fluorescence Explorer (FLEX). Dubuisson et al. (2009) [16] present a method to retrieve the altitude of aerosol plumes over ocean from the ratio of reflectances in the two O_2 A band channels of the Medium Resolution Imaging Spectrometer (MERIS) and the Polarization and Directionality of the Earth's Reflectance (POLDER) instrument. Finally, we mention the work by Van Diedenhoven et al. (2005) [59] who showed that retrieved apparent surface pressure (i.e. retrieved surface pressure when ignoring aerosol scattering) with SCIAMACHY depends systematically on aerosol parameters. This illustrates in yet another way that the O_2 A band contains aerosol information available for retrieval.

Absorption by oxygen in the A band has been or is being used in operational cloud retrieval for the GOME instruments (Fast Retrieval Scheme for Clouds from the Oxygen A Band (FRESCO) [30]) and for SCIAMACHY (Semi-Analytical Cloud Retrieval Algorithm (SACURA)[45]). There are indications that the FRESCO cloud retrieval algorithm may also provide information on aerosols in case of optically thick aerosol layers (Wang et al., 2012) [64]. However, FRESCO uses a Lambertian surface to model cloud layers, which may be an inaccurate approximation for aerosol layers since typical aerosol layers have significant transmission. The forward model of the Aerosol Layer Height algorithm is developed specifically for retrieval of aerosol height.

Finally, we remark that the O_2 A band is often used for an atmospheric scattering correction as part of more convolved trace gas retrieval algorithms (e.g. [40] [5]; [43]; [66]).

4.3 Product requirements

Science requirements for the Aerosol Layer Height product are described in [AD2]. The target requirement on the accuracy and precision of retrieved Aerosol Layer Height is 0.5 km or 50 hPa. The threshold requirement on accuracy and precision is 1 km or 100 hPa. A minimum aerosol optical thickness for which these requirements should be met is not specified. Note that an accuracy and precision requirement is defined for retrieved aerosol height but not for retrieved aerosol optical thickness.

Furthermore, the Aerosol Layer Height product will be delivered in near real-time, which means that Level-2 data should be available within three hours after observation.

4.4 Overview of the retrieval algorithm

The Aerosol Layer Height algorithm presently has the following key features:

- Spectral fit estimation of reflectance across the O_2 A band (wavelengths ~758–770 nm) using a neural network;
- Retrieval method is Optimal Estimation;
- Main fit parameters are: aerosol layer mid pressure (p_{mid}) and aerosol optical thickness (τ_0);
- Error estimates are provided to improve the usability of the product;
- Assumed aerosol profile: single uniform scattering layer with a fixed pressure thickness.

We assume that aerosols are confined to a single layer with a fixed pressure difference between top and bottom of the layer, and with a constant aerosol volume extinction coefficient and aerosol single scattering albedo within the layer. This parameterization is most suited for aerosol profiles that are dominated by a single, elevated, optically thick aerosol layer. The product's name explicitly refers to this particular profile parameterization. The reported height parameter is the mid pressure of the layer defined as the sum of top pressure and bottom pressure divided by two. The aerosol layer mid pressure (p_{mid}) is converted into an aerosol layer mid altitude (z_{mid}) using an appropriate temperature profile. In addition to aerosol layer mid pressure, also the aerosol optical thickness is retrieved. The retrieved aerosol optical thickness holds for wavelengths of the O_2 A band (i.e. at 760 nm). The wavelength range of the O_2 A band is too small to provide information on the spectral dependence of the optical thickness. The Aerosol Layer Height product contains error estimates as well as other relevant diagnostics so that the user can evaluate the retrieval result.

From retrieval simulation experiments and a validation study for SCIAMACHY ALH retrievals, we have learned that the retrieved mid pressure of the assumed aerosol layer can in general be regarded as an average aerosol scattering height (manuscript in preparation).

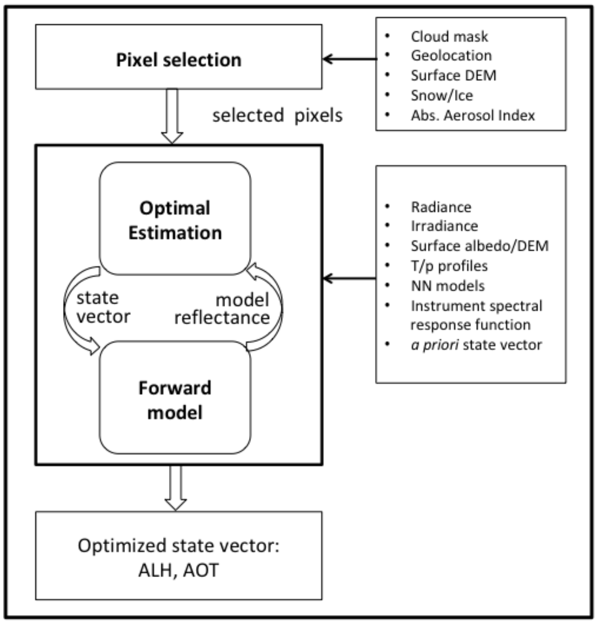

Figure 3: Flow chart for the Aerosol Layer Height retrieval algorithm.

The baseline fit window extends from 758 to 770 nm and covers the entire O_2 A band. The error analysis reported in Section 8 is performed for this fit window so that it provides a benchmark against which alternative implementations can be compared.

A basic flow chart of the algorithm is given in Figure 3. Calibrated radiances, irradiances and their associated measurement errors are the main inputs for the algorithm. Aerosol Layer Height is retrieved for cloud-free pixels only. Furthermore, pixels covered by snow or (sea) ice are initially excluded from analysis as well. In addition, in order to process pixels that contain a minimum amount of aerosols, we select pixels based on the UV Aerosol Index. High values for this index indicate the presence of elevated absorbing aerosol. Dynamic input data further comprise meteorological data. Static input includes oxygen absorption parameters, a high-resolution solar irradiance spectrum, slit functions for the radiance and irradiance, and surface altitude (digital elevation model). Finally, a surface albedo climatology is used to provide a priori values for retrieval.

Aerosol optical properties show a large variation in time and space. However, the forward model used in operational retrieval assumes a single, average aerosol model (e.g. single scattering albedo ω_0 of 0.95 and Henyey-Greenstein phase function with asymmetry parameter g of 0.7). Sensitivity analyses for the Aerosol Layer Height algorithm (Section 8) and experiments with GOME–2 spectra [49] have shown that a single, fixed aerosol model is sufficient for a reasonably accurate (i.e. compared to science requirements) retrieval of aerosol pressure, which is the primary objective of this product. We remark that retrieved aerosol optical thickness holds for the particular aerosol model assumed in retrieval (phase function and single scattering albedo) and should thus be understood as an effective quantity in this respect.

Development of the operational Aerosol Layer Height algorithm is ongoing work. In this document, the most recent implementation of the operational algorithm is described. Updates and new versions of the ATBD are foreseen during the development phase and the lifetime of the product when there are significant changes to the algorithm. The current implementation of the algorithm is based on a neural network forward model and an optimal estimation scheme in the retrieval. A detailed description of the Aerosol Layer Height retrieval algorithm is given in Section 5.2 and Section 6. The sensitivity analyses presented in Section 8 illustrate the algorithm's expected performance and provide further support to the choices we made in the design of the algorithm.

4.5 Development risks

The current version of the ALH algorithm implemented in the Level-2 processor does not fit the surface albedo but keeps it fixed in retrieval at climatological values. When applying the algorithm to real spectra from GOME-2 ([49]; see also Section 9) and SCIAMACHY (manuscript in preparation), we found that when fitting the surface albedo retrieved aerosol pressures often have substantially lower values (i.e. aerosol layer placed higher in the atmosphere) compared to the case of not fitting the surface albedo. The comparison with lidar measurements

confirms that retrieved Aerosol Layer Heights are indeed too high when fitting the surface albedo but attain realistic values when not. First retrieval simulations relate this effect to the presence of boundary layer aerosols. When fitting the surface albedo, part of the aerosol scattering near the surface is attributed in retrieval to reflection by the surface, which in turn biases retrieved Aerosol Layer Height into the direction we observe with real data retrievals. An explanation of this mechanism is given in Sanders et al. (2015) and in Section 9. The important observation here is that in this case the retrieved Aerosol Layer Height parameter does not properly represent an average aerosol scattering height. Since boundary layer aerosols are typically present, we currently do not fit the surface albedo. Based on the GOME-2 and particularly the SCIAMACHY case studies ([49]), it was expected that climatological surface albedo values for sea surfaces are sufficiently accurate for our purposes. First results from TROPOMI confirm this. Over land, the accuracy of the retrievals are strongly dependent on the surface albedo, with low accuracy for bright surfaces. Fitting the surface albedo may be beneficial for land retrievals, but this depends strongly on the accuracy of the surface albedo database itself. Currently, a surface equivalent reflectance (LER) database and a directional LER (DLER) database based on TROPOMI data are under development. The implementation of these databases will be investigated when they become available.

Another critical point concerns the presence of residual clouds in the scene after cloud masking (see Section 5.1.1). The off-line cloud mask is based on observations by the Visible / Infrared Imaging Radiometer Suite (VIIRS). The near real-time cloud mask is primarily based on an assessment of the homogeneity of the scene using TROPOMI's so-called small-pixel columns. For the profile parameterization of the baseline algorithm (single aerosol layer assumed), a sensitivity analysis has shown that optically thin clouds that typically remain undetected by a cloud mask can cause substantial biases in retrieved Aerosol Layer Height (Section 8.8). Cirrus clouds occur abundantly, particularly in the tropics [39]. An accurate retrieval of aerosol height in the near real-time processing stream is particularly important for aviation safety applications. First results [38] show that the VIIRS cloud masks are sufficient to isolate cloud-free scenes for aerosol layer height retrievals. However, in near-real time cirrus affects the retrievals.

4.6 Foreseen update approach

The initial focus of the product is to use the oxygen A band to provide height information for optically thick aerosol layers in the free troposphere. We foresee, however, the following two updates to the algorithm.

First, we anticipate an alternative profile parameterization that explicitly takes into account boundary layer aerosols. As mentioned above, we found that retrieved height of the elevated layer is biased when significant boundary layer aerosols are present and the surface albedo is retrieved simultaneously with aerosol parameters. We are planning to extend DISAMAR so that aerosol properties of two atmospheric intervals can be fitted. One interval then represents the elevated aerosol layer and the other represents boundary layer aerosols.

Second, we anticipate that at a later stage an update of the algorithm includes the O_2 B band. The wavelength range of the O_2 A band (~759-770 nm) is contained in TROPOMI spectral band 6 (725–775 nm), while the O_2 B band (~685–689 nm) is covered on the same detector by spectral band 5 (675–725 nm). Although the O_2 B band is weaker than the O_2 A band, this absorption band might provide additional aerosol information (e.g. [51]), particularly because land surfaces typically have different reflectivities at the two absorption bands (red edge). At the same time, co-registration errors might be relatively small [RD4].

4.7 Terminology

The deviation of a measured or calculated value from its true value is called the *error*. The error has a random and a systematic component. Throughout this document, a distinction is made between the *precision* and the *accuracy* of a retrieved parameter. These terms are defined as follows:

- Precision: This term refers to the random error component. A measure for the precision is the standard deviation (σ) of the fit parameter's (*a posteriori*) distribution. A large standard deviation indicates a poor precision.

- Accuracy: This term refers to the systematic error component. A measure for the accuracy is the bias defined as the fit parameter's (*a posteriori*) expected value minus its true value. A large bias indicates a poor accuracy.

Furthermore, within the context of the Optimal Estimation retrieval method, the terms *a priori error* and *a posteriori error* of a state vector element are often used. Both errors specifically refer to the random error

component (1-σ error). The term *measurement noise* similarly refers to the random error component of the measurement error. The measurement error, however, may comprise other error terms as well, such as *calibration errors*.

The term *forward model* indicates the model that is used to calculate reflectance spectra. Its main use is in the retrieval procedure (inversion) in which modeled reflectance spectra are fitted to actual measurements. In this case, the forward model is called the *forward model for retrieval*. In the operational processor this step is comprised of a fast neural network estimation of the spectra. In the sensitivity studies in this ATBD, this step comprised of line-by-line calculation by DISAMAR, when actual measurements are replaced by simulated measurements. The forward model used for these simulations is called the *forward model for simulation*. We restrict the use of the term simulation to simulation of measurements or retrievals with DISAMAR when performing sensitivity analyses.

Finally, the effect of systematic errors on retrieval can be investigated by introducing differences between parameters in the forward model for simulation and the forward model for retrieval (*model biases*). Typically, the forward model for simulation is more complex and comprehensive than the forward model for retrieval. For example, the forward model for simulation may include a phase function from Mie calculations to describe the angular dependence of scattering by aerosols, whereas the forward model for retrieval always uses the neural network, trained with the same aerosol model.

5 Algorithm description

5.1 Spatial data selection

Aerosol Layer Height is retrieved for cloud-free pixels outside the sun glint region. In addition, pixels with the highest chance of containing significant amounts of aerosol are selected for processing first. We also exclude from analysis pixels covered by snow or ice.

5.1.1 Cloud mask

A cloud mask for the off-line processing and reprocessing modes is based on observations by VIIRS aboard Suomi-NPP [RD5]. VIIRS is a multispectral imager that is well suited for the detection of clouds, particularly of clouds at high altitude such as cirrus. S5P flies in formation with Suomi-NPP and observes within approximately 5 min from Suomi-NPP's overpass. Observations by VIIRS are re-gridded to the TROPOMI observation grid and a cloud mask is constructed for different definitions of the TROPOMI field-of-view [RD5].

The standard VIIRS Cloud Mask determines a cloud classification for every VIIRS ground pixel based on a set of threshold tests using radiances in the visible, near-infrared, shortwave infrared and thermal infrared wavelength range. VIIRS pixels are eventually classified as confidently clear, probably clear, probably cloudy or confidently cloudy. The VIIRS cloud mask for TROPOMI gives the fraction of VIIRS pixels with a particular cloud classification out of the total number of VIIRS pixels within each defined TROPOMI field-of-view. The VIIRS cloud mask for TROPOMI also contains the mean and the standard deviation of radiances for the VIIRS pixels within a TROPOMI field-of-view. A dedicated cirrus test using the 1.38 μm channel is part of the standard VIIRS Cloud Mask, but thin cirrus may still be missed as illustrated in [RD5]. For our purposes, detection of thin cirrus is important and next to using the VIIRS cloud classifications re-gridded to the TROPOMI grid, we therefore also apply a separate threshold test to the mean radiance at 1.38 μm. As a starting point, we closely follow threshold tests implemented by the methane retrieval algorithm [23]. Accurate cloud screening is important for methane retrieval as well and the development of the VIIRS cloud mask for TROPOMI is mainly driven by this requirement.

The cloud mask from VIIRS is not available in near real-time. Cloud masking for the near real-time processing mode consists of a number of threshold tests based on TROPOMI observations. An important parameter concerns the homogeneity of the scene. It is planned to downlink radiance measurements for one wavelength ('column') per spectral band every exposure time, instead of every co-addition period. The homogeneity of the scene can then be assessed based on the variability of the radiance across these so-called small-pixel columns. Additional parameters include radiance levels in the visible wavelength range and their wavelength dependence (color). Cloud parameters from the FRESCO algorithm, which are delivered near real-time, are also used. Setting thresholds for cloud mask tests will primarily be a matter of experience.

The VIIRS cloud mask may have difficulty detecting clouds at low altitude. It would therefore be reasonable to take an assessment of the homogeneity of the scene also into account in off-line cloud masking. More generally, TROPOMI threshold tests used for cloud masking in near real-time are considered a fallback option for the off-line processing stream in case the VIIRS cloud mask is unavailable. We expect that the near real-time cloud mask will have difficulty detecting cirrus clouds. So-called high cloud cover parameters from ECMWF may perhaps provide additional information useful for masking of persistent cirrus. However, this is an experimental option and it needs to be further investigated whether the temporal resolution is sufficient for this purpose.

Finally, we note that cloud masking is problematic over snow or ice covered areas. Pixels covered by snow or ice are therefore excluded from analysis at present.

5.1.2 Snow or ice covered pixels

In case of drifting sea ice or land temporarily covered with snow or ice, the true surface albedo substantially deviates from its climatological value. In addition to the surface albedo climatology, we need information on snow or ice cover. This information might be used to provide a better a priori value for the surface albedo, or to exclude snow or ice covered pixels from analysis. (It is very well possible to retrieve Aerosol Layer Height over bright surfaces, but cloud masking is often problematic in that case.) Information on snow or ice cover is provided, for example, by the National Snow & Ice Data Center (NSIDC) or by ECMWF. The spatial resolution should preferably be comparable to the resolution of TROPOMI.

5.1.3 Sunglint

The strongest violation of the Lambertian approximation for the reflectivity of the ground surface occurs for surfaces exhibiting specular reflection of direct sunlight. Oceanic pixels for which the viewing geometry is such that sunglint is to be expected are excluded from analysis. A threshold (e.g. 18°) is put on the sunglint angle, i.e. the angle between the viewing direction and the direction of specular reflection. The threshold needs to be large enough so that effects related to sea surface roughness are taken into account. The sunglint angle α is given by

$$\cos\alpha = \cos\theta_0 \cos\theta + \sin\theta_0 \sin\theta \cos(\phi - \phi_0) \quad (1)$$

in which θ_0 is the solar zenith angle, θ the viewing zenith angle and $\phi - \phi_0$ the relative azimuth angle.

5.1.4 Pixels containing aerosol

Initially, only pixels are selected for processing that contain a significant amount of aerosol. The UV Aerosol Index is used to select pixels that contain elevated absorbing aerosol. Calculation of this index is a very fast operation. Scattering aerosol and aerosol close to the surface will be missed. In the future, pixels containing scattering aerosols can perhaps be selected by setting a threshold on maximum negative UVAI values in combination with a high-quality cloud mask [41]. Typical aerosol cases that are detected are desert dust, biomass burning aerosol and volcanic ash plumes. Particularly detection of the latter case is important in near real-time processing for aviation safety. In addition, SO_2 measurements, news reports of volcanic eruptions and the like can be used to incidentally select geographical areas. Note that it would be desirable in the end to process all cloud-free pixels.

5.1.5 Pixel selection scheme

Below, the currectly implemented scheme that selects the pixels for ALH retrieval is described. This selection scheme will be further expanded and optimized in the coming time, after assessments of the ALH product. Note that selection step 7 is not available for near real-time processing. As a starting point, the Aerosol Layer Height implementation of the VIIRS cloud mask for TROPOMI follows the implementation by the methane retrieval algorithm (threshold values T1, T2 and T3 are currently taken from there; see [RD5]).

Process pixels for which the following criteria are met (logical AND, tests are ordered):

1. Solar zenith angle is smaller than 75° .
2. For pixels over water, sun glint angle is larger than 18° .
3. Standard deviation of elevation inside pixel is smaller than 300 m.
4. Pixel is completely land OR completely water.
5. Pixel does not contain snow / ice according to dynamic input (NSIDC or ECMWF) AND climatological surface albedo at VIS wavelength is smaller than 0.5.
6. FRESCO effective cloud fraction is smaller than 0.05.
7. Fraction of confidently clear VIIRS pixels within TROPOMI nominal NIR field-of-view is smaller than threshold T1 AND fraction of confidently clear VIIRS pixels within TROPOMI extended NIR field-of-view is smaller than threshold T2 AND mean VIIRS cirrus reflectance (1.38 μm) within TROPOMI nominal NIR field-of-view is smaller than threshold T3. This selection step is not available for near real-time processing. Threshold values T1, T2 and T3 are currently taken from the methane retrieval algorithm.
8. UVAI is larger than 2.0.
9. The absolute value of the difference between the scene albedo at 380 nm from the UVAI calculation and the climatological surface albedo at 380 nm is smaller than a particular threshold. This difference threshold is the maximum of an absolute value (0.05) and a relative value (25% of the climatological surface albedo at 380 nm). This is a first test to filter out clouds.

5.2 Forward model

This section provides a detailed description of the current implementation of the forward model for the Aerosol Layer Height retrieval algorithm. The forward model is based on a neural network (NN) trained to estimate the irradiances, radiances and their derivatives with respect to ALH and AOT in the O2-A band wavelength window. This approach replaces the original line-by-line computation done with the RTM DISAMAR [RD6], [RD7], which was used to develop and test the ALH algorithm. The NN implementation improves the forward computation speed by several orders, which makes it possible to retrieve ALH for all TROPOMI pixels on a near-real time basis. The NN implementation reduces the accuracy of the ALH, but several tests (see section 8) show that the reduction is limited. The training of the neural network was done with spectra that were simulated with DISAMAR, and all the test results described in this ATBD are valid also for the NN forward model implementation.

Section 5.2 describes the forward model of the baseline algorithm. There are, however, alternative parameterizations, settings etc. that we may implement as options in the operational algorithm. These options are briefly discussed where appropriate, because this is important for developers of the Level-2 processor.

5.2.1 Overview

The forward model calculates reflectances for an atmosphere in which Rayleigh scattering, gas absorption, and scattering and absorption by aerosol and clouds can take place. The atmosphere is bounded from below by a reflecting and possibly emitting ground surface. The forward model is used for the inversion in which modeled reflectance spectra are fitted to actually measured reflectance spectra.

The Radiative Transfer Model (RTM), at the core of the algorithm, computes the monochromatic, or high spectral resolution, reflectance R at the top-of-atmosphere at a wavelength λ, defined as [RD2]

$$R(\lambda) = \frac{\pi I(\lambda)}{\mu_0 E_0(\lambda)}, \tag{2}$$

where $I(\lambda)$ is the radiance at the top-of-atmosphere at wavelength λ, E_0 is the solar irradiance at the top-of-atmosphere at wavelength λ, perpendicular to the direction of the incident sunlight, and μ_0 the cosine of the solar zenith angle. The RTM-calculated high-resolution reflectance spectrum is convolved with the instrument's spectral response function (ISRF, [RD8]), to obtain reflectances $R(\lambda_i)$ at the instrument's spectral resolution,

$$R(\lambda_i) = \frac{\pi I(\lambda_i)}{\mu_0 E_0(\lambda_i)}, \tag{3}$$

where λ_i is the central wavelength at the i^{th} spectral point on the sensor, and $I(\lambda_i)$ and $E_0(\lambda_i)$ are the measured radiance and irradiance for that spectral point, respectively.

5.2.2 Radiative transfer model

Monochromatic (high-resolution) reflectances are calculated in DISAMAR with the layer-based orders-of-scattering (LABOS) method. This is a variant of the doubling-adding method (e.g. [13], [25]) in which the adding of the different layers is replaced by orders of scattering for the atmospheric layers.

The atmosphere is first divided into homogeneous layers. Reflection and transmission properties for individual layers are calculated using the doubling method. The orders-of-scattering method is then used to calculate the internal radiation field and the field at the top of the atmosphere. The order of scattering refers to the number of times radiation has been scattered by atmospheric layers instead of atmospheric volume elements. Within a single layer, however, many scattering events can take place. LABOS is more efficient than both the adding method and the classical orders-of-scattering method. A detailed description of this method is given in [RD9].

We now briefly discuss current settings for the most important parameters of the radiative transfer calculations used in the NN model. For an explanation of other settings, for example construction of the high-resolution wavelength grid used for the line-by-line calculations, we refer the reader to [RD9].

- Multiple scattering is taken into account, as this can be significant inside aerosol layers.
- Polarization is currently ignored, as this substantially reduces computation time. Approximate calculations using scalar radiative transfer will introduce errors due to polarizing aerosols and multiply Rayleigh scattered light. A preliminary sensitivity analysis using the 'Fine mode weakly absorbing' aerosol model

(Section 8.3.2) has shown that the effect on retrieved aerosol mid pressure is typically much smaller than about 20 hPa. It is in principle possible to include polarization in radiative transfer calculations with DISAMAR .

- Inelastic scattering (rotational Raman scattering) is currently not implemented. The effect on the O_2 A band reflectance is small (e.g. [62]; [54]), particularly for a nadir-viewing instrument such as TROPOMI. A preliminary sensitivity analysis has shown that the effect on retrieved parameters is much smaller than the effect of other model errors so that we can ignore rotational Raman scattering.
- The atmosphere is assumed plane-parallel, but a correction for the attenuation of direct incident sunlight in a spherical atmosphere is made if the solar zenith angle is 60° or larger [8].
- The number of Gaussian points needed for integration over the polar angle depends on the phase function of the aerosol (or cloud particle). We have found that we typically need about ten Gaussian points (twenty streams) in case of a Henyey-Greenstein phase function with asymmetry parameter g of 0.7 to get an accurate calculation of the radiance fields. This phase function is the standard phase function assumed in the NN forward model, see section 5.2.4.6.

5.2.2.1 Derivatives of reflectance

Derivatives of reflectance with respect to the fit parameters are used to find the solution in an iterative manner (see Eq. 8) and to determine the a posteriori error covariance matrix (see Eq. 6 below). In DISAMAR, special attention is given to the derivatives. All derivatives, except those for wavelength calibration, are calculated in a semi-analytical manner using reciprocity (equivalent to the adjoint method; e.g. [35]). Such an approach is preferred over numerical techniques (e.g. finite-difference methods), because derivatives can be calculated much faster and much more accurately. Detailed expressions for various specific derivatives are discussed in [RD9].

It seems particularly important for the Aerosol Layer Height retrieval algorithm to have accurate derivatives. For example, both aerosol optical thickness and surface albedo are fit parameters. Errors of these parameters are typically highly correlated. The correlation coefficient can be well above 0.9. Hence, the effect of inaccurate derivatives on the stability of retrieval may be large, because convergence becomes problematic in case of highly correlated fit parameters.

5.2.3 The Neural Network forward model

In total, 3980 absorption lines have been identified in the oxygen A band to retrieve ALH with sufficient accuracy. Line-by-line (LBL) monochromatic calculation of TOA reflectance, and its derivatives with respect to z_p and τ, on such a high resolution wavelength grid requires approximately 20–30 seconds to complete on a computer equipped with Intel®Xeon®CPU E3-1275 v5 at a clock speed of 3.60 GHz. In an iterative (OE) framework, the retrieval of z_p takes between 3–6 iterations, depending on the amount of aerosol information available in the observed spectra, which controls the derivatives that drive the OE. With a monochromatic forward RTM this would mean a severe limitation of the number of processable pixels, since the computation time for one pixel is very much larger than the measurement time. E.g. for the TROPOMI ALH processor, a time frame of approximately half an hour is available to process a number of 1.4 million spectra. Obviously, LBL computations are unsuitable for the necessary high-speed processing of spectra. To reduce the computational time required for retrieving z_p, a neural network forward model was implemented to predict the radiances and derivatives in the forward model step.

A neural network (NN) model was trained using the Tensorflow™ module developed at Google®[ER1]. The choice for using Tensorflow™ is based on its simplicity in training the neural network model, and building it into operational level-2 processors. The standard architecture of the NN-augmented operational ALH processor includes three types of NN models, one estimating the top of atmosphere sun-normalised radiance, and two estimating the derivatives of the reflectance with respect to z_aer (in hPa^{-1}), and τ. All three neural network models share the same input model parameters, listed in Table 1. Where the parameter is part of the NN feature space, the parameters is listed in the so-called feature vector, while parameters that are constant for all NN trainings are called fixed. E.g. aerosol fraction is set to 1.0 for the entire NN space, since pixels are assumed to be cloud-free and entirely aerosol-filled. Typical parameters to vary are the solar-satellite geometry, meteorological and surface parameters, which should span all possibilities that are encountered in the measurements as best as possible. Since the various aerosol parameters (the aerosol single scattering

albedo, scattering phase function, asymmetry factor and Ångström exponent), are fixed in the operational ALH retrieval algorithm, they are fixed in the NN training as well.

Generally, the required training data size increases with increasing non-linearity between input an output layers in a neural network. Once the input model parameters in Table 1 have been gathered, the RTM calculates TOA sun-normalised radiance and the derivative of reflectance with respect to aerosol and surface parameters. This is, by far, the most time consuming step, since each model run requires LBL computations. For TROPOMI, by trial and error, a training set of 500,000 samples was found to produce sufficiently accurate results. The solar-satellite geometry for this training set was determined from a random S5P orbit, the meteorological parameters were derived from the 2017 60-layer ERA-Interim Reanalysis data [RD10], and aerosol and surface parameters were generated randomly.

There are 5 NN models for ALH, all consisting of 4 files, with a total size of 9.1Mb.

5.2.4 NN configuration and training

To train the NN and to test the training, the generated spectra were randomly split in a 0.85:0.15 ratio. One part was used to the train the NN, while the other part was used to test the trained NN. In Figure 4 an example of a LBL-generated and an NN-generated Sun-normalised radiance spectrum is shown.

The RTM-calculated and convolved reflectances are fitted to the measured reflectances (Equation 3) using an optimal estimation scheme. The influence of the atmosphere on the TOA reflectance is characterised using an atmosphere-surface model, consisting of, at least, these relevant components: (1) surface reflectance, (2) surface pressure, (3) fluorescence emission, (4) temperature profile, (5) aerosol model, (6) aerosol profile, and (7) oxygen absorption.

5.2.4.1 High-resolution solar irradiance model

The solar irradiance spectrum is based on [RD11]. The near-infrared wavelength region of this spectrum has a full width at half maximum (FWHM) of 0.04 nm and is oversampled by a factor of four, while the rest of the spectrum is equal to the high-resolution solar reference spectrum described in [RD11]. Differences between the two spectra in the ALH fit window are less than 0.2%.

Table 1: Scene-dependent input model parameters for the NN model.

Parameter class	**Model Parameters**	**Remarks**	limits
Geometry	Solar zenith angle (θ_0)	feature vector	0–75°
	Solar azimuth angle (ϕ_0)	feature vector	-180–180°
	Viewing zenith angle (θ)	feature vector	full swath
	Viewing azimuth angle (ϕ)	feature vector	-180–180°
Aerosol parameters	Aerosol fraction	fixed	1.0
	Single scattering albedo (ω)	fixed	0.95
	Aerosol optical thickness (τ)	feature vector	0.0–15.0
	Aerosol mid pressure (p_{mid})	feature vector	100–1020 hPa
	Aerosol layer thickness (p_{thick})	fixed	50 hPa
	Scattering phase function	fixed	Henyey-Greenstein
	asymmetry factor (g)	fixed	0.7
	Ångström exponent (Å)	fixed	0.0
Meteorological parameters	Temperature	feature vector	temperature at z_{p}
Surface parameters	Surface pressure (p_s)	feature vector	520–1048.5 hPa
	Surface reflectance model	LER	
	Surface albedo (A_s)	feature vector	$2.0 \cdot 10^{-7}$ – 0.70

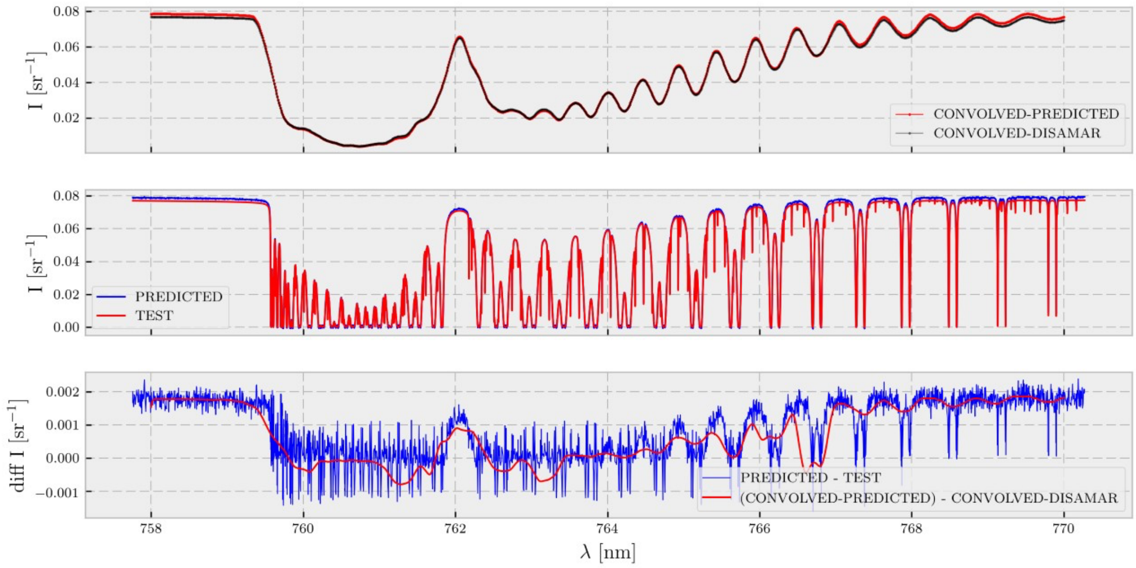

Figure 4: Example of the Sun-normalised radiance spectrum in the Oxygen-A band as computed by the RTM and by the NN model. The top panel shows the spectra after convolution with the S5P slit function, the middle panel shows a comparison between the high resolution spectra, and the bottom show the difference between the LBL and NN spectra, for the high resolution and convoluted spectra.

5.2.4.2 Wavelength calibration

Since the ALH algorithm relies heavily on the correct placement of absorption lines, and shifts of 0.002 nm already yield a strong degradation of the end result, both the irradiance and radiance wavelength grids will be fitted to Fraunhofer lines in the 758–770 nm wavelength range. The Aerosol Layer Height algorithm focuses on cloud-free scenes, and wavelength offsets due to inhomogeneous illumination of the slit from clouds in the field of view can be expected to be minimal. Therefore, a wavelength calibration, which is normally non-linear [RD12], can be kept linear for the ALH algorithm, using a wavelength offset $\delta\lambda$ only, in a fit window between 758 and 770 nm. Changes due to ozone absorption can be ignored.

The offsets $\delta\lambda$ are determined using an optimal estimation fit, starting with a shift of zero. The shift is at most one third of the spacing of the wavelength grid.

The wavelength calibration has to be performed before the optimal estimation is started, because the forward model expects calibrated radiances and irradiances.

5.2.4.3 Surface reflection

The ground surface is modeled as an isotropically reflecting (Lambertian) surface. The surface albedo is specified at a number of wavelength nodes and polynomial interpolation is used to calculate intermediate values. Spectral variation in the reflectivity of the ground surface across the O_2 A band is expected for vegetated land and deserts [31]. In the forward model, we assume a linear wavelength dependence of the surface albedo to account for this variation. Hence, the albedo is specified at two wavelength nodes (the edges of the fit window at 758 and 770 nm) and other values are found by linear interpolation.

A priori values are taken from a surface albedo climatology, such as the MERIS black-sky albedo (BSA) climatology [42] or the SCIAMACHY Lambertian-equivalent reflectivity (LER) climatology [ER2]. Particularly over land, climatological albedo values may sometimes be inaccurate, which would then lead to biased or non-convergent retrievals (Section 8.5).

Our experience with retrievals using GOME-2 and SCIAMACHY spectra suggests that the Lambertian surface reflectance model is sufficient for our purposes. Currently, the GOME-2 LER datavbase is used. However, the impact of BRF effects may be more pronounced for the substantially smaller TROPOMI ground pixel. Nadir pixel sizes are 40 km x 80 km for GOME-2, 30 km x 30/60 km for SCIAMACHY and 3.5 km x 5.6 km for TROPOMI. Future sensitivity studies should estimate the impact of BRF effects for different surface types on retrieval of Aerosol Layer Height. When the TROPOMI LER and DLER databases become available, they may be implemented in the ALH retrieval, and fitting of the surface albedo may also be attempted.

5.2.4.4 Surface pressure

Accurate surface pressures are needed, as they determine the oxygen column. We use surface pressures from the same ECMWF fields as the temperature profiles. The error analysis of Section 8.7.2 indicates that surface pressures on a 1° by 1° grid, possibly interpolated in space and time to the satellite observation are sufficient, although a finer spatial grid is preferable. There are methods to convert surface pressures on an ECMWF spatial grid to surface pressures on an even finer grid using a digital elevation model (e.g. [67]). This would be appropriate for mountainous areas. To compensate for remaining errors in the surface pressure, it may be needed to fit the surface pressure with appropriate a priori errors but this is currently not foreseen.

5.2.4.5 Temperature profiles

Accurate temperature profiles are needed for retrieval, because of the temperature and pressure dependence of oxygen absorption. We use temperature profiles that are made available through the European Centre for Medium-Range Weather Forecasts (ECMWF). Based on the error analysis of Section 8.7.1, we estimate that profiles on a 1° by 1° spatial grid, possibly interpolated in space and time to the satellite observation, are sufficient for our purposes. To compensate for remaining errors in the temperature profile, it may be needed to fit the temperature profile (or perhaps only a temperature offset) with appropriate a priori errors. The error analysis of Section 8.7.1 shows that aerosol parameters and the temperature profile can be simultaneously retrieved for expected a priori errors in ECMWF profiles.

5.2.4.6 Aerosol model

An aerosol layer is modeled as a layer of particles with an associated aerosol optical thickness (τ_0). The ratio of scattering and absorption is controlled by the single scattering albedo (ω_0). The phase function $P(\theta)$ describes the angular distribution of scattered light. We have very limited prior knowledge of the aerosol type available: even aerosol climatologies are not sufficient, since these typically miss distinct aerosol episodes, such as volcanic ash plumes. The operational algorithm therefore initially assumes a single, average aerosol model. For example, we may assume the aerosol to have a fixed single scattering albedo of 0.95 and a fixed phase function that is given by a Henyey-Greenstein (HG) function with asymmetry parameter of 0.7. These are average values for the single scattering albedo and asymmetry parameter in this wavelength range for all main aerosol types as found in long-term Aerosol Robotic Network (AERONET) observations by Dubovik et al. (2002)[15]. The Henyey-Greenstein function is given by

$$P_{HG} = \frac{1-g^2}{(1+g^2-2g\cos\theta)^{3/2}} \tag{4}$$

where g is the asymmetry parameter and θ the scattering angle.

The error analyses in Section 8.4 show that if the assumed aerosol model deviates from the true aerosol type, biases in retrieved aerosol pressure generally remain relatively small, particularly when the surface albedo is a fit parameter. Retrieved aerosol optical thickness and surface albedo, however, show significant biases in response to model biases in single scattering albedo and phase function. Retrieved values for these two parameters should therefore be understood as effective quantities. Aerosol Layer Height retrievals with GOME-2 and SCIAMACHY spectra [49] confirm that the particular choice of the aerosol model is not that critical, even when the surface albedo is fixed in retrieval. We remark that we assume the single scattering albedo, phase function and optical thickness (extinction cross section) to be independent of wavelength across the fit window (758 - 770 nm). The optical thickness that we retrieve holds for wavelengths at the O_2 A band and is denoted by τ_0 (760 nm) or occasionally as τ_0(O_2 A).

5.2.4.7 Aerosol profile

Although the O_2 A band is a strong line absorption spectrum that spans a large range of absorption optical thicknesses, it contains limited aerosol profile information (e.g. [22]; [53]; [9]; cf. [11]). Since we are developing an operational algorithm, we retrieve only a single profile parameter in the baseline implementation. If the algorithm proves to be robust enough, we may consider retrieving additional profile parameters in the future. Note that current operational O_2 A band cloud algorithms also retrieve just a single (cloud) height parameter (e.g. FRESCO and SACURA).

Hence, it is not useful to specify an extinction profile at a large number of pressure levels, as is often done for trace gases. We prefer instead a simple profile parameterization in which aerosols are uniformly distributed

in a single atmospheric layer. In DISAMAR's forward model, the atmosphere is divided into a small number of pressure intervals that do not overlap. These intervals may be aerosol-free and cloud-free, or contain aerosol or clouds with a certain aerosol / cloud fraction. Aerosol or cloud properties of only one atmospheric interval can be fitted. Below we will describe the parameterizations of the aerosol profile and associated fit parameters.

5.2.4.8 Oxygen absorption cross section

A study by De Haan [RD13] has shown that using O_2 line parameters from the most recent HITRAN database [ER3] and assuming a simple Voigt profile for the shape of the absorption line is not sufficient for a reasonably accurate retrieval of aerosol properties. The most prominent issues concern inclusion of line mixing (LM) and collision-induced absorption (CIA) into the absorption cross section. Sensitivity analyses in [RD13] show that ignoring LM and CIA leads to significant biases in retrieval of aerosol properties, much more than in retrieval of cloud properties.

At present, DISAMAR includes first-order line mixing and collision-induced absorption by O_2-O_2 and O_2-N_2 according to [57] and [58]. We mention that HITRAN data currently available for CIA by these two collision complexes are indeed based on Tran et al. (2006) [57]. As a minor remark, we note that for the O_2 A band, we have replaced the HITRAN 2008 database by a database from Jet Propulsion Laboratory (JPL), because there are indications that line parameters in the JPL database are slightly more accurate [58]. The JPL database was part of a code that was kindly provided by J.-M. Hartmann.

Based on data published in Tran and Hartmann (2008) [58], De Haan [RD13] estimates the uncertainty in the improved model for collision-induced absorption and line mixing to be of the order of 20%. He shows that significant biases in retrieved aerosol height remain in that case for optically thin aerosol layers close to the surface. For example, an aerosol layer with τ_0 of 0.2 at 850 hPa over vegetated land shows a bias of approximately 100 hPa, while retrieval for layers closer to the surface does not converge. Hence, it is recommended that an effort is made to obtain more accurate data on O_2 line mixing and collision-induced absorption for atmospheric retrievals. In Section 9, we further investigate the effect of spectroscopic uncertainties on retrieval of aerosol height.

5.2.4.9 Instrument model

The instrument model for retrieval contains radiance and irradiance slit functions for the convolution of high-resolution radiance spectra, irradiance spectra and derivatives. Furthermore, it contains various instrumental effects that can be applied to the (ir)radiance spectra. We mention two effects that are important for the O_2 A band algorithm. First, we known that stray light can bias retrieval of aerosol / cloud properties from the O_2 A band (Section 8.11.1), because of the low signal inside the absorption band. It may be necessary to fit stray light parameters to account for any stray light that remains after the default corrections in the Level-1b processor have been performed. However, in the GOME-2 and SCIAMACHY case studies [49] fitting stray light did not improve the retrieval in a convincing way and therefore in the baseline setup for these retrievals stray light was excluded from the state vector. Second, the Level-1b processor performs the wavelength calibration of the irradiance but for the radiance only a wavelength assignment is done. The wavelength calibration for the radiance spectra is part of the Level-2 processor and is performed in a separate step before the main Level-2 retrievals take place. The wavelength calibration uses strong Fraunhofer lines and for the calibration of O_2 A band spectra Fraunhofer lines to the shorter wavelength end of the band are used [RD14]. These wavelength calibrations are essential for the correc retrieval of the ALH using the absorption lines in the O_2 A band.

6 Algorithm description: Retrieval method

This section provides a description of the retrieval method for the Aerosol Layer Height retrieval algorithm and it discusses *a priori* information for its main fit parameters.

6.1 Optimal Estimation

We take a Bayesian approach to the inverse problem and follow the formulation by Rodgers (2000)[44], which is conventionally referred to as Optimal Estimation. The implementation of Optimal Estimation in DISAMAR is described in [RD9]. We briefly discuss key aspects of the retrieval method.

Optimal Estimation is a form of regularization that constrains the least-squares solution by a priori knowledge. The cost function that is minimized is given by

$$\chi^2 = [\mathbf{y} - \mathbf{F}(\mathbf{x},\mathbf{b})]^T \mathbf{S}_\varepsilon{}^{-1} [\mathbf{y} - \mathbf{F}(\mathbf{x},\mathbf{b})] + (\mathbf{x} - \mathbf{x_a})^T \mathbf{S_a}{}^{-1} (\mathbf{x} - \mathbf{x_a}), \tag{5}$$

where $\mathbf{y}$ is the vector of measured reflectance, which contains values for the different wavelengths; $\mathbf{F}(\mathbf{x},\mathbf{b})$ is the vector of calculated reflectances, which is also called the forward model; $\mathbf{x}$ is the state vector containing the parameters that are fitted; $\mathbf{b}$ is the vector containing the model parameters; is the error covariance matrix of the measurement; $\mathbf{x_a}$ is the a priori state vector; and $\mathbf{S_a}$ is the error covariance matrix associated with the a priori state vector. One can recognize the familiar weighted least-squares solution in the first part and the a priori constraint in the second part of the cost function. The rationale and derivation of the cost function is given in Rodgers (2000)[44].

An important advantage of the Optimal Estimation formalism is that it provides a proper error analysis. Minimization of χ^2 gives the retrieved state vector : the associated (a posteriori) error covariance matrix is given by

$$\hat{\mathbf{S}} = (\mathbf{K}^T \mathbf{S}_\varepsilon \mathbf{K} + \mathbf{S_a}{}^{-1})^{-1}. \tag{6}$$

where $\mathbf{K}$ is the matrix of derivatives (evaluated at in Eq. 5),

$$K_{ij} = \frac{dF_i}{dx_j}. \tag{7}$$

Note that matrix $\mathbf{K}$ provides the derivatives of measured reflectance, i.e. high-resolution derivatives after appropriate convolution with the slit functions. For other diagnostic information that can be used to interpret the retrieval result we refer the reader to [44].

Generally, the forward model is non-linear so that minimization of the cost function has to be solved in an iterative manner. The standard implementation in DISAMAR uses the Gauss-Newton method. The update of the state vector during iteration is given by

$$\mathbf{x}_{n+1} = \mathbf{x_a} + (\mathbf{K_n}{}^T \mathbf{S}_\varepsilon{}^{-1} \mathbf{K_n} + \mathbf{S_a}{}^{-1})^{-1} \mathbf{K_n}{}^T \mathbf{S}_\varepsilon{}^{-1} [\mathbf{y} - \mathbf{F}(\mathbf{x_n}) + \mathbf{K_n}(\mathbf{x_n} - \mathbf{x_a})], \tag{8}$$

where $\mathbf{x_n}$ are subsequent iterates of the state vector or linearization points of the forward model. Hence, $\mathbf{K_n}$ is the derivative matrix evaluated at $\mathbf{x_n}$. In some cases exceptions are made. For example, when the change in the state vector is very large, the update is reduced. Also, if elements of the state vector are assigned non-physical values (e.g. negative surface albedo) they are reset to physical values. The iteration is typically started with $\mathbf{x_1} = \mathbf{x_a}$.

A χ^2-minimum has been found and the fit has converged if during iteration the state vector's update is small compared to the expected precision. An appropriate measure for the size of the update is

$$d_n^2 = (\mathbf{x_{n+1}} - \mathbf{x_n})^T \mathbf{S_n}{}^{-1} (\mathbf{x_{n+1}} - \mathbf{x_n}), \tag{9}$$

where is $\mathbf{S_n}$ the *a posteriori* covariance matrix for the n^{th} iteration. If $d_n{}^2$ becomes smaller than a predefined threshold, iteration is stopped, and $\mathbf{x_{n+1}}$ and $\mathbf{S_n}$ become $\hat{\mathbf{x}}$ and $\hat{\mathbf{S}}$, respectively. The convergence criterion is typically equal to the number of state vector elements *m*. It is important to note here that a convergence test only ensures that a local minimum has been reached. It does not ensure that the minimum is actually the correct solution (global minimum). A test for convergence should therefore be supplemented by an evaluation of the actual value of χ^2 (a high value would indicate a non-global minimum), inspection of the residue spectrum or a check of the consistency of retrieval results with neighbor pixels.

Within the TROPOMI Level-1b team, an effort is currently being made to supply the future (ir)radiance products with accurate estimates of calibration errors, which can then be included in the measurement error

covariance matrix . Accurate derivatives (Eq. 7) and accurate estimates of the measurement error will improve convergence (Eq. 8) and estimates of the a posteriori error covariance matrix (Eq. 6).

6.2 State vector elements and *a priori* information

In the current implementation of the Aerosol Layer Height retrieval algorithm, the state vector contains the elements printed in bold in Table 2. Other parameters given in Table 2 may be added to improve the retrieval, as they influence the accuracy of the ALH. We have also indicated typical *a priori* values and errors, however, implementatin is not currently foreseen.

Table 2: State vector elements and typical a priori values and errors for the Aerosol Layer Height retrieval algorithm. In the current implementation, the state vector contains the parameters printed in bold. For an explanation, see text.

State vector element	*a priori value*	*a priori* error (1σ)	Remark
Aerosol mid pressure $\boldsymbol{p}_{\mathrm{mid}}$	800 hPa	500 hPa	Alternative profile parameterizations (5.3.8) are optional.
Aerosol optical thickness (τ_0)	0.2	1.0	At 760 nm
Surface albedo (A_s) at 758 nm Surface albedo (A_s) at 770 nm	climatology	0.2	GOME-2 LER
Surface pressure (p_s)	ECMWF	3 hPa	
Temperature offset ΔT	0 K	3 K	Offset to the *a priori* ECMWF temperature profile
Fluorescence emission (F_s) at 758 nm Fluorescence emission (F_s) at 770 nm	0.0 0.0	$1.0 \cdot 10^{12}$ ph. cm^{-2} s^{-1} nm^{-1} sr^{-1} $1.0 \cdot 10^{12}$ ph. cm^{-2} s^{-1} nm^{-1} sr^{-1}	Over vegetated land only.
Stray light	0%	1%	Additive radiance offset defined as a percentage of the radiance at 758 nm

The main fit parameters are the aerosol layer's mid pressure and optical thickness. A priori values and errors are such that the range of realistic values for these parameters is covered. Currently the assumed pressure thickness of the aerosol layer is 50 hPa. The optical thickness is retrieved for wavelengths of the O_2 A band and it is assumed wavelength independent across the spectral window. Alternative profile parameterizations and corresponding fit parameters are discussed in Section 6.2.2.

The surface albedo at two wavelength nodes may be retrieved but this is currently not foreseen. A priori Lambertian-equivalent reflectivities are taken from the GOME-2 climatology [31]. Climatological values at two channels near the O_2 A band (around 754 and 775 nm) are available, which are used as a priori values for the surface albedo at 758 nm and 770 nm. Because of the very large GOME pixel size, scenes identified as cloud-free in the histogram analysis of [31] may still contain clouds. Recently, a Lambertian-equivalent reflectivity climatology from SCIAMACHY has become available. Because of smaller ground pixel sizes (over sea) and better instrument calibration, this climatology may be more accurate.

Other fit parameters are surface pressure and an offset to the a priori temperature profile. A priori values are provided by ECMWF as described in Section 5.3. We set an a priori error on the surface pressure in agreement with Salstein et al. (2008) [46] who report an rms error in 1° by 1° ECMWF surface pressures of 2–3 hPa. The a priori error in the temperature offset is 3 K. Fluorescence emissions at two wavelength nodes can be fitted for retrievals over land. *A priori* we assume zeros emissions. The *a priori* error covers the range of realistic fluorescence values (e.g. [21]; [17]). Finally, also an additive radiance offset (stray light) can be fitted.

6.2.1 Height variable

Pressure is taken as the independent height variable. Assuming hydrostatic equilibrium and given a temperature profile, the pressure grid can be converted into an altitude grid (in km). As a consequence, an atmospheric

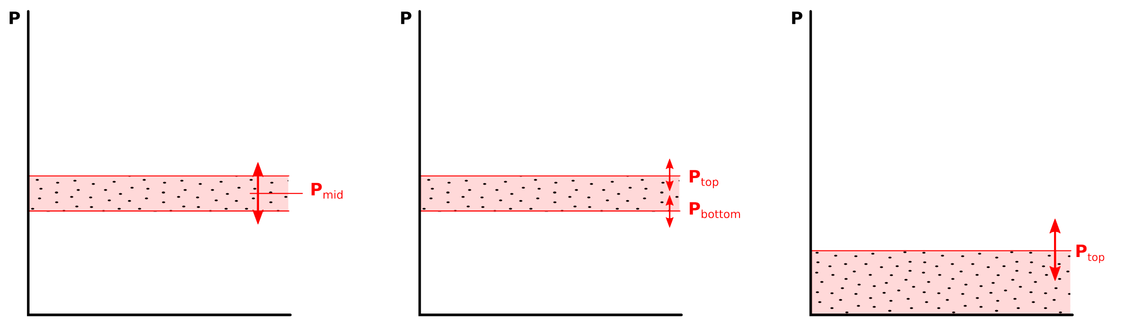

Figure 5: Aerosol profile parameterizations for the TROPOMI Aerosol Layer Height product. (A) The baseline profile parameterization assumes an elevated layer with a fixed pressure difference between top and bottom of the layer. The layer's mid pressure is retrieved. (B) If the aerosol optical thickness is large enough, it will perhaps be possible to simultaneously fit the top and bottom pressure. (C) An alternative parameterization that might be used, depending on the aerosol case, assumes an aerosol layer extending down to the ground. The layer's top pressure is retrieved.

layer (e.g. an aerosol layer) with a fixed pressure thickness has different geometric thicknesses as a function of pressure and temperature.

The TROPOMI Level-2 processor ingests quite accurate meteorological data. If the temperature profile or an offset is fitted (Section 5.2.4.5), we still suggest using the a priori temperature profile, rather than the retrieved temperature profile, to convert retrieved aerosol pressures into retrieved aerosol altitudes. In our GOME-2 and SCIAMACHY retrievals, we found that fitting a temperature offset can result in large offset values, which are probably related to model errors other than errors in meteorological data. For example, we see that fitting a temperature offset helps to reduce residuals caused by spectral calibration errors. The a priori temperature profile therefore probably represents actual meteorological conditions better than the retrieved profile. We recall that retrieved layer mid pressure is always calculated as the sum of top pressure and bottom pressure divided by two. This layer mid pressure is then converted into a layer mid altitude using the a priori meteorological temperature profile.

6.2.2 Profile parameterization

In the baseline algorithm, we assume that the aerosols are uniformly distributed in a single layer with a fixed pressure difference between top and bottom of the layer, a constant aerosol volume extinction coefficient and aerosol single scattering albedo, and an aerosol fraction of one (Figure 5A). The pressure of the interval is retrieved keeping the pressure thickness constant. The reported pressure is the layer's mid pressure (mean of the top and bottom pressure). Without further clarification, the term aerosol pressure will always refer to the layer's mid pressure. The optimal pressure thickness will be determined in future investigations.

If the aerosol optical thickness is large enough, it will perhaps be possible to simultaneously fit top and bottom pressure (Figure 5B), in which case we are effectively retrieving the pressure thickness of the layer in addition to the mid pressure. Section 8.8 provides a sensitivity analysis for this profile parameterization. Alternatively, we may assume that aerosols are uniformly distributed in an atmospheric interval that extends down to the ground surface with an aerosol fraction of one (Figure 5C), in which case the algorithm would retrieve the top pressure of the interval. We will implement this alternative parameterization in the Level-2 processor as an option to the baseline algorithm. Finally, we mention that it is possible to put aerosols or clouds in other atmospheric intervals too, although we can fit properties of only a single target interval. This option may help to account for example for background sea salt near the ocean surface or residual cirrus at high altitude.

6.3 Convergence of retrieval and uniqueness of solution

During numerical experiments (see also Section 8.3), we found that the cost function may sometimes be relatively flat or even have more than one local minimum (cf. Hollstein et al., 2012 [24], figure 19). If the cost function exhibits multiple minima, the solution obtained depends on the initial values and might be a wrong local

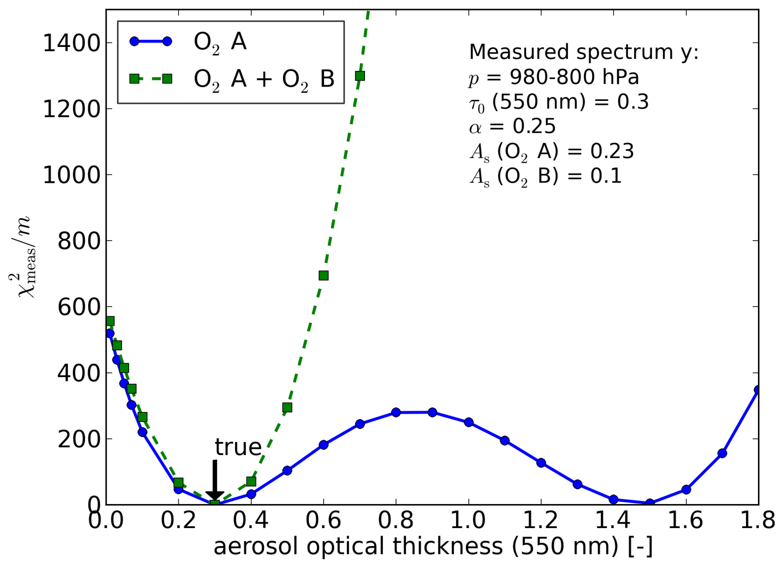

Figure 6: χ^2 of the (simulated) measurement (first term of Eq. 5) for an aerosol layer between 980 and 800 hPa with optical thickness of 0.3 at 550 nm over vegetated land. The measurement vector **y** includes the O_2 A band, or the O_2 A and B bands. Note that the surface is much brighter in the O_2 A band. The modeled spectrum **F**(**x**) differs from the measurement with respect to optical thickness. One can clearly see multiple minima in the cost function if only the O_2 A band is taken into account.

minimum. Also, convergence for our GOME-2 retrievals sometimes depended on the initial values. However, in many cases stable convergence to the correct solution was found.

If finding an incorrect local χ^2-minimum or non-convergence becomes a problem, steps will be taken to use different initial values (multiple runs) or improve convergence. A sensitivity analysis indicated that the convergence rate improves if we assume in retrieval purely scattering aerosols (as opposed to partly absorbing aerosol, e.g. SSA of 0.95). Local χ^2-minima, particularly for land scenes, may be removed by including the O_2 B band in the measurement vector (Figure 6).

7 Feasibility

7.1 Estimated Computational Effort

A test was performed to assess the computation time spent by the ALH processor with a NN implemented in the forward model, using one day of TROPOMI data, shown in Fig. 7. On this day a severe dust storm can be found over the Atlantic Ocean, producing a large number of pixels with sufficiently high TROPOMI AAI. Furthermore, more high AAI hotspots can be identified around the globe. This means many pixels have to processed by the AER_LH processor during this day, which can be considered a normal, but more than average load for the ALH processor.

The result of the test run is shown in the bottom panel of Fig. 7. All pixels with an AAI $>$ 0.4 and FRESCO cloud fraction CF$<$ 0.8 were processed. As the figure shows, a large number of pixels were (successfully) processed by the processor. Table 3 shows the number of pixels selected, processed and failed. It also shows the time spent by the processor. The processor was run on 36 cores. The Total time is the total time spent by the processors on one orbit, the Processing time is the time spent on processing the selected pixels, and the difference is the time spent on initialisation, pixel selection, and writing of the files.

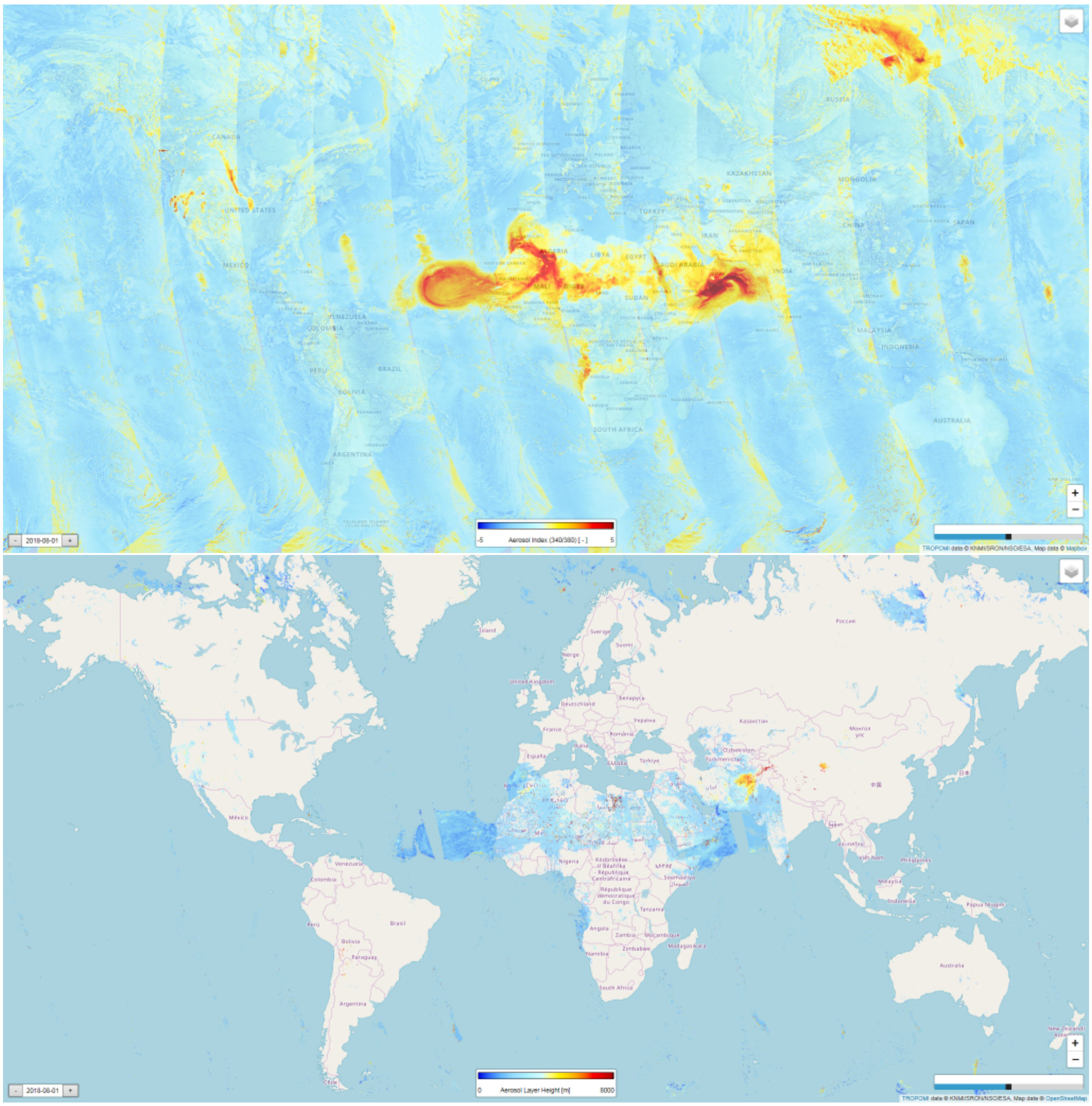

Figure 7: Top panel: TROPOMI AAI on 1 August 2018 showing a large aerosol (dust) plume over the Atlantic Ocean originating from the Sahara, and several other hotspots of high AAI from smoke and dust. Bottom panel: TROPOMI AER_LH retrieval results from an initial test run of the ALH processor with NN implemented in the forward model.

Table 3: Statistics of the NN AER_LH processing of 1 August 2018 measurements.

Orbit	total # pixels	selected pixels	successfull pixels #	successfull pixels %	Not Con-verged	Total time [s]	Processing Time [s]	Δ [s]
4138	1301888	4645	4378	94.3	267	511	79	432
4139	1453760	7489	7322	97.8	167	562	104	458
4140	1453760	5322	4973	93.4	349	533	68	465
4141	1453760	8874	8725	98.3	149	449	87	362
4142	1453760	129198	125819	97.4	3379	1660	1295	365
4143	1453760	112009	102422	91.4	9587	2263	1720	543
4144	1454280	107077	83318	77.8	23764	2595	2063	532
4145	1453760	124462	106657	85.7	17805	3050	2450	600
4146	1453760	69804	69502	99.6	302	1414	879	535
4147	1454280	7792	7472	95.9	320	442	93	349
4148	1453760	5479	5008	91.4	471	418	70	348
4149	1453760	17080	16761	98.1	319	512	154	358
4150	1453760	3749	3488	93.0	261	395	46	349
Day	18,748,048	602,980	545,845	90.5	57,140	14804 4h 6’44"	9108 2h31’48"	5696 1h34’56"

System: HP Blade Server
CPU: 2 AMD Opteron^{TM} Processor 6376 (2.3GHz,16 core), total 32 cores [ER4]
Memory: 128 GB memory
OS: Red Hat Enterprise Linux Server release 7.3 (Maipo)
Kernel: 3.10.0-514.10.2.el7.x86_64

7.2 Timeliness

The Aerosol Layer Height product has a near real-time requirement. With the test above the average time spend per pixel in a normal day can be estimated. 32% of the pixels were selected for processing this day, with the setting used, and selecting them (and including other overhead), took one and a half hour on 32 cores,

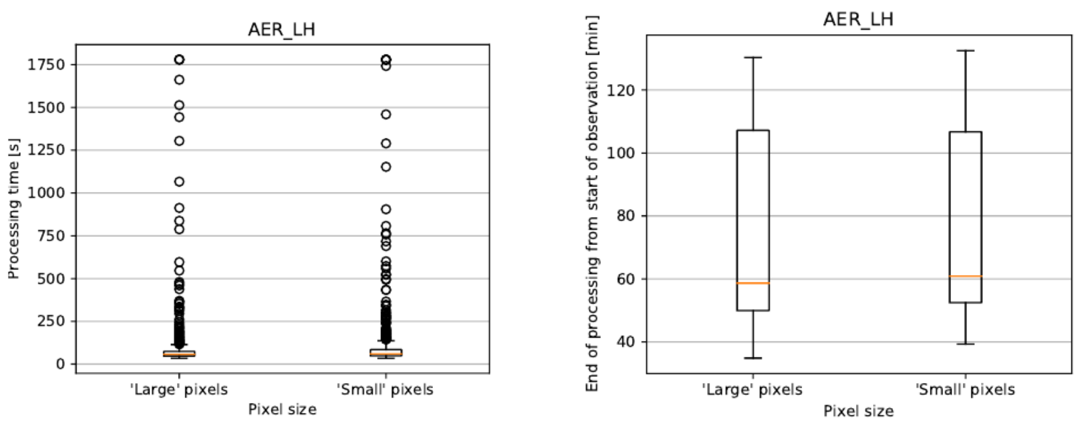

Figure 8: Timeliness of the AER_LH processor. The upper panel shows the processing time per near-real time granule. The bottom panel shows the timeliness of the end of the processing time. ‘Large’ pixels refer to pixels with an integration time of 1080 ms, yielding pixel sizes of 7×7 km^2 at nadir, ‘small’ pixels refer to an integration time of 840 ms, yielding pixel sizes of about 7×5.6 km^2.

which is 38.5% of the total time spent. 90.5% of the selected pixels were succesfully processed (actually yielding an ALH), and only 9.5% failed due to retrieval error or warnings. The total time spent on the retrieval was about 4 hours, which yields an average processing time (of the entire day) of 0.0246 s per selected pixel, with 32 parallel processors. This includes initialisation, and also the non-successful pixels, which take longer to process on average, since non-convergence pixel take at most 12 iterations before they are excluded, while successful pixels can converge to an answer in 3-4 iterations.

The timeliness was tested for AER_LH for two periods: from 2019-08-04 00:04:19 UTC, orbit 9358 to 2019-08-06 01:59:19 UTC, orbit 9387, and from 2019-08-06 02:39:29 UTC, orbit 9388, to 2019-08-08 07:46:09 UTC, orbit 9419. The first period consists of 375 near-real time granules and the second period consists of 372 granules. The two periods mark the change of TROPOMI footprint sizes from 7×7 km^2 to 7×5.6 km^2. Between these periods a transition in the operational settings to a shorter integration time (IT), from 1080 ms to 840 ms, of the TROPOMI measurements was implemented. The total processing time and the processing time per pixel were recorded during both periods and compared. Timeliness for all products are described in [55]. Figure 8 shows the results for AER_LH. No violations of the three hour near-real time timeliness were recorded for AER_LH for either 'large' pixels (1080 ms IT) and 'small' pixels (840 ms IT).

The timeliness of AER_LH is strongly dependent on the number of selected pixels. At present only scenes with strongly UV-absorbing aerosols are selected, and the processor is fast enough to process all pixels well within the set period of three hours. This allows the relaxation of the pixel selection, to also include scattering aerosols, provided that suitable selection criteria can be found to include these.

7.3 Input data for the Aerosol Layer Height algorithm

7.3.1 TROPOMI Level-1b

The following Level-1b data are needed for the Aerosol Layer Height algorithm (Table 4):

Table 4: TROPOMI Level-1b input data.

Name/Data	Symbol	Unit	Pre-process needs	Backup if not available	Comments
Radiance data for band 6	I	mol s^{-1} m^{-2} nm^{-1} sr^{-1}	Per 3.5 km x 5.6 km nadir ground pixel.	No retrieval.	The O_2 A band is contained in band 6; product includes geolocation data.
Irradiance data	E_0	mol s^{-1} m^{-2} nm^{-1}	-	Use previous measurement.	-
Small-pixel column radiance data for band 6	I	mol s^{-1} m^{-2} nm^{-1} sr^{-1}	-	Skip cloud test that uses small-pixel column data.	So-called small-pixel column radiance data are used in the near real-time cloud mask (see Section 5.1).
Radiance data for band 4	I	mol s^{-1} m^{-2} nm^{-1} sr^{-1}	-	Skip cloud test that uses band 4 radiance data.	Radiances in the visible wavelength range are used in the near real-time cloud mask (see Section 5.1).

Finally, we foresee that at a later stage we might want to include the O_2 B band as an option to the baseline algorithm. The O_2 B band is included in Level-1b data for spectral band 5.

7.3.2 Dynamic input

Dynamic input data are discussed in Section 5.1 and Section 5.2. Dynamic input for off-line processing and reprocessing modes is summarized in Table 5.

Table 5: Dynamic input data for off-line processing and reprocessing.

Name/Data	Symbol	Unit	Source	Pre-process needs	Backup if not available	Comments
Temperature profiles	$T(p_i)$	K	ECMWF (forecast fields)	Interpolation towards TROPOMI ground pixel	Temperature profiles from TOMS version 8 ozone climatology (static).	Temporal resolution: 3-hour intervals (forecast fields). Spatial resolution: 1° by 1° or finer.
Surface pressures	p_s	Pa	ECMWF (forecast fields)	Interpolation towards TROPOMI ground pixel: e.g. linear (temporal) and nearest-neighbor (spatial).	Assume 1013 hPa at sea level; use digital elevation model and scale factor of 8.3 km to calculate surface pressure for elevated scenes.	Temporal resolution: 3-hour intervals (forecast fields). Spatial resolution: 1° by 1°, preferably finer.
Snow / ice cover	-	-	NSIDC or ECMWF	Collocation with TROPOMI ground pixel.	GOME-2 LER climatology (static).	Spatial grid comparable to resolution of TROPOMI.
UV Aerosol Index	-	-	TROPOMI Level-2	-	Skip pixel selection step.	UVAI needed for pixel selection.
KNMI Clouds	-	-	TROPOMI Level-2 support	-	Skip pixel selection step.	FRESCO cloud fraction needed for pixel selection.
VIIRS cloud mask	-	-	TROPOMI Level-2 support	-	TROPOMI near real-time cloud mask (Section 5.1).	Cloud mask based on observations with VIIRS, which are regridded to TROPOMI observation grid.

Dynamic input for the near real-time processing mode is summarized in Table6.

Table 6: Dynamic input data for near real-time processing.

Name/Data	Symbol	Unit	Source	Pre-process needs	Backup if not available	Comments
Temperature profiles	$T(p_i)$	K	ECMWF (forecast fields)	Interpolation towards TROPOMI ground pixel: e.g. linear (temporal) and nearest-neighbor (spatial).	Temperature profiles from TOMS version 8 ozone climatology (static).	Temporal resolution: 3-hour intervals (forecast fields).Spatial resolution: 1° by 1° or finer.
Surface pressures	p_s	Pa	ECMWF (forecast fields)	Interpolation towards TROPOMI ground pixel: e.g. linear (temporal) and nearest-neighbor (spatial).	Assume 1013 hPa at sea level; use digital elevation model and scale factor of 8.3 km to calculate surface pressure for elevated scenes.	Temporal resolution: 3-hour intervals (forecast fields). Spatial resolution: 1° by 1°, preferably finer.

Snow / ice cover	-	-	NSIDC or ECMWF	Collocation with TROPOMI ground pixel.	GOME-2 LER climatology (static).	Spatial grid comparable to resolution of TROPOMI.
UV Aerosol Index	-	-	TROPOMI Level-2	-	Skip pixel selection step.	UVAI needed for pixel selection.
KNMI Clouds	-	-	TROPOMI Level-2 support	-	Skip pixel selection step.	FRESCO cloud fraction needed for pixel selection.

7.3.3 Static input

Static input data are discussed in Section 5 and summarized in Table7.

Table 7: Static input data.

Name/Data	Symbol	Unit	Source	Pre-process needs	Comments
GOME-2 LER climatology	A_s	-	[56].	Collocation with TROPOMI ground pixel.	Resolution: monthly, on a 0.25° by 0.25° grid.
O_2 absorption parameters	-	-	Oxygen line parameters according to [57];[58]. This includes line mixing. Collision-induced absorption cross sections for O_2-O_2 and O_2-N_2 from HITRAN [ER3].	Oxygen absorption cross sections are pre-calculated and stored in look-up tables.	-
Surface altitude	z_s	m	GMTED2010[12]; preprocessing according to [RD15].	For TROPOMI ground pixel, calculate mean, standard deviation, maximum and minimum elevation.	A digital elevation model at high spatial resolution.
Slit functions for the radiance and irradiance	-	-	TROPOMI Level-1b product.	-	-
High-resolution solar irradiance spectrum	E_0	mol s^{-1} m^{-2} nm^{-1}	TROPOMI project reference spectrum [RD6] or [RD11].	-	-

7.4 Robustness against instrumental errors

Instrument errors most relevant for the Aerosol Layer Height algorithm are errors related to the Level–1b stray light correction, wavelength calibration and slit function calibration. Section 8.11 provides an error analysis investigating the effects of these instrument errors on retrieval. Biases in retrieved pressure for typical instrument errors can be significant, depending on the scenario. A wavelength calibration for the radiance measurement is not provided by the TROPOMI Level-1b processor, but is part of the Level-2 algorithm. Stray light for the radiance measurement can in principle be fitted, although the result depends on the accuracy of the stray light model.

7.5 Data product description

A single Level-2 file in the off-line processing stream will contain a complete TROPOMI orbit. Such a Level-2 file contains main groups PRODUCT and METADATA. Main data fields (on a pixel level) are stored in the PRODUCT group and its subgroup SUPPORT_DATA. As we will process only a small subset of all pixels (Section 5.1), arrays contain many fill values and compression will thus reduce the file size considerably. The METADATA group contains a subgroup called QA_STATISTICS (quality assurance statistics). Quality assurance statistics and metadata items are data fields on an orbit level. These will contribute little to the overall Level-2 file size. Table8 provides an overview of data fields in the PRODUCT group. More data fields may be added in the course of algorithm development; see also Table 2 for an overview of the state vector elements.

Table 8: Level-2 output data.

Name/Data	**Symbol**	**Unit**	**Description**	**Number of Values**
aerosol_mid_pressure	p_{mid}	Pa	Mid pressure of an aerosol layer with an assumed pressure thickness of (currently) 50 hPa and a constant aerosol volume extinction coefficient and single scattering albedo. Mid pressure is equal to top pressure plus bottom pressure divided by two (Section 5.3.8).	1
aerosol_mid_altitude	z_{mid}	m	Mid altitude is calculated from aerosol mid pressure using the a priori temperature profile (Section 5.3.3).	1
aerosol_optical_thickness	τ_0	-	Aerosol optical thickness of the assumed aerosol layer. The optical thickness holds for 760 nm (Section 5.3.6).	1
surface_albedo	A_s	-	Surface albedo at two wavelength nodes. Polynomial interpolation is used to determine the surface albedo at other wavelengths (e.g. linear wavelength dependence if two nodes are specified, Section 5.3.1).	2
a_posteriori_covariance_-matrix	**S**	<various>	A posteriori covariance matrix of the state vector. Units of matrix elements are derived from units of state vector elements.	*[variable]*
*[variable]*_precision			Precision of *[variable]*.	*[variable]*.
latitude	-	degrees	Latitude of pixel center.	1
longitude	-	degrees	Longitude of pixel center.	1
solar_zenith_angle	-	degrees	-	1
solar_azimuth_angle	-	degrees	-	1
viewing_zenith_angle	-	degrees	-	1
viewing_azimuth_angle	-	degrees	-	1

Data types for all fields are floats. Assuming ~1 042 800 pixels per orbit and 7 state vector elements, the uncompressed size of an ALH Level-2 file for the data fields of Table 8 is ~360 MB. More state vector elements may be added in the course of algorithm development. Since only a small fraction of all pixels is processed, matrix dimensions other than along track and across track pixel should perhaps be considered for storing retrieval results.

8 Error analysis

The purpose of the error analysis is to illustrate the performance of the baseline algorithm. Settings for the radiative transfer calculations are such that the algorithm is accurate. The sensitivity analyses presented in this section thus provide a benchmark against which the performance of future optimizations of the algorithm (e.g. for computational speed) can be compared.

8.1 Performance of the neural network forward model

All the sensitivity studies presented in this section the *f*orward model of simulation steps have been performed using DISAMAR. In the operational processor the *f*orward model of retrieval is performed using the neural network (NN) spectral estimation. In order to assess the accuracy of the NN, and to estimate the representativeness of the error analyses in this section for the operational processor, we start first with an analysis of the NN implementation alone.

In Figure 9 the retrieval of the ALH on 9 November 2018 is shown. It depicts the situation on the west coast of the US, when severe wild fires scourged the surroundings of Paradise, Ca., and large smoke plumes were visible from VIIRS onboard Suomi/NPP, and TROPOMI. In the top-left image the smoke plume is depicted, overlaid with ALH retrievals using line-by-line (LBL) calculation from DISAMAR, which are time-consuming, and therefore not as complete as the ALH retrievals in the top-right picture, which is the same picture overlaid with NN calculation of the ALH. The bottom-left picture shows the difference between the retrievals, while the bottom-right shows a scatterplot of the differences. Clearly, the NN implementation performs very well for this case, showing only minimal differences between the retrieved mid-layer heights using different forward models.

In Figure 10 the scatterplots of the differences between the LBL ALH and NN ALH on the next two days are shown. Again, the differences introduced by the NN iplementation are limited. The largest differences are on

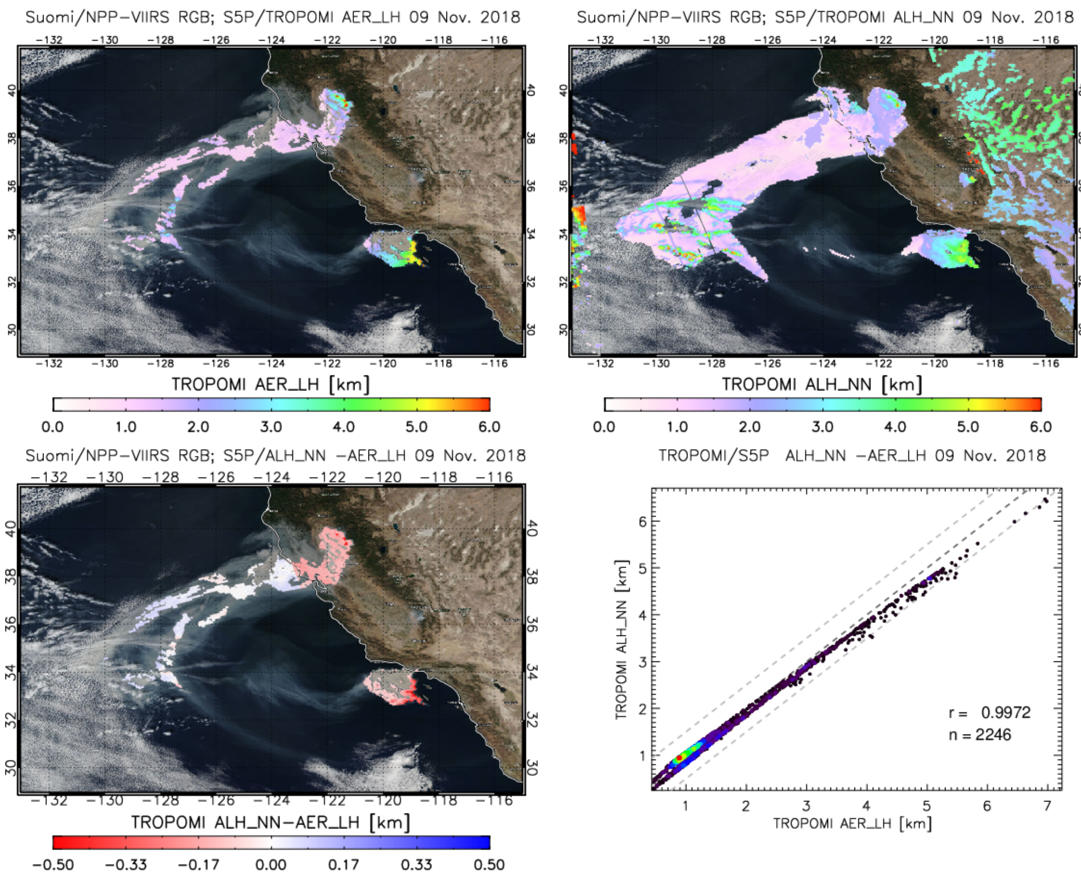

Figure 9: (top-left) Suomi/NPP VIIRS RGB on 9 Nov. 2018, overlaid with LBL ALH ; (top-right) Suomi/NPP VIIRS RGB on 9 Nov. 2018, overlaid with NN ALH; (bottom-left)Suomi/NPP VIIRS RGB on 9 Nov. 2018, overlaid with difference of NN-LBL ALH; (bottom-right) Scatterplot of NN ALH versus LBL ALH for the pixels in the left panels.

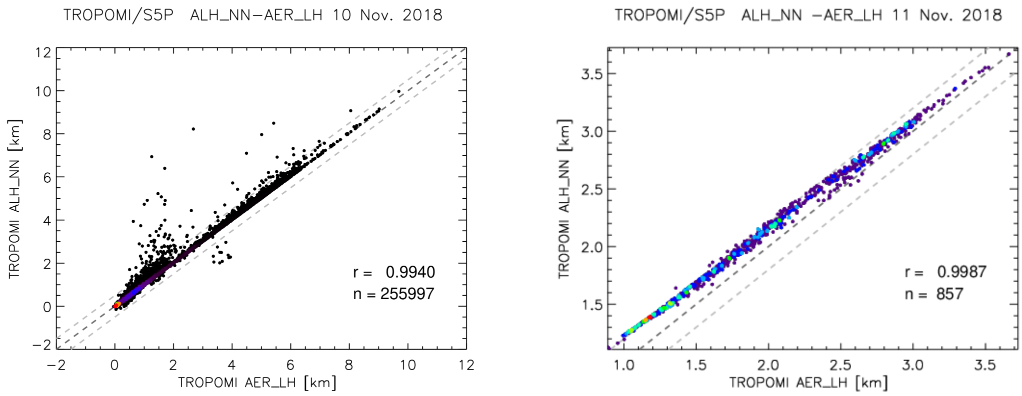

Figure 10: (left) Scatterplot of NN ALH versus LBL ALH on 10 Nov 2018 for the area in Fig 9; (right) Same as the left panel for 11 Nov. 2018.

10 Nov. 2018, when sub-pixel clouds make the retrieval unreliable. The NN forward model treats these pixels differently than DISAMAR is some cases. Therefore, the representativeness of the NN ALH is different from the LBL ALH, because the NN will always give a solution within the trained domain, while LBL calculation may fail. However, the accuracy is not so much affected by the NN.

8.2 Default settings for the error analysis

We will first describe the default settings used in the error analysis; these settings are used unless explicitly stated otherwise.

The instrument model used in simulation and retrieval consists of anticipated instrument characteristics for TROPOMI described in Veefkind et al. (2012)[63]. Note that these instrument characteristics are slightly different from the more recent TROPOMI instrument properties described in citeRDS5P-KNMI-L2-0010-RP. The radiance and irradiance slit functions *S* at the O_2 A band are flat-topped functions with a full width at half maximum of 0.5 nm:

$$S(\lambda_i, \lambda) = \text{const} \cdot 2^{\left(\frac{\lambda_i - \lambda}{\text{FWHM}/2}\right)^4} \tag{10}$$

The constant const normalizes the slit function to unit area. The spectral sampling interval is 0.10 nm.

A noise model associates simulated reflectance spectra with noise spectra. We assume that the measurement error is dominated by shot noise. Hence, the measurement error covariance matrix is diagonal and the signal-to-noise ratio (SNR) of the radiance *L* is proportional to the square root of the radiance (in photons). In addition, we assume the proportionality factor to be independent of wavelength. If we know the signal-to-noise ratio for some reference radiance level L^{ref} at some reference wavelength ${\lambda_i}^{\text{ref}}$, we can thus calculate the signal-to-noise ratio for any other radiance level at any other wavelength following

$$\text{SNR}(L(\lambda_i)) = \text{SNR}(L^{\text{ref}}(\lambda_i^{\text{ref}})) \cdot \sqrt{\frac{L(\lambda_i)}{L^{\text{ref}}(\lambda_i^{\text{ref}})}}. \tag{11}$$

The signal-to-noise ratio at 758 nm (continuum) is 500 for a reference radiance L^{ref}(758 nm) of $4.5 \cdot 10^{12}$ photons s^{-1} cm^{-2} sr^{-1} nm^{-1} and for the spectral sampling interval of 0.1 nm. The reference radiance spectrum, which is used for specification of the SNR within the Sentinel-5 and Sentinel-5 Precursor projects, corresponds to a dark scene (‘tropical dark’, meaning a pure molecular atmosphere with a surface albedo of 0.02, a solar zenith angle of 0° and a viewing zenith angle of 0°). Hence, if clouds or aerosols are present, or if the surface albedo is larger than 0.02, the actual SNR will be (much) larger than 500. Finally, we assume the signal-to-noise ratio of the irradiance to be a factor of ten higher than the signal-to-noise ratio of the radiance. Note that we do not add noise to the radiance spectra nor do we apply by default any other instrumental effects.

The temperature profile in simulation and retrieval corresponds to the mid-latitude summer atmosphere, and the ground pressure is 1013 hPa. Oxygen has a constant volume mixing ratio of 21%. Oxygen absorption cross section parameters are taken from the HITRAN 2008 database [ER3]: a Voigt profile is assumed, only

the most abundant isotopologue is taken into account, and line mixing and collision-induced absorptions are ignored. We consider the following surface types

Table 9: Surface types and corresponding albedos considered in the error analysis

Surface type	**Surface albedo**	
	758 nm	**770 nm**
Sea / ocean	0.025	0.025
Vegetated land	0.20	0.25
Desert / arid land	0.30	0.35
Snow / ice	0.6	0.6

These values are in agreement with Koelemeijer et al. (2003) [31]. Fluorescence emissions for vegetated land are zero. The pressure difference between top and bottom of an aerosol layer is 20 hPa in both simulation and retrieval. Hence, a mid pressure of, for example, 800 hPa corresponds to an aerosol layer with a top and bottom pressure of 790 hPa and 810 hPa, respectively. The default aerosol model in simulation and retrieval has a single scattering albedo of 0.95, a Henyey-Greenstein phase function with asymmetry parameter of 0.7 and an Angstrom coefficient of zero. Radiative transfer settings are as described in 5.4 (e.g. polarization is ignored in simulation and retrieval).

8.3 Baseline precision of Aerosol Layer Height

First we describe the baseline precision of retrieved mid pressure and we investigate its dependence on mid pressure, aerosol optical thickness, surface albedo and observation geometry. We also show that the inversion can be problematic for specific combinations of atmospheric state and observation geometry.

Approach

For a number of atmospheric states and observation geometries, we simulate reflectance spectra of the O_2 A band at TROPOMI's resolution and we calculate corresponding noise spectra according to TROPOMI's anticipated noise model. We then use the derivatives of reflectance provided by the forward model, to propagate the measurement noise and calculate 1-σ errors in fit parameters. The state vector contains the main fit parameters p_{mid}, τ_0, A_{s} (758 nm) and A_{s} (770 nm).

In symbols this can be expressed as follows. If the forward model is linearized around the (retrieved) state for the purposes of an error analysis, we write

$$\mathbf{R} \approx \mathbf{F}(\hat{\mathbf{x}}) + \mathbf{K}(\mathbf{x} - \hat{\mathbf{x}}), \tag{12}$$

where $\mathbf{R}$ is the vector of simulated measurements. The covariance matrix describing the error in retrieved parameters due to the measurement error in $\mathbf{R}$ follows from Eq. 8-3 using rules for error propagation:

$$\hat{\mathbf{S}} = \mathbf{K}\hat{\mathbf{S}}\mathbf{K}^T \Rightarrow \hat{\mathbf{S}} = (\mathbf{K}^T\mathbf{S}^{-1}\mathbf{K})^{-1}. \tag{13}$$

Note that a column of **K** corresponds to the derivative of reflectance with respect to a particular fit parameter as a function of wavelength (Eq. 7). If certain columns of **K** become strongly linearly dependent (i.e. spectral shapes of derivatives are similar), matrix is nearly singular. Errors in corresponding parameters (diagonal elements of) become large and it will be difficult to simultaneously fit these parameters with precision levels that meet scientific user requirements. In addition, the solution is sensitive to systematic errors, such as numerical inaccuracies, model biases or calibration errors (ill-conditioning).

We are not taking into account a priori information here, since our aim is to investigate precision levels that can be achieved by the measurement alone. The state vector used for the present analysis indeed contains all main fit parameters for which we in practice have little a priori knowledge available. If more fit parameters are added to the state vector, precision levels might deteriorate, depending on the respective a priori errors. In the remainder of the error analysis, we will describe how precision levels change in response to adding parameters to the state vector where appropriate. The results presented in this section thus provide a description of the algorithm's baseline precision.

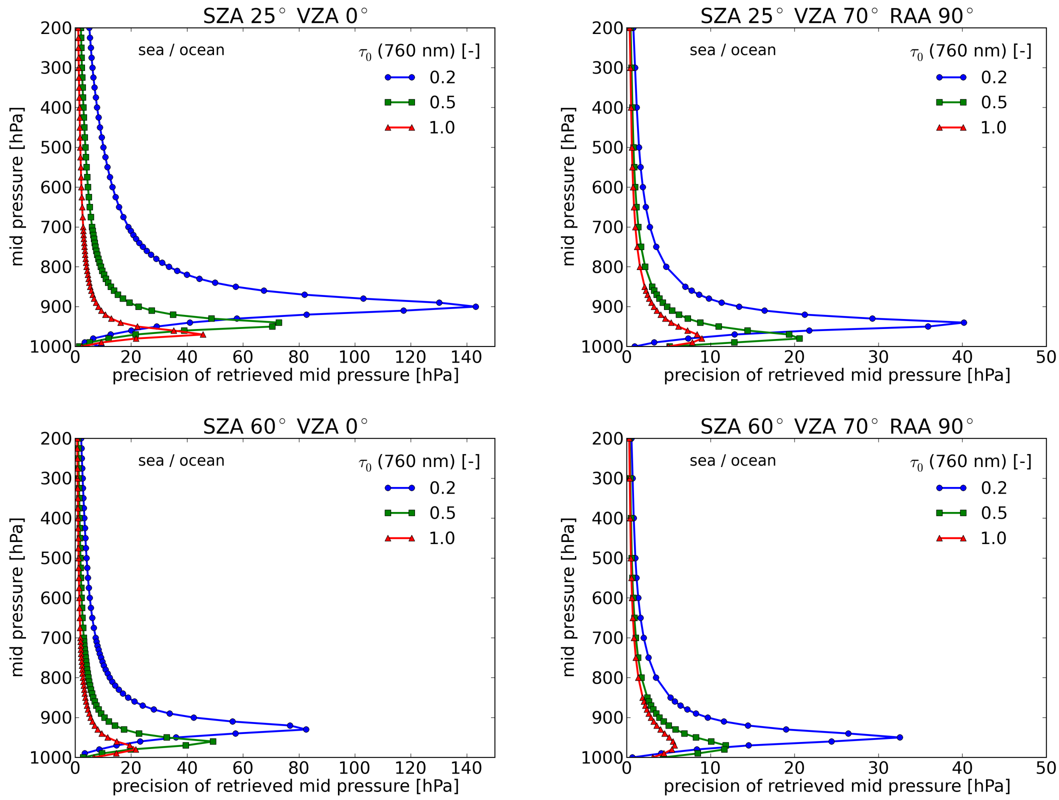

Figure 11: Precision of retrieved aerosol mid pressure as a function of mid pressure for three values of the aerosol optical thickness. Panel A shows retrieval precision for an aerosol layer over sea / ocean; Each of the four subplots in a panel corresponds to a different observation geometry: SZA 25°, VZA 0° (top left); SZA 25°, VZA 70°, RAA 90° (top right); SZA 60°, VZA 0° (bottom left); and SZA 60°, VZA 0°, RAA 90° (bottom right). Note the different scales of the x-axis.

Results

We simulated reflectance spectra for a large range of mid pressures, optical thicknesses, surface albedos and solar zenith angles (SZAs). We also tested a number of viewing zenith angles (VZAs) and relative azimuth angles (RAAs). We used the default aerosol model ω_0 of 0.95, HG phase function with asymmetry parameter of 0.7); the aerosol layer has a pressure thickness of 20 hPa. We summarize the main findings below.

Figures 11 and 12 illustrate the precision of retrieved mid pressure for four representative TROPOMI observation geometries. Every subplot of these figures shows precision of retrieved mid pressure as a function of mid pressure for three values of the aerosol optical thickness. Figures 11 corresponds to retrievals over sea / ocean and Figures 12 corresponds to vegetated land, respectively. The four subplots within a panel correspond to four different observation geometries: solar zenith angles of 25° and 60°, and viewing zenith angles corresponding to pixels at nadir (0°) and near the end of the swath (70°).

Overall, the figures show that the baseline precision is usually well below the TROPOMI target requirement of 50 hPa for optical thicknesses above 0.2. In incidental cases, however, precision may significantly deteriorate and increase up to 100 hPa or even above.

Precision of mid pressure generally improves with decreasing pressure (increasing altitude). At larger pressure differences between aerosol layer and ground surface, it is easier to distinguish aerosol contributions from surface contributions. Precision of mid pressure generally improves with increasing optical thickness (stronger aerosol signal). Note, however, that exceptions to these trends exist. There is no clear dependence of precision on the albedo of the surface.

Precision of mid pressure generally improves with increasing solar zenith angle. If the solar zenith angle increases, a unit area of surface receives less light (weaker aerosol signal) but path lengths through the aerosol layer are longer (stronger aerosol signal). Apparently, the latter effect dominates. Precision of mid pressure also tends to improve with increasing viewing zenith angle (longer path lengths through aerosol layer, hence stronger aerosol signal). As before, exceptions to these trends exist.

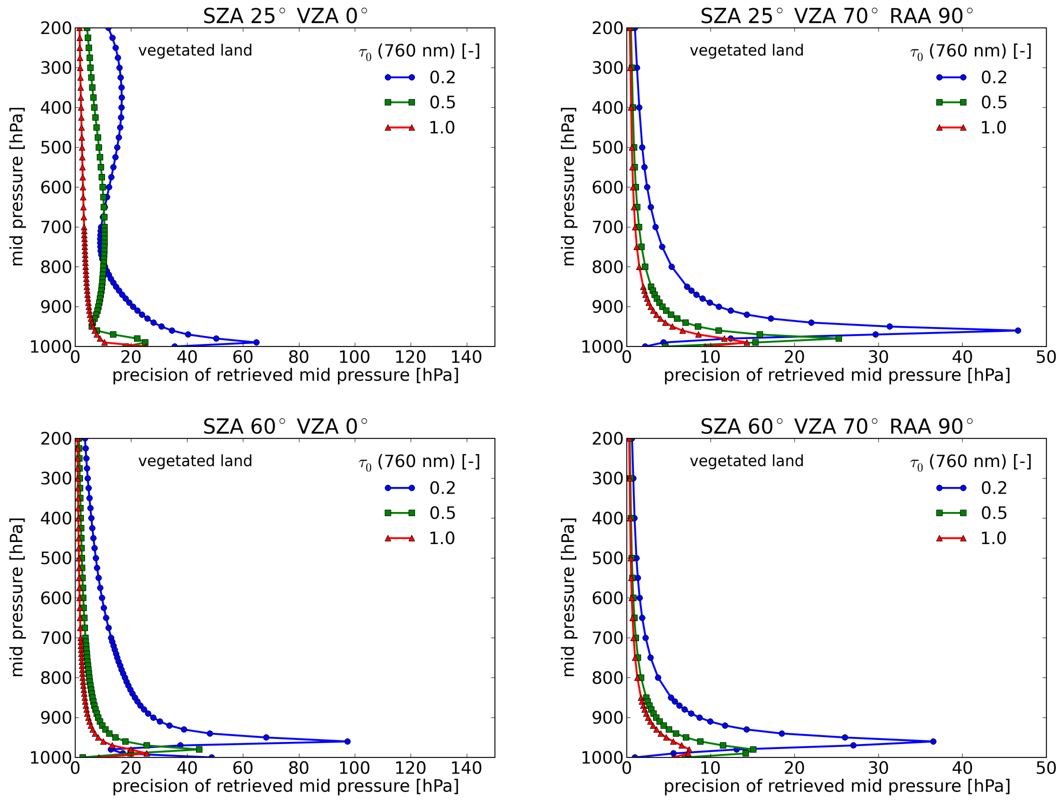

Figure 12: Precision of retrieved aerosol mid pressure as a function of mid pressure for three values of the aerosol optical thickness. Panel A shows retrieval precision for an aerosol layer over vegetated land. Each of the four subplots in a panel corresponds to a different observation geometry: SZA 25°, VZA 0° (top left); SZA 25°, VZA 70°, RAA 90° (top right); SZA 60°, VZA 0° (bottom left); and SZA 60°, VZA 0°, RAA 90° (bottom right). Note the different scales of the x-axis.

Figure 13 depicts precision of retrieved mid pressure as a function of surface albedo for three arbitrary atmospheric states and observation geometries. It illustrate once more that the inversion can become nearly singular for specific atmospheric states and observation geometries. Furthermore, aerosol retrieval is not more precise over darker (or brighter) surfaces in a general sense. This stands in contrast with conventional spectral aerosol optical thickness retrieval algorithms, which are typically less precise over land. Spectral optical thickness retrievals using continuum reflectances rely heavily on external surface reflectance models or climatologies. Such reflectance models or climatologies are generally less accurate for land surfaces. Finally, it shows that it is very well possible to retrieve aerosol pressure over snow covered surfaces.

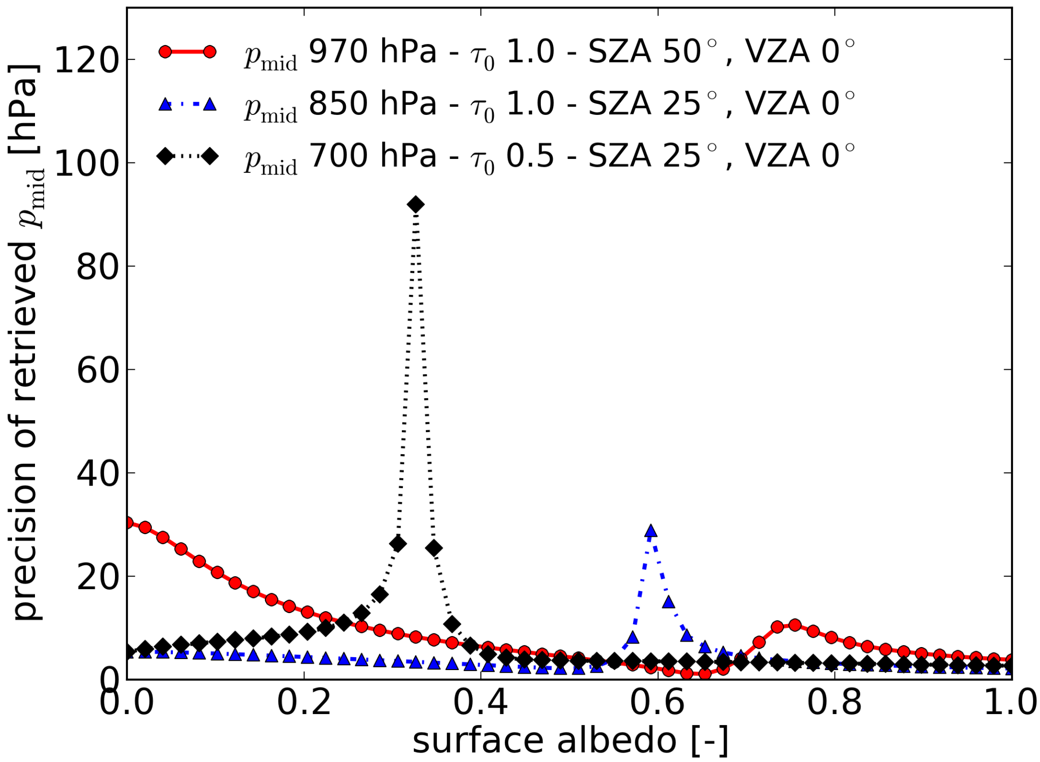

Figure 13: Precision of retrieved mid pressure as a function of surface albedo for three arbitrary atmospheric states and observation geometries.

Finally, we mention that errors in the fit parameters are usually highly correlated. To give an impression, Table 10 shows correlation coefficients between errors in all fit parameters for an aerosol layer with optical thickness of 0.5 at 800 hPa over sea / ocean and vegetated land. Although correlation coefficients can be as high as 0.999, precision of retrieved pressure is good (cf. Figures 11 and 12, bottom left plot). This conforms to the finding that the degrees of freedom for the signal for these two cases is 4.0, which is equal to the number of fit parameters. Thus, derivatives are still sufficiently linearly independent to retrieve all four parameters simultaneously. It is our experience from simulation studies that a retrieval with such high correlation coefficients is generally stable.

Table 10: Correlation coefficients between errors in fit parameters for an aerosol layer with optical thickness of 0.5 at 800 hPa over sea / ocean and vegetated land. The solar zenith angle is 60° and the viewing direction is nadir. The height variable is altitude (in km) instead of pressure (in hPa).

Correlation coefficient	Sea/Ocean	Vegetated land
$z_{mid} - \tau_0$ (760 nm)	-0.9945	-0.9895
$z_{mid} - A_s$ (758 nm)	0.9929	0.9721
$z_{mid} - A_s$ (770 nm)	0.9937	0.9383
τ_0 (760 nm) $- A_s$ (758 nm)	-0.9996	-0.9900
τ_0 (760 nm) $- A_s$ (770 nm)	-0.9997	-0.9562
A_s (758 nm) $- A_s$ (770 nm)	0.9991	0.9354

8.4 Required knowledge of aerosol type

Retrieval of aerosol pressure from the O_2 A band requires an assumed aerosol model, because the measurement does not contain enough information to simultaneously retrieve aerosol optical properties. However, the aerosol type present in the target pixel is generally unknown and shows a large variation in time and space. In this section, we show that biases in retrieved aerosol pressure generally remain small in response to model errors in the single scattering albedo and phase function. Biases in retrieved aerosol optical thickness on the other hand are significant.

8.4.1 Single scattering albedo

Approach

First we investigate the sensitivity of retrieval to model errors in the single scattering albedo. We simulate reflectance spectra for a range of optical thicknesses and for a number of single scattering albedos, mid pressures and surface albedos. We then retrieve aerosol mid pressure assuming in retrieval a single scattering albedo of 0.95. The forward models for simulation and retrieval are the same, except for this model error in the single scattering albedo. The state vector contains the main fit parameters p_{mid}, τ_0, A_s (758 nm) and A_s (770 nm).

Results

We discuss a set of representative retrieval results. True values, a priori values and a priori errors for the fit parameters are given in Table 11. The single scattering albedo in the simulation is either 0.9 or 1.0. In both simulation and retrieval we have a single aerosol layer with a pressure thickness of 20 hPa and a Henyey-Greenstein phase function with asymmetry parameter of 0.7. The solar zenith angle is 50° and the viewing direction is nadir.

Table 11: True values, a priori values and a priori errors used in the retrieval simulations of Figure 12 investigating the sensitivity of retrieval to the assumed single scattering albedo.

Fit parameter	True value	AP value	AP error (1-σ)
p_{mid}	600 hPa 800 hPa	True	500 hPa
τ_0 (760 nm)	Range: 0.025 – 1.0	True	2.0
A_s (758 nm)-A_s (770 nm)	0.025 – 0.025 0.0 – 0.25 (vegetated land)	True	0.2

Figure 14 shows the results from these retrievals. The left and right panels correspond to the two surface albedos. We show the bias in retrieved mid pressure (first row), precision of retrieved mid pressure (second row), and the bias in retrieved optical thickness with precision indicated by error bars (third row). Note that the *x*-axis has a logarithmic scale.

One would perhaps expect retrieved aerosol parameters to be inaccurate in case of a model error in the single scattering albedo. However, we see that biases in retrieved pressure are typically very small compared to the TROPOMI target requirement on accuracy of 50 hPa. Moreover, biases tend to decrease for optically thicker aerosol layers (stronger aerosol signal). On the other hand, we see that retrieved optical thickness is biased significantly and so is retrieved surface albedo (not shown). These two fit parameters respond to a model error in the singe scattering albedo. Indeed, biases in retrieved optical thickness and surface albedo increase with increasing aerosol optical thickness.

For the vegetated land case (panel B), we see that pressure biases rapidly increase up to and sometimes even above 50 hPa in a small range of optical thicknesses between 0.1 and 0.2 and particularly for the near-surface aerosol layer. This result is not so much illustrative of the effect of a model error in the single scattering albedo. Rather, as indicated by the poor precision levels in this range, spectral shapes of the derivatives are similar and the inversion is sensitive to any model error.

A model error of 0.05 in the single scattering albedo is used to represent a typical a priori uncertainty. However, we have tested model errors up to 0.2 (e.g. single scattering albedo of 0.6 in the simulation and 0.8 in retrieval). Even for such a large error, the conclusions stated above hold. Hence, retrieved aerosol pressure is robust against inaccurate knowledge of the single scattering albedo. In Section 8.5 we show that it is essential in this respect that surface albedo, next to aerosol optical thickness, is a fit parameter.

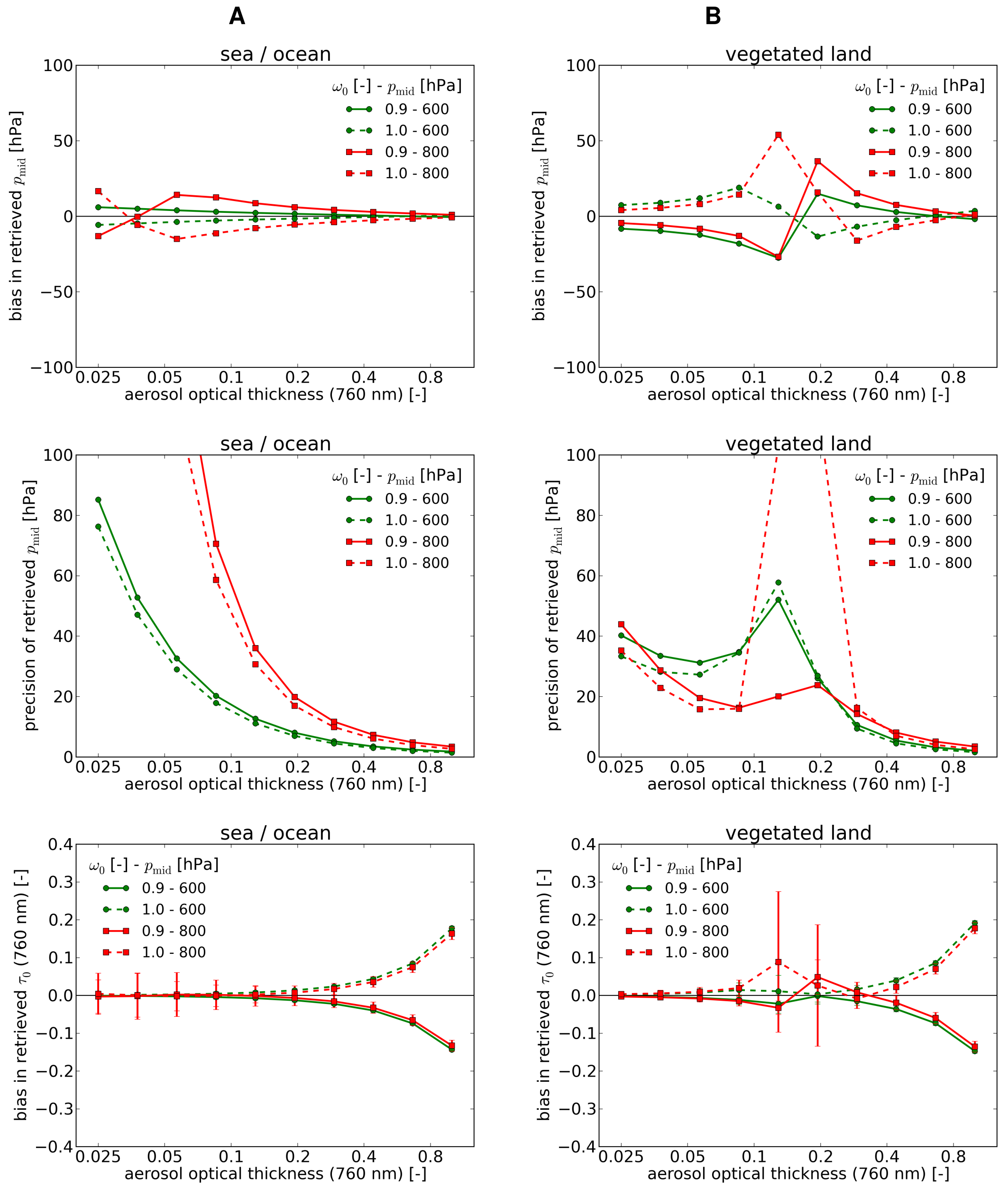

Figure 14: Effect of a model error in the single scattering albedo on retrieved mid pressure and aerosol optical thickness as a function of optical thickness. We assume a single scattering albedo of 0.95 in retrieval, while the true single scattering albedo is either 0.90 (solid lines) or 1.0 (dashed lines). The aerosol layer is located at 600 hPa (green lines) or 800 hPa (red lines). First row: bias in retrieved mid pressure; second row: precision of retrieved mid pressure; third row: bias in retrieved optical thickness with error bars indicating precision. Panel A (left column) shows retrieval simulations over sea / ocean; panel B (right column) shows retrieval simulations over vegetated land. The x-axis has a logarithmic scale.

We have repeated these retrieval simulations and fitted the single scattering albedo with an a priori error of 0.05. Overall, precision of retrieved aerosol pressure remains the same but precision of retrieved aerosol optical thickness deteriorates. In addition, we find that biases in both retrieved pressure and optical thickness remain the same. Thus, retrieval does neither improve nor deteriorate with respect to aerosol pressure when fitting the single scattering albedo. However, these preliminary investigations also indicate that the near-singular behavior for the aerosol layer with optical thickness between 0.1 and 0.2 over vegetated land is mitigated.

Fitting the single scattering albedo is implemented as an option to the baseline algorithm. Perhaps fitting the single scattering albedo will improve retrieval of aerosol optical thickness for optically thick aerosol layers (optical thickness larger than, say, 1.0).

8.4.2 Phase function

Approach

Second we investigate the sensitivity of the retrieval to model errors in the phase function. We simulate reflectance spectra using generic aerosol models that are used within the framework of the aerosol project in ESA's Climate Change Initiative program [ER5]. We test three somewhat realistic atmospheric scenarios for a range of optical thicknesses and for a number of aerosol pressures. The three scenarios are based on the 'Dust', 'Fine mode weakly absorbing' and 'Fine mode strongly absorbing' aerosol models [14]. The fourth aerosol model, 'Sea salt', is not considered here. For one scenario we retrieve top pressure instead of mid pressure, following the parameterization described in section 6.2.2 and illustrated in Figure5C. In retrieval we assume the Henyey-Greenstein phase function with asymmetry parameter of 0.7. To isolate the effect of a model error in the phase function, the single scattering albedo assumed in retrieval is equal to the true value. The state vector contains the main fit parameters p_{mid}, τ_0, A_{s} (758 nm) and A_{s} (770 nm).

Results

Optical properties for the three aerosol models are summarized in Table 12. Figure 15 makes a comparison of the phase functions used in simulation and retrieval. The three atmospheric scenarios, and true values, a priori values and a priori errors for the fit parameters are given in Table 13. For the first two scenarios the profile consists of a single aerosol layer with a pressure thickness of 20 hPa and we are retrieving mid pressure. For the Boundary layer pollution scenario, the aerosol layer extends down to the ground surface and we are retrieving the top pressure of the aerosol layer. The solar zenith angle is 50° and the viewing direction is nadir.

Table 12: Optical properties at the O_2 A band for the three aerosol models used in the retrieval simulations of Figure 16 (based on [14]). Properties for the Dust model are based on T-matrix calculations, which are kindly provided by Oleg Dubovik and co-workers; for the other two models we performed Mie calculations.

Aerosol model	**Single scattering albedo (760 nm)**	**Asymmetry parameter**	**Normalized extinction cross section at 760 nm (w.r.t. 550 nm)**
Dust	0.97	0.71	1.05
Fine mode strongly absorbing	0.76	0.57	0.57
Fine mode weakly absorbing	0.97	0.58	0.50

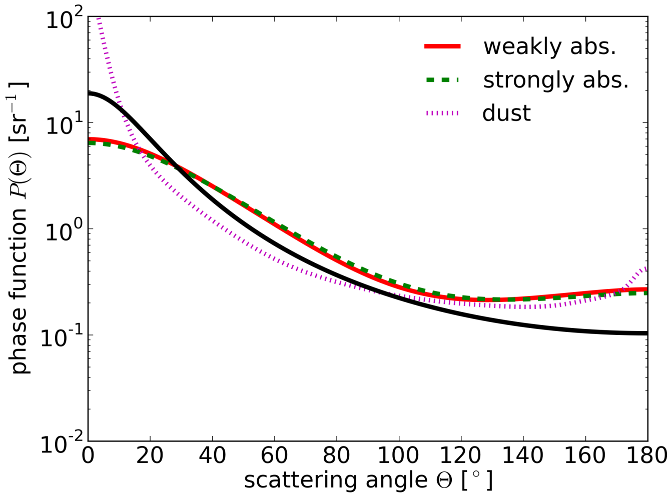

Figure 15: Phase functions for the three aerosol models used in the retrieval simulations of Figure 16. The black line corresponds to a Henyey-Greenstein phase function with asymmetry parameter of 0.7, which is used in retrieval.

Table 13: True values, a priori values and a priori errors used in the retrieval simulations of Figure 16 investigating the sensitivity of retrieval to the assumed phase function.

Scenario	**Fit parameter**	**True value**	**AP value**	**AP error (1-σ)**
'Dust over ocean'	p_{mid}	600 hPa 750 hPa 850 hPa	True	500 hPa
	τ_0(550 nm)	Range: 0.05–2.0	True	2.0
	A_s (758 nm)-A_s (770 nm)	0.025 – 0.025	True	0.2
'Biomass burning over ocean'	p_{mid}	600 hPa 750 hPa 850 hPa	True	500 hPa
	τ_0(550 nm)	Range: 0.05–2.0	True	2.0
	A_s (758 nm)-A_s (770 nm)	0.20 – 0.25 (vegetated land)	True	0.2
'Boundary layer pollution'	p_{top}	850 hPa 900 hPa 950 hPa	True	500 hPa
	τ_0(550 nm)	Range: 0.05–2.0	True	2.0
	A_s (758 nm)-A_s (770 nm)	0.20 – 0.25 (vegetated land)	True	0.2

Figure 16 shows the results from these retrievals. Each panel corresponds to one of the three scenarios. We show the bias in retrieved aerosol pressure (left) and precision of retrieved pressure (right). Note that the *x*-axis has a logarithmic scale. We remark that the effect of a model error in the phase function depends on (interactions between) the observation geometry, aerosol parameters and surface albedo. This effect is harder to generalize from a limited set of retrieval simulations than the effect of a model error in the single scattering albedo.

For the 'Dust over ocean' scenario (panel A), we see that the effect of a model error in the phase function on retrieved pressure is small, even though the phase function for the coarse mode aerosol differs most pronouncedly from the Henyey-Greenstein function (particularly in the forward scattering direction). The inversion for dark surfaces (e.g. sea / ocean) is generally well conditioned. These retrieval simulations then suggest that aerosol pressure retrieval over a dark surface is robust against inaccurate knowledge of the phase function.

The retrieval simulations for the 'Biomass burning over land' scenario (panel B) are more difficult to interpret, because the inversion is nearly singular for optical thicknesses at 550 nm between about 0.2 and 0.3. Precision is poor and retrieval is sensitive to model errors in that range. However, for optical thicknesses at 550 nm above 0.4, biases in retrieved mid pressure due to the model error in the phase function, are much smaller than the target requirement of 50 hPa. Retrieved aerosol optical thickness is biased significantly (not shown).

At first sight, the retrieval simulations for the 'Boundary layer pollution' scenario (panel C) seem to have similar results. Biases in retrieved top pressure increase in a range of optical thicknesses (around 0.8) for two out of three aerosol top pressures. However, precision of retrieved pressure in this range is good and well below the target requirement of 50 hPa. For optical thicknesses at 550 nm above around 1.3, biases in retrieved pressure are small, but biases in retrieved aerosol optical thickness are significant (not shown).

8.4.3 Conclusion

The retrieval simulations presented in this section indicate that retrieved aerosol pressure is robust to model errors in the single scattering albedo. They also suggest that retrieved aerosol pressure is robust to a model error in the phase function, particularly over dark surfaces (e.g. sea / ocean). The operational algorithm will therefore initially assume a single, average aerosol model.

We have also shown that aerosol retrieval over relatively bright land (e.g. vegetated land) can be problematic. Since vegetated land is much darker at the O_2 B band around 685 nm (the O_2 A and B bands are located on opposite sides of the so-called red-edge; e.g. [31]), including the O_2 B band in the fit may help to mitigate or remove near-singularities for vegetated land cases. Retrieval of aerosol pressure over land needs to be further investigated.

We prefer to assume a phase function in retrieval that is smooth and can serve as an approximate phase function for many aerosol types. A smooth phase function is advantageous because radiative transfer calculations are faster (less streams needed).

8.5 Role of a priori knowledge of the surface albedo

A surface albedo climatology, such as the MERIS BSA database [42], can provide model or a priori values for the surface albedo in retrieval. In this section, we show that the typical uncertainties associated with climatological values make it sometimes problematic to treat the surface albedo as a model parameter: large pressure biases and non-convergent retrievals occur. On the other hand, biases and non-convergences disappear if the surface albedo is included in the state vector. We also show that imposing a small a priori error in the surface albedo corresponding to the uncertainty in climatological values, does not improve precision of retrieved pressure.

Before presenting the sensitivity analysis, we first illustrate in Figure 17 that the surface albedo and aerosol optical thickness can be retrieved simultaneously from the O_2 A band. The figure shows reflectance spectra for two different combinations of optical thickness and surface albedo that yield the same reflectance in the continuum. All other parameters, including the aerosol pressure, are the same. The two cases can be distinguished from the shape of absorption: photons reflected by the surface have to pass through the atmosphere below the aerosol layer, in which additional oxygen absorption takes place.

Approach

We investigate the effect on retrieval if the true surface albedo differs from the value provided by a surface albedo climatology. We compare three types of retrieval: the surface albedo being a model parameter, the surface albedo being fitted in a retrieval constrained by the climatology, and the surface albedo being fitted in an unconstrained retrieval. These three retrieval types are summarized in Table 14. We investigate a sea / ocean case and a vegetated land case and assume that the typical random (1-σ) error in climatological albedo values is 0.01 and 0.02, respectively. (Thus, events such as incidental snow cover are not incorporated.) For simplicity, we assume in this sensitivity analysis that the surface albedo is wavelength independent. The state vector contains parameters p_{mid}, τ_0, and A_s.

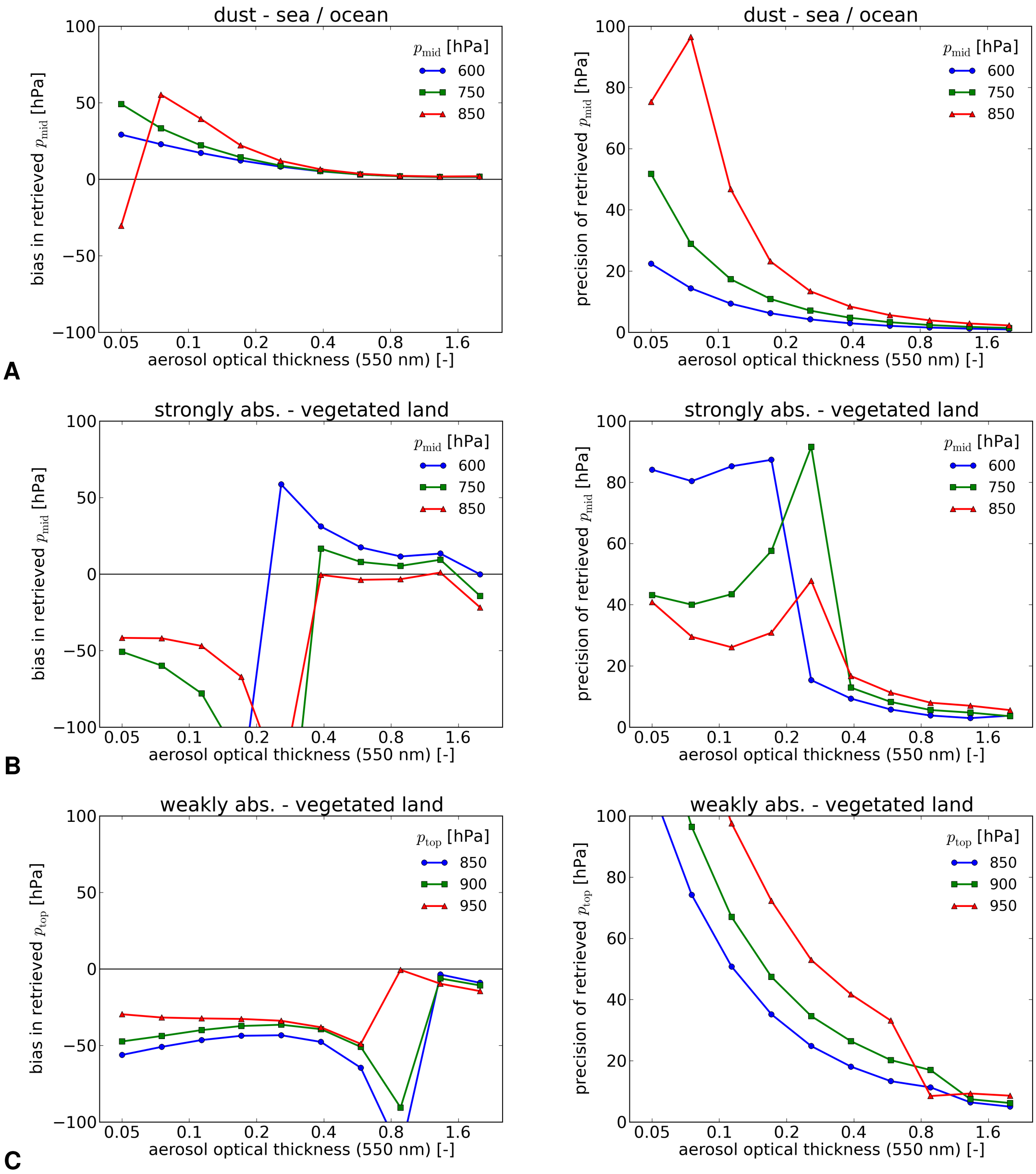

Figure 16: Effect of a model error in the phase function on retrieved aerosol pressure as a function of optical thickness for three values of aerosol pressure. Panel A (first row): 'Dust over ocean'; panel B (second row): 'Biomass burning over land'; panel C (third row): 'Boundary layer pollution'. For details of these scenarios, see the text and Table 13. In each panel, the left plot shows the bias in retrieved aerosol pressure and the right plot shows precision of retrieved pressure. We assume a Henyey-Greenstein phase function with asymmetry parameter of 0.7 in retrieval. Note that for the 'Boundary layer pollution' scenario, we assume an aerosol profile consisting of a single layer extending down to the ground surface. In this case, we retrieve the layer's top pressure p_{top}. The x-axis has a logarithmic scale.

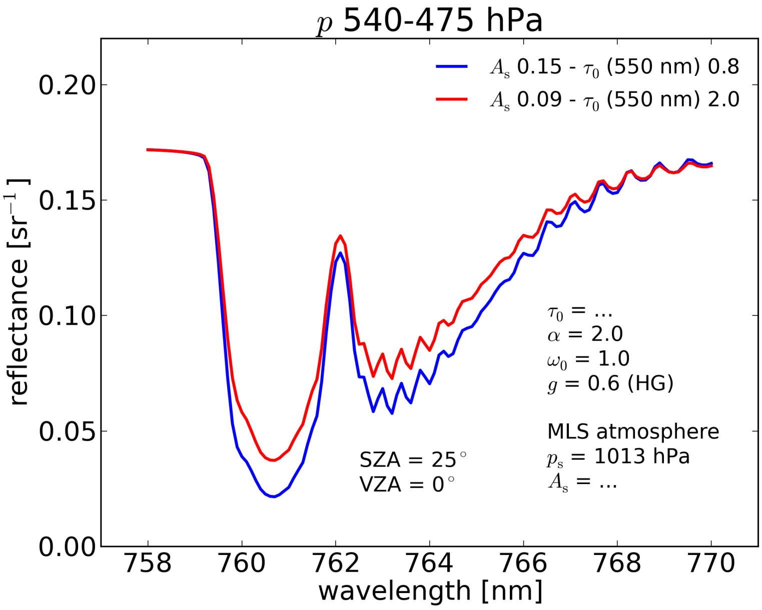

Figure 17: Reflectance spectra for two different combinations of optical thickness and surface albedo that yield the same continuum reflectance. All other parameters are the same. The aerosol layer is between 540 and 475 hPa; the single scattering albedo is 1.0; the solar zenith angle is 25° and the viewing direction is nadir. From the shape of absorption we can simultaneously fit surface albedo and aerosol optical thickness.

Table 14: *A* priori error in the surface albedo for the three types of retrieval investigating the effect of an error in climatological surface albedo values.

Retrieval type	AP error (1-σ) in A_s	Comment
'No fit A_s (σ=0.0)'	0.0	Surface albedo is a model parameter: the model value is provided by the surface albedo climatology
'Fit A_s (σ=0.01)' 'Fit A_s (σ=0.02)'	0.01 (sea/ocean) 0.02 (vegetated land)	Surface albedo is a fit parameter: the *a priori* value is provided by the surface albedo climatology and the *a priori* error is the random error associated with the climatological value
'Fit A_s (σ=0.2)'	0.2	Surface albedo is a fit parameter: measurement determines surface albedo (large *a priori* error); climatology provides starting value for the fit

Results We have tested a number of atmospheric scenarios, but show results for only two of them. The results for these scenarios are representative of all the other scenarios. Atmospheric scenarios and associated a priori values and errors are given in Table 15. We vary the true surface albedo within 3ω around the climatological value. In both simulation and retrieval, the aerosol layer's pressure thickness and the aerosol model have default values. The solar zenith angle is 50° and the viewing direction is nadir.

Table 15: True values, a priori values and a priori errors used in the retrieval simulations of Figure 18 investigating the sensitivity of retrieval to the assumed phase function.

Fit parameter	True value	AP value	AP error (1-σ)
p_{mid}	500 hPa 800 hPa	True	500 hPa
τ_0(760 nm)	0.2 0.5 1.0	True	2.0
A_s (760 nm)	Range: 0.025 $\pm$ 3*0.01 (sea/ocean) Range: 0.02 $\pm$ 3*0.02 (vegetated land)	0.025 0.2	Three cases: see table 8-6

Figure 18 shows results for an aerosol layer with optical thickness of 0.5 at 500 hPa over sea / ocean (panel A) and an aerosol layer with optical thickness of 0.5 at 800 hPa over vegetated land (panel B). We show the bias in retrieved aerosol pressure (left) and precision of retrieved pressure (right) as a function of the true surface albedo for each of the three retrieval types. The climatological surface albedo value that is used in retrieval (either as model value, a priori value or starting value), is indicated by the arrow. Missing data points indicate that retrieval does not converge.

If the surface albedo is not fitted, non-convergences and pressure biases much larger than 50 hPa occur. For example, if the true surface albedo is 0.21 while a value of 0.20 is assumed in retrieval, the aerosol layer at 800 hPa over vegetated land shows a pressure bias of 94 hPa. If the true surface albedo is 0.19, retrieval for that layer does not even converge. Note that these deviations of the true surface albedo from the model value are representative of current surface albedo climatologies. On the other hand, if the surface albedo is fitted, the non-convergent retrievals and pressure biases disappear.

Precision of retrieved pressure is the same when fitting the surface albedo with an a priori error corresponding to the climatological uncertainty, or when fitting the surface albedo with a relatively large a priori error of 0.2. This indicates that the information about the surface reflectivity contained in the measurement is so pronounced that the a priori information provided by a surface albedo climatology does not constrain retrieval.

So far we have focused on the question whether a surface albedo climatology improves (a posteriori) precision of retrieved pressure. However, a surface albedo climatology can also help to stabilize retrieval by providing starting values for the iterative fit procedure. The outcome of an iterative fit is particularly sensitive to the starting value in case of highly non-linear forward models or multiple minima in the cost function. A surface albedo climatology can provide starting values for the fit that are supposedly closer to the surface albedo's true values. If starting values of fit parameters are closer to their true values, the convergence rate may improve, the number of iterations may be reduced, or retrieval may more often converge to the correct (global) χ^2-minimum.

The stability of retrieval is difficult to assess in a simulation environment. However, we have done extensive experiments with GOME-2 and SCIAMACHY spectra (Sanders et al., 2015; manuscript in preparation) and so far we found that the retrieval is considerably stable. For example, for a set of 1844 SCIAMACHY pixels over sea with high UVAI values, 1835 pixels had a converging retrieval after the first attempt (the starting values were the default, constant values). We also saw in these case studies that repeated retrieval attempts with different starting values does not improve convergence substantially.

8.6 Fitting surface albedo to compensate errors in single scattering albedo

In Section 8.3 we have shown that retrieved aerosol pressure is a robust quantity with respect to the assumed single scattering albedo but retrieved aerosol optical thickness and surface albedo are not. In Section 8.4 we have discussed the various ways to treat the surface albedo in retrieval with respect to the available surface albedo climatology (Table 14). We have shown that retrieval of aerosol pressure is sometimes problematic when not fitting the surface albedo in view of anticipated uncertainties in climatological albedo values. In this section, we return to the question of the effect of model errors in the single scattering albedo on retrieval and argue that the surface albedo should be included in the state vector for yet another reason.

The purpose of this section is to show that in order for retrieved pressure to be robust against inaccurate knowledge of the single scattering albedo it actually helps when the surface albedo is a fit parameter. Simultaneously fitting aerosol optical thickness as well as the surface albedo compensates for a model error in the

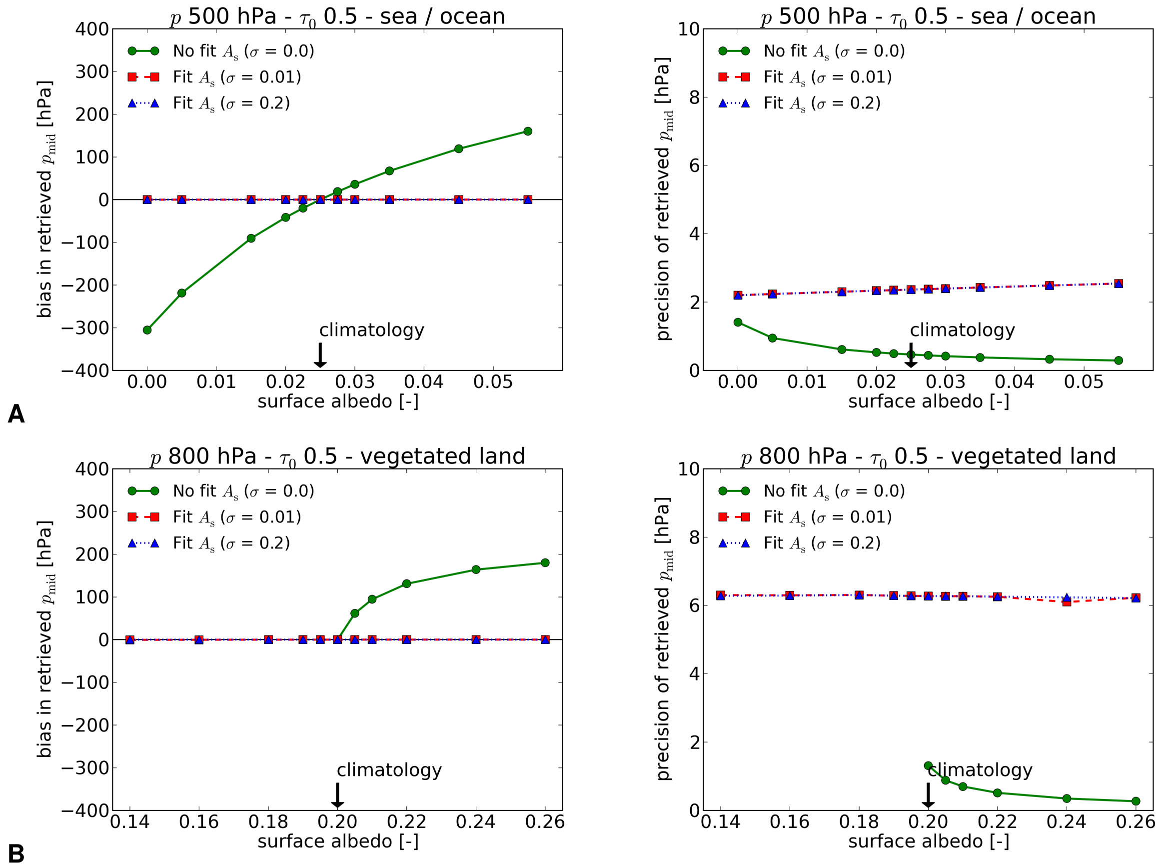

Figure 18: Effect of an error in climatological albedo values on retrieved aerosol pressure as a function of the true surface albedo for three retrieval types (Table 14). Panel A (first row): aerosol layer with optical thickness of 0.5 at 500 hPa over sea / ocean; panel B (second row): aerosol layer with optical thickness of 0.5 at 800 hPa over vegetated land. In each panel, the left plot shows the bias in retrieved aerosol pressure and the right plot shows precision of retrieved pressure. The climatological surface albedo value, which is used in retrieval, is indicated by the arrow. Missing data points indicate that retrieval does not converge.

single scattering albedo.

Approach

We again investigate the effect on retrieval of a model error in the single scattering albedo, but this time we compare the three retrieval types of Table 14. The retrieval type in which the surface albedo is fitted in an unconstrained retrieval (‘Fit A_s (ω = 0.2)’) corresponds to the retrieval simulations of Section 8.3. The single scattering albedo assumed in retrieval is 0.95; the true single scattering albedo varies in a wide range between 0.80 and 1.0. For simplicity, we assume that the surface albedo is wavelength independent. The state vector contains parameters p_{mid}, τ_0, and A_s.

Results

The atmospheric scenarios and retrieval settings are the same as in the previous section (Table 15), except for the true surface albedo, which is not varied but equal to its climatological (a priori) value. We show results for two scenarios, which are representative of all the other scenarios. The solar zenith angle is 50° and the viewing direction is nadir.

Figure 19 shows the pressure bias as a function of the true single scattering albedo for an aerosol layer with optical thickness of 0.5 at 500 hPa over sea / ocean (left plot) and an aerosol layer with optical thickness of 0.5 at 800 hPa over vegetated land (right plot). The single scattering albedo assumed in retrieval is 0.95. Missing data points indicate that retrieval does not converge.

If the surface albedo is not fitted, non-convergences and pressure biases much larger than 50 hPa occur. For example, if the true single scattering albedo is 1.0 while a value of 0.95 is assumed in retrieval, the aerosol layer at 800 hPa over vegetated land shows a pressure bias of 119 hPa. If the true single scattering albedo is 0.90, retrieval for that layer does not even converge. On the other hand, if the single scattering albedo is

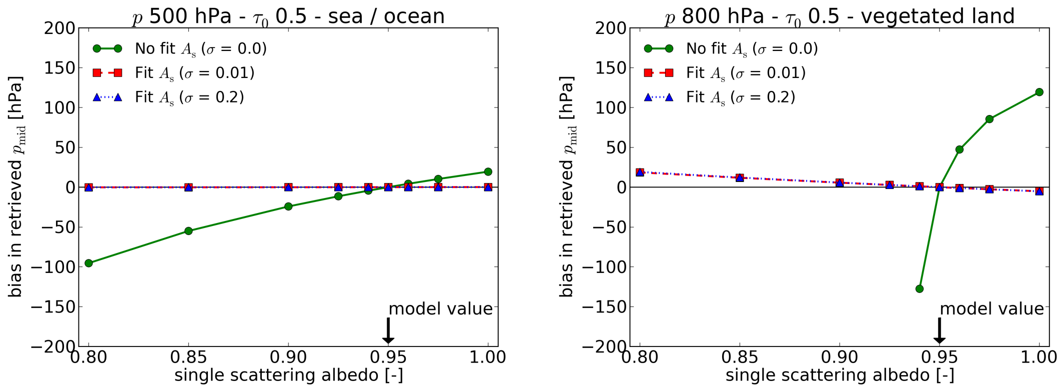

Figure 19: Effect of a model error in the single scattering albedo on the bias in retrieved pressure as a function of the true single scattering albedo for three retrieval types (Table 14). The single scattering albedo assumed in retrieval is 0.95. Left: aerosol layer with optical thickness of 0.5 at 500 hPa over sea / ocean; right: aerosol layer with optical thickness of 0.5 at 800 hPa over vegetated land. Missing data points indicate that retrieval does not converge.

fitted, the non-convergent retrievals disappear and pressure biases become very small. As mentioned before, retrieved aerosol optical thickness and surface albedo are biased (not shown).

Since fitting the surface albedo can compensate for typical model errors in the single scattering albedo, it is important to check whether the a priori error in the surface albedo is sufficiently large in this respect. The surface albedo should have enough flexibility to deviate from its true value in order to respond to model errors in aerosol optical properties. We find that even with a priori errors as small as 0.01 to 0.02, the retrieval can accommodate model errors in the single scattering albedo.

We have only investigated the effect of a model error in the single scattering albedo here, but we expect the conclusions stated above to also hold for model errors in the phase function.

8.7 Effect of uncertainty in a priori meteorological data

Temperature profiles and surface pressures are input data for the Aerosol Layer Height algorithm and they are provided by ECMWF. The purpose of this section is to show that if the temperature profile or surface pressure is not fitted, the expected uncertainties in meteorological input data can cause significant biases in retrieved aerosol pressure. On the other hand, if we include the temperature profile or surface pressure in the state vector with a priori errors corresponding to these expected uncertainties, we find that the decrease of precision of retrieved aerosol pressure is negligible (temperature profile) or limited (surface pressure).

8.7.1 Temperature profile

Approach

We assume that for the stable meteorological conditions that are targeted by the ALH algorithm (cloud-free pixels), a representative temperature error is 1-2 K for temperature profiles on a 1° by 1° grid. If the temperature profile is incorrect, biases in the number density and oxygen absorption cross section propagate into aerosol pressure biases.

We first investigate the effect of a temperature error on retrieved aerosol pressure by adding a temperature offset of 1, 2.5 or 5 K to the mid-latitude summer profile in the simulation while not fitting the temperature profile in retrieval. Next, we investigate retrieval precision when varying the a priori error in the temperature profile between 0 and 5 K. We assume a correlation length of 6 km for the a priori errors (i.e. starting with perfectly correlated a priori errors for adjacent levels the correlation coefficient drops off by a factor 1/*e* every 6 km). The state vector then contains fit parameters p_{mid}, τ_0, A_s(758 nm) and A_s (770 nm) in the first case, while $T(p_i)$ is added in the second case.

Results

We simulated reflectance spectra for two aerosol mid pressures (800 and 500 hPa), two aerosol optical thicknesses (0.2 and 0.5) and two surface albedos (sea / ocean and vegetated land); a priori errors are the usual 500 hPa, 2.0 and 0.20, respectively. The solar zenith angle is 50° and the viewing direction is nadir.

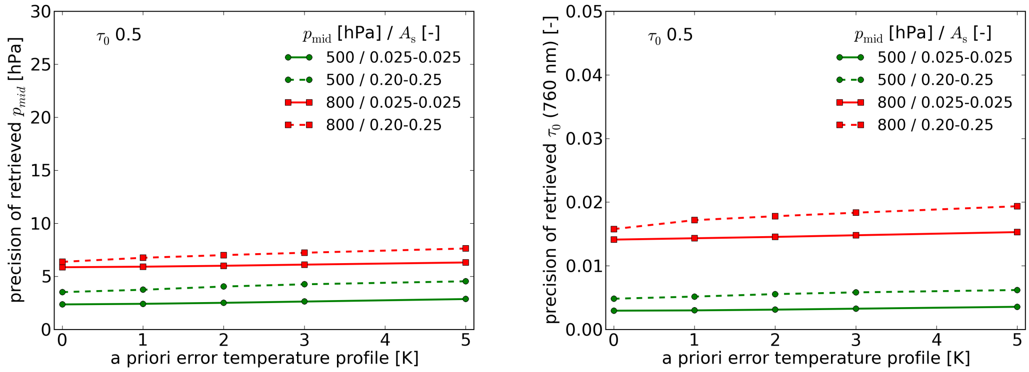

Figure 20: Precision of retrieved aerosol pressure (left plot) and optical thickness (right plot) as a function of the a priori error in the temperature profile. The aerosol layer has optical thickness of 0.5 and is located at 500 hPa (green lines) or 800 hPa (red lines), over sea / ocean (solid lines) or vegetated land (dashed lines). Retrieval precision shows the same behavior if the optical thickness is 0.2.

Table 16 gives retrieved aerosol mid pressures for every atmospheric scenario and for a temperature offset of 1 K if the temperature profile is not fitted. We have also tested offsets of 2.5 and 5 K, and found that pressure biases scale linearly with the temperature offset in this range (sometimes retrieval does not converge). In case of an offset of 1 K, pressure biases are of the order of a few hPa for retrievals over sea, but they increase up to 83 hPa for the aerosol layer with optical thickness of 0.2 at 800 hPa over vegetated land.

Table 16: Retrieved aerosol pressures for a number of atmospheric scenarios when an offset of 1 K is applied to the mid-latitude summer temperature profile in the simulation.

Surface albedo: A_s(758 nm)–A_s(770 nm)	**Aerosol optical thickness: τ_0**	**Aerosol pressure: p_{mid}**	**Pressure bias: retrieved - true**
0.025–0.025 (sea/ocean)	0.2	800 hPa	*+8 hPa*
		500 hPa	*-2 hPa*
	0.5	800 hPa	*+3 hPa*
		500 hPa	*-2 hPa*
0.2–0.25 (vegetated land)	0.2	800 hPa	*+83 hPa*
		500 hPa	*-33 hPa*
	0.5	800 hPa	*+20 hPa*
		500 hPa	*+3 hPa*

Figure 20 shows precision of retrieved aerosol pressure and optical thickness as a function of the a priori error in the temperature profile $T(p_i)$ for an aerosol layer with optical thickness of 0.5. The aerosol layer was at 500 or 800 hPa and over sea / ocean or vegetated land. We find that the deterioration of retrieval precision for these two parameters is negligible if the a priori error is increased from 0 K (temperature profile not fitted) up to 5 K. Note that we expect the uncertainty in ECMWF meteorological data to be smaller than (a 1-σ error of) 5 K. We have also verified that the pressure biases reported in Table 16 now disappear. Hence, fitting the temperature profile with an a priori value provided by ECMWF and a corresponding a priori error avoids the pressure biases described above while precision of retrieved aerosol pressure is retained.

8.7.2 Surface pressure

Approach

Salstein et al. (2008) report root-mean-square differences of 2-3 hPa between ground station observations and spatiotemporally interpolated 6-hourly 1° by 1° ECMWF surface pressures from operational analysis fields. These differences tend to be somewhat larger for high latitude and high topography regions. We take this value as a starting point for a sensitivity analysis of the effect of an error in the surface pressure.

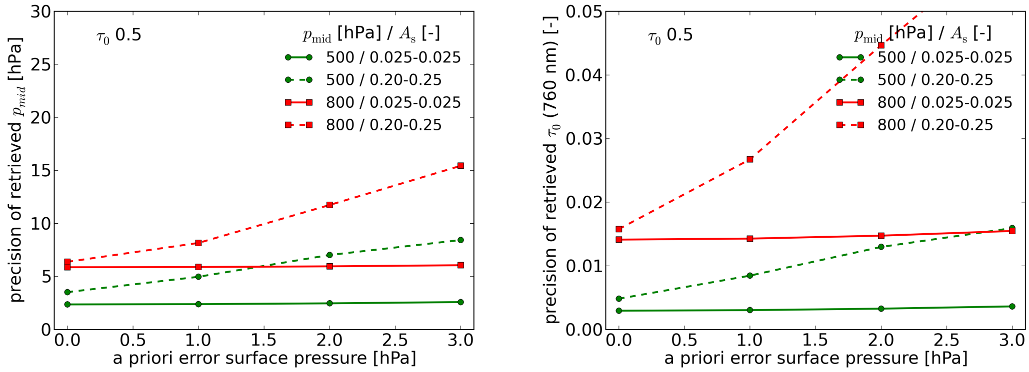

Figure 21: Precision of retrieved aerosol pressure (left plot) and optical thickness (right plot) as a function of the a priori error in the surface pressure. The aerosol layer has optical thickness of 0.5 and is located at 500 hPa (green lines) or 800 hPa (red lines), over sea / ocean (solid lines) or vegetated land (dashed lines). Retrieval precision shows the same behavior if the optical thickness is 0.2.

For the same atmospheric scenarios we first investigate the effect of a model error in the surface pressure by decreasing the true surface pressure by 2 and 4 hPa compared to the value of 1013 hPa assumed in retrieval. Next, we investigate retrieval precision when varying the a priori error in the surface pressure between 0 and 3 hPa. The state vector then contains fit parameters $p_{\rm mid}$, τ_0, A_s (758 nm) and A_s (770 nm) in the first case, while P_s is added in the second case.

Results

We simulated reflectance spectra for two aerosol mid pressures (800 and 500 hPa), two aerosol optical thicknesses (0.2 and 0.5) and two surface albedos (sea / ocean and vegetated land); a priori errors are the usual 500 hPa, 2.0 and 0.20, respectively. The solar zenith angle is 50^{circ} and the viewing direction is nadir.

Table 17 gives retrieved aerosol mid pressures for every atmospheric scenario when there is a model bias of 2 hPa in the surface pressure. We have also tested a model bias of 4 hPa and found that pressure biases double (sometimes retrieval does not converge). In case of a model bias of 2 hPa, pressure biases are of the order of a few hPa for retrievals over sea, but they increase up to 56 hPa for the aerosol layer with optical thickness of 0.2 at 800 hPa over vegetated land.

Table 17: Retrieved aerosol pressures for a number of atmospheric scenarios when the true surface pressure is 1011 hPa while the surface pressure assumed in retrieval is 1013 hPa.

Surface albedo: A_s(758 nm)–A_s(770 nm)	**Aerosol optical thickness: τ_0**	**Aerosol pressure: $p_{\rm mid}$**	**Pressure bias: retrieved - true**
0.025–0.025 (sea/ocean)	0.2	800 hPa	*+4 hPa*
		500 hPa	*+2 hPa*
	0.5	800 hPa	*+1 hPa*
		500 hPa	*+1 hPa*
0.2–0.25 (vegetated land)	0.2	800 hPa	*+56 hPa*
		500 hPa	*+43 hPa*
	0.5	800 hPa	*+10 hPa*
		500 hPa	*+7 hPa*

Figure 21 shows precision of retrieved aerosol pressure and optical thickness as a function of the a priori error in the surface pressure p_s for an aerosol layer with optical thickness of 0.5. The aerosol layer was at 500 or 800 hPa and over sea / ocean or vegetated land. We find that retrieval precision for these two parameters deteriorates somewhat if the a priori error is increased from 0 hPa (surface pressure not fitted) up to 3 hPa (surface pressure fitted). This deterioration of precision of retrieved pressure may be acceptable. However, we also find that the pressure biases in Table 17 are only partly removed when fitting surface pressure with an a priori error of 3 hPa (not shown). This indicates that the cost function is quite flat along the dimension of

surface pressure.

8.7.3 Conclusion

Expected uncertainties in the temperature profile and surface pressure can cause significant biases in retrieved aerosol pressure. Biases due to temperature uncertainties can be avoided by fitting the temperature profile with an appropriate a priori error. Biases due to surface pressure uncertainties can be partly removed by fitting the surface pressure with an appropriate a priori error. We therefore implement fitting of the temperature profile and surface pressure as options to the baseline algorithm. Perhaps it is possible to fit the temperature profile only in the lower atmosphere or even to simply fit an offset to the a priori profile. Based on the sensitivity analysis, we expect ECMWF temperature profiles on a 1° by 1° grid to be sufficient for our purposes. As to surface pressure, we find that accurate a priori data is needed. Compared against Salstein et al. (2008) [46], our results indicate that ECMWF surface pressures should preferably be delivered on a spatial grid finer than 1° by 1°.

8.8 Aerosol pressure biases due to cloud contamination

Since retrieved aerosol pressure does not depend strongly on the assumed particle model (Section 8.4), the Aerosol Layer Height algorithm is in principle capable of retrieving the height of any scattering layer—aerosols or clouds. However, since the spectrum provides little profile information, we do not consider multi-layered aerosol / cloud profiles in our forward model. Pixels are screened for the presence of clouds (Section 5.1) and we assume in retrieval that remaining scenes are fully cloud-free and dominated by a single aerosol layer (cf. the profile parameterizations for retrieval shown in Figure 5). However, residual clouds may still be present in the target pixel after having applied a cloud mask.

In this section, we illustrate biases in retrieved aerosol pressure for two typical cases of cloud contamination: an optically thin, homogeneous cirrus cloud and a low-altitude broken cumulus cloud. We show that expected biases for cloud-contaminated scenes put strict requirements on cloud masking, which are probably difficult to meet by the TROPOMI cloud masks. It is therefore necessary to devise post-retrieval tests to further remove retrievals likely affected by cloud contamination (e.g. analysis of χ^2 or residue spectrum).

Approach

We investigate the sensitivity of retrieved aerosol pressure to the presence of a cloud layer that is not accounted for in the forward model for retrieval. In addition to the aerosol layer, the atmospheric scenarios contain either a cirrus layer between 330 and 300 hPa with cloud fraction of 1.0 for which we vary cloud optical thickness, or a cumulus cloud between 910 and 890 hPa with optical thickness of 10 for which we vary the cloud fraction. The state vector includes the main fit parameters p_{mid}, τ_0, A_s (758 nm) and A_s (770 nm).

Results

We simulated reflectance spectra for a number of aerosol optical thicknesses (0.2, 0.5 and 1.0), aerosol mid pressures (800, 700 and 600 hPa) and surface albedos (sea / ocean and vegetated land). We only show results for the aerosol layer at 700 hPa over sea / ocean, which are representative of results for all the other scenarios tested. Cirrus and cumulus cloud particles have a single scattering albedo of 1.0 and a Henyey-Greenstein phase function with asymmetry parameter of 0.8. The fit parameters' *a priori* values are equal to their true values; *a priori* errors for aerosol pressure, optical thickness and surface albedo are the usual 500 hPa, 2.0 and 0.20, respectively. The solar zenith angle is 50° and the viewing direction is nadir.

Figure 22 shows retrieved aerosol pressures for the aerosol layer at 700 hPa over sea / ocean as a function of cirrus optical thickness (left plot) and cumulus cloud fraction (right plot). Retrieved aerosol pressures are biased towards cloud pressures and sometimes retrieval does not even converge. We find larger biases and more non-convergent retrievals for optically thinner aerosol layers and larger separations between cloud layer and aerosol layer. The surface albedo has no pronounced effect on retrieval biases or lack of convergence due to cloud contamination (not shown).

Focusing on the aerosol layer with optical thickness of 0.5, we see that aerosol pressure biases become larger than 100 hPa if the cirrus optical thickness rises above 0.1. We expect that a cirrus optical thickness of 0.1 will be below the detection limit of the VIIRS cloud mask [1]. For the same aerosol layer, aerosol pressure biases become larger than 50 hPa if the cumulus cloud fraction rises above 0.2. Thus, some of the clouds that will typically pass a cloud mask can cause substantial biases in retrieved aerosol pressure.

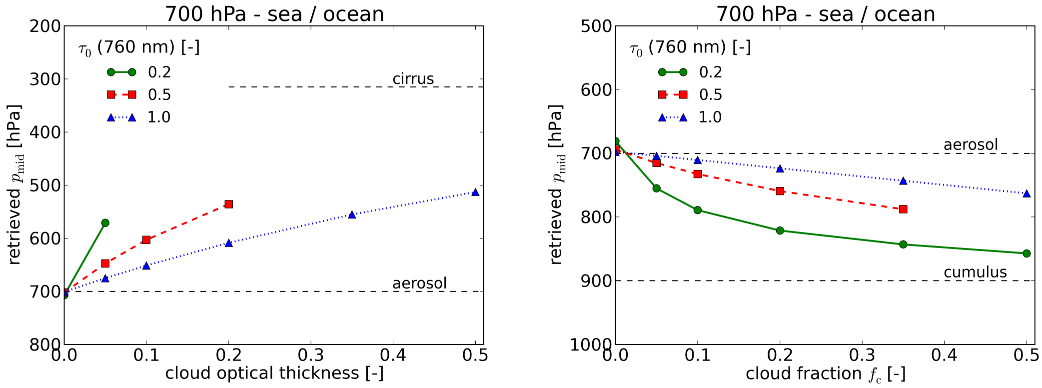

Figure 22: Effect of an unscreened cloud layer on retrieved aerosol pressure for three values of the aerosol optical thickness. Left: cirrus layer between 330 and 300 hPa with cloud fraction 1.0 and varying cloud optical thicknesses; right: cumulus cloud between 910 and 890 hPa with cloud optical thickness of 10 and varying cloud fractions. The aerosol layer is at 700 hPa over sea / ocean. The profile parameterization in retrieval assumes one scattering layer. Missing data points indicate that retrieval does not converge.

8.9 Alternative profile parameterization: aerosol layer with variable pressure thickness

The baseline algorithm assumes a single aerosol layer with a fixed pressure difference between top and bottom of the layer. We also implement alternative profile parameterizations as options to the baseline algorithm. These parameterizations are discussed in Section 6.2.2 and illustrated in Figure 5. The purpose of this section is to investigate precision if both mid pressure and pressure thickness are retrieved (Figure 5B). Precision of retrieved top pressure for the boundary layer pollution profile parameterization (Figure 5C) is illustrated in Section 8.4.2.

We compare precision of retrieved mid pressure p_{mid} and pressure thickness Δp for the alternative implementation with precision of retrieved mid pressure p_{mid} for the baseline algorithm. The state vector for the alternative implementation thus contains an additional profile parameter. We also investigate the dependence of precision on the a priori error in the surface albedo. The results show that if pressure thickness is included in the fit, precision of retrieved mid pressure hardly deteriorates. We also find that mid pressure is much easier to determine from the measurement than pressure thickness.

Approach

The current implementation of the algorithm with DISAMAR fits top pressure and bottom pressure. For a proper comparison of the alternative profile parameterization with the baseline parameterization, we report errors in mid pressure and pressure thickness, which are calculated from errors in top and bottom pressure. The state vector then basically contains fit parameters p_{mid}, τ_0, A_s (758 nm) and A_s (770 nm) with Δp being added for the alternative implementation.

Results

We simulated reflectance spectra for a number of aerosol optical thicknesses (0.2, 0.5 and 1.0), aerosol mid pressures (800 and 500 hPa) and surface albedos (sea / ocean and vegetated land). We assume a somewhat more realistic pressure thickness of 100 hPa in simulation and retrieval, because the spectral shape of derivatives for mid pressure and pressure thickness can also depend on this parameter.

We show results for two scenarios, which form the extremes between which the results for all other scenarios are. The a priori error in the surface albedo is varied between 0.001 and 1.0; a priori errors for mid pressure and pressure thickness are 354 hPa and 707 hPa, respectively (errors of 500 hPa for fit parameters top and bottom pressure); and the a priori error for aerosol optical thickness is 2.0. The solar zenith angle is 50° and the viewing direction is nadir.

Figure 23 shows precision of retrieved mid pressure and pressure thickness as a function of the *a priori* error in the surface albedo for an aerosol layer with optical thickness of 0.5 at 500 hPa over vegetated land and an aerosol layer with optical thickness of 0.5 at 800 hPa over sea / ocean. The green solid line represents results for the baseline algorithm; red dashed lines indicate results for the alternative profile parameterization.

If pressure thickness is also fitted, the deterioration of precision of retrieved mid pressure is limited and for

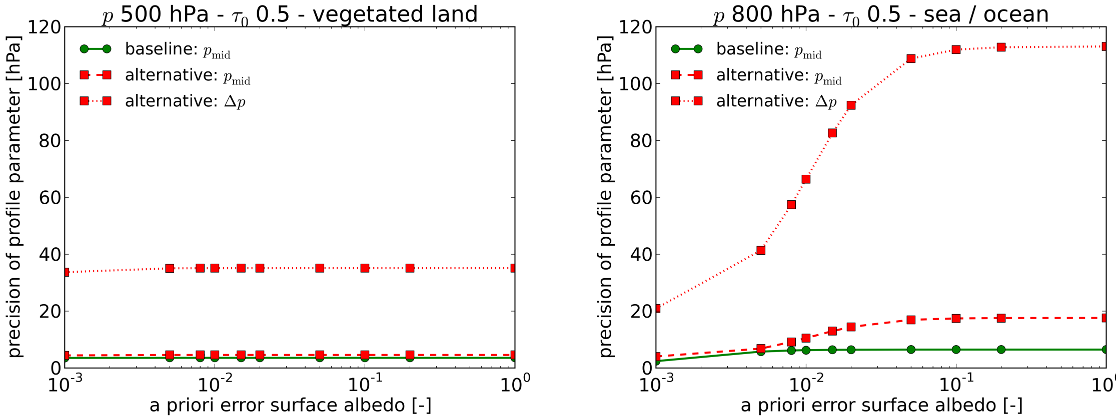

Figure 23: Precision of retrieved profile parameters as a function of the *a priori* error in the surface albedo for the baseline profile parameterization of a layer with fixed pressure thickness and the alternative implementation of a layer with variable pressure thickness. Left: aerosol layer with optical thickness of 0.5 at 500 hPa over vegetated land; right: aerosol layer with optical thickness of 0.5 at 800 hPa over sea / ocean. The baseline algorithm fits mid pressure (green solid line) and the alternative implementation fits mid pressure and pressure thickness (red dashed lines). Note the logarithmic scale of the x-axis.

many scenarios precision of retrieved mid pressure even is the same. Errors in mid pressure and pressure thickness are thus not highly correlated and in this respect it is a viable option to include pressure thickness in the state vector. However, we also see that precision of retrieved pressure thickness is much poorer than precision of retrieved mid pressure, although for some scenarios precision of pressure thickness may still be acceptable (e.g. below 50 hPa).

Over the range of *a priori* errors in the surface albedo, the elevated layers at 500 hPa hardly show an improvement in precision of profile parameters. For the near-surface layer at 800 hPa, precision of pressure thickness starts improving if the *a priori* error becomes smaller than 0.01 to 0.03. Here, accurate *a priori* knowledge of the surface albedo may in principle benefit retrieval, although we do not expect available a priori knowledge to be more accurate than this threshold.

8.10 Interference of chlorophyll fluorescence

Terrestrial vegetation exhibits fluorescence in the red and near-infrared wavelength range, which may thus interfere with aerosol retrieval from the O_2 A band. The purpose of this section is to briefly illustrate the effect of chlorophyll fluorescence on aerosol retrieval from the O_2 A band and to show that fluorescence and aerosol parameters can be retrieved simultaneously. A detailed discussion of aerosol retrieval from the O_2 A band in the presence of chlorophyll fluorescence can be found in Sanders and De Haan (2013) [47].

Approach

For an aerosol layer over vegetated land with typical fluorescence emissions, we compare accuracy and precision of retrieved aerosol pressure when fitting fluorescence emissions with accuracy and precision when not fitting emissions. We assume an average fluorescence emission at the O_2 A band of $1.0 \cdot 10^{12}$ photons s^{-1} cm^{-2} sr^{-1} nm^{-1}; as a maximum value we take three times the average fluorescence emission. These values are in agreement with Joiner et al. (2011) [27], although somewhat large compared to Guanter et al. (2012) [21] and Frankenberg et al. (2011) [18]. The state vector contains parameters p_{mid}, τ_0, A_s (758 nm) and A_s (770 nm), while F_s (758 nm) and F_s (770 nm) are added if fluorescence is fitted.

Results

We have simulated retrieval of aerosol layers at a number of different pressures over vegetated land with varying optical thickness. We report results for an aerosol layer at 600 hPa. True values, *a priori* values and *a priori* errors can be found in Table 18. The solar zenith angle is 50° and the viewing direction is nadir.

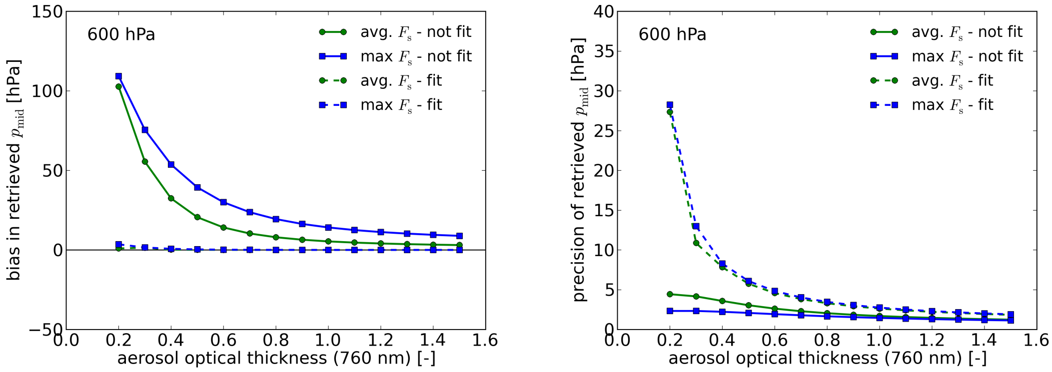

Figure 24: Accuracy (left plot) and precision (right plot) of retrieved aerosol pressure as a function of optical thickness when the vegetated land surface exhibits chlorophyll fluorescence. Solid lines correspond to a retrieval in which fluorescence is present in the simulation but not accounted for in the forward model for retrieval. Dashed lines correspond to a retrieval in which fluorescence emissions are included in the forward model and retrieved simultaneously with aerosol parameters.

Table 18: True values, a priori values and a priori errors used in the retrieval simulations of Figure 14 investigating the sensitivity of retrieval to the assumed single scattering albedo.

Fit parameter	**True value**	**AP value**	**AP error (1-σ)**
p_{mid}	600 hPa	True	500 hPa
τ_0 (760 nm)	Range: 0.2 – 1.5	True	2.0
A_s (758 nm) – A_s (770 nm)	0.20 – 0.25 (vegetated land)	True	0.2
A_s (758 nm) – A_s (770 nm)	$1.0 \cdot 10^{12}$ – $1.0 \cdot 10^{12}$ 'avg. F_s' $3.0 \cdot 10^{12}$ – $3.0 \cdot 10^{12}$ 'max F_s' photons s^{-1} $cm^{-2} sr^{-1}$ nm^{-1}	0.0–0.0	$1.0 \cdot 10^{12}$ – $1.0 \cdot 10^{12}$ photons s^{-1} $cm^{-2} sr^{-1}$ nm^{-1}

Figure 24 compares accuracy (left plot) and precision (right plot) of retrieved aerosol pressure when fluorescence emissions are fitted and when they are not. We assume fluorescence emissions to be absent a priori. If fluorescence emissions are ignored in the forward model, significant pressure biases occur, particularly for optically thinner layers. If the aerosol layer is placed lower in the atmosphere, we also find that retrieval often does not converge. Hence it is important to take fluorescence emissions into account in retrieval.

When fitting fluorescence emissions, retrievals converge and pressure biases disappear. For small aerosol optical thicknesses, precision of retrieved aerosol pressure deteriorates to some extent. There is of course a trade-off between accuracy and precision. Preliminary tests indicate that retrieval is stable when fitting fluorescence parameters. Even when *a priori* values differ strongly from true values, the true state is retrieved.

One may consider a fast fluorescence retrieval using Fraunhofer lines in a pre-processing step for the actual aerosol height retrieval (cf. Buchwitz et al., 2013 [4]). Fluorescence emissions from the Fraunhofer line retrieval may then provide a constraint for the O_2 A band algorithm. However, an a priori fluorescence emission from such a pre-retrieval step also has an associated error (e.g. [4]). Sanders and De Haan (2013) [50] have investigated the dependence of retrieval precision on the a priori error in the fluorescence emission. For the cases considered, they find that precision of retrieved aerosol parameters hardly improves if the *a priori* error is decreased towards values that can typically be associated with a Fraunhofer line retrieval. This then indicates that if the objective of the O_2 A band retrieval is the retrieval of aerosol parameters, precision will hardly benefit from such a pre-retrieval step. Providing a better a priori value in the sense of a starting value for the fit might still help to improve the convergence rate or convergence to the global χ^2-minimum in case of a strongly non-linear forward model. This needs to be further investigated.

8.11 Instrumental errors

In this section we investigate the effect of instrumental errors on retrieval. Instrumental errors most relevant to the ALH algorithm are errors related to the Level-1b stray light correction, wavelength calibration and slit function calibration. We show that biases in retrieved pressure for typical instrument errors can be significant, depending on the scenario.

8.11.1 Stray light

Approach Part of the Level-1b processor is a stray light correction algorithm, which corrects the output of the detector for the stray light signal [RD16]. This correction step will very likely not remove the full stray light signal under all conditions. Here we investigate the effect of uncorrected stray light on retrieval. Since optical paths for the radiance and irradiance are almost identical, we assume the same amount of stray light as a fraction of the respective continuum signal. Stray light is modeled as a spectrally constant additive offset to the radiance and irradiance spectrum. Offsets are defined as percentages of the continuum (ir)radiance at 758 nm. Note that the relative stray light contribution is much larger inside the absorption band. We investigate offsets of 1%, 3% and 5%. The state vector contains fit parameters p_{mid}, τ_0, A_s (758 nm) and A_s (770 nm).

Results We simulated retrievals for an aerosol layer with optical thickness of 0.5 at 700 hPa over sea / ocean and vegetated land); *a priori* errors are the usual 500 hPa, 2.0 and 0.20, respectively. The solar zenith angle is 50° and the viewing direction is nadir.

Table 19 gives pressure biases and optical thicknesses in case of stray light offsets. Within precision margins of retrieved aerosol pressure, pressure biases scale linearly with offsets. For this scenario, a stray light offset of 1% gives a pressure bias of 6 hPa (sea / ocean) or 13 hPa (vegetated land).

Stray light for the radiance is expected to have the largest impact on retrieval, as the contribution is relatively large at strong absorption lines of the O_2 A band. Stray light for the earth radiance can in principle be fitted, but an instrument stray light model is needed in that case. Note that the stray light signal can be strongly dependent on wavelength.

Table 19: Pressure biases and retrieved optical thicknesses in case of additive offsets applied to the radiance and irradiance spectrum. The aerosol layer has an optical thickness of 0.5 and is at 700 hPa over sea / ocean or vegetated land. Stray light offsets are constant with wavelength and they are defined as percentages of the (ir)radiance at 758 nm.

Surface albedo: $\mathbf{A_s}$ **(758 nm) –** $\mathbf{A_s}$ **(770 nm)**	**Stray light offset**	**Pressure bias: retrieved - true**	**Pressure precision**	**Retrieved optical thickness**
0.025 – 0.025 (sea/ocean)	+1%	*-6 hPa*	3.9 hPa	0.49
	+3%	*-17 hPa*	3.9 hPa	0.48
	+5%	*-28 hPa*	3.8 hPa	0.47
0.20 – 0.25 (vegetated land)	+1%	*-13 hPa*	5.1 hPa	0.49
	+3%	*-37 hPa*	5.2 hPa	0.48
	+5%	*-61 hPa*	5.2 hPa	0.47

8.11.2 Wavelength calibration

Approach

A wavelength calibration of the solar irradiance measurement is foreseen in the Level-1b processor. The radiance measurement, however, is only assigned a nominal wavelength grid [RD16]. The reason for this is that inhomogeneous illumination of the slit (e.g. partly cloudy scenes) causes the most significant changes to the radiance wavelength scale. An accurate wavelength calibration of the radiance measurement should thus be part of the Level-2 processor, as inhomogeneous slit illumination is an atmospheric effect. Note, however, that inhomogeneous illumination of the slit is not expected for the Aerosol Layer Height algorithm, since the focus of this algorithm are cloud-free scenes

Here we investigate the effect of an error in the nominal wavelength grid for the radiance. The nominal radiance wavelength grid is shifted by 0.005 nm, 0.01 nm and 0.02 nm with respect to the true grid. We remark that the spectral bin size is 0.10 nm, so that a wavelength shift of 0.01 nm or 10% is already quite large. The

state vector contains fit parameters p_{mid}, τ_0, A_s (758 nm) and A_s (770 nm).

Results
We simulated retrievals for an aerosol layer with optical thickness of 0.5 at 700 hPa over sea / ocean and vegetated land); *a priori* errors are the usual 500 hPa, 2.0 and 0.20, respectively. The solar zenith angle is 50° and the viewing direction is nadir.

Table 20 gives pressure biases and optical thicknesses in case of wavelength shifts applied to the nominal radiance wavelength grid. Within precision margins of retrieved aerosol pressure, pressure biases scale linearly with offsets. For this scenario, a wavelength shift of 0.005 nm gives a pressure bias of 3 hPa (sea / ocean) or 11 hPa (vegetated land).

Table 20: Pressure biases and retrieved optical thicknesses in case the width of the radiance and irradiance slit functions in the simulation differs from the width of the slit functions assumed in the retrieval. The aerosol layer has an optical thickness of 0.5 and is at 700 hPa over sea / ocean or vegetated land. The FWHM of the radiance and irradiance slit functions in retrieval is 0.5 nm.

Surface albedo: A_s (758 nm) – A_s (770 nm)	**FWHM slit functions in the simulation**	**Pressure bias: retrieved - true**	**Pressure precision**	**Retrieved optical thickness**
0.025 – 0.025 (sea/ocean)	0.51 nm	*-1 hPa*	3.9 hPa	0.50
	0.52 nm	*-2 hPa*	3.8 hPa	0.50
	0.54 nm	*-6 hPa*	3.8 hPa	0.50
0.20 – 0.25 (vegetated land)	0.51 nm	*+3 hPa*	4.9 hPa	0.51
	0.52 nm	*+5 hPa*	4.7 hPa	0.53
	0.54 nm	*+5 hPa*	4.5 hPa	0.55

It is possible to fit the width of the slit function as well as its nominal wavelength (see previous section) in the main algorithm. As an alternative, we may also consider performing the wavelength calibration in a pre-processing step, if this is accurate enough. Removing the wavelength shift from the state vector when performing online radiative transfer calculations will probably increase computation speed.

9 Application to GOME-2 spectra

9.1 Introduction

ESA's AEROPRO project was executed at KNMI between May 2012 and March 2014. AEROPRO stands for Aerosol Profile Retrieval Concept Development and Validation for Sentinel-4. The purpose of the project is to pre-develop an aerosol profile retrieval concept for the UVN spectrometer aboard the Meteosat Third Generation - Sounder (MTG-S) platform. The AEROPRO project has been run in close collaboration with the Sentinel-5 Precursor / TROPOMI project: the aerosol height algorithm used for AEROPRO is basically the same retrieval algorithm as described in this document. Within the AEROPRO project, the aerosol height algorithm has been tested on spectra measured by the Thermal and Near Infrared Sao ensor for Carbon Observations Fourier-Transform Spectrometer (TANSO-FTS) aboard the Greenhouse Gases Observing Satellite (GOSAT [34]) and on spectra measured by GOME-2 on MetOp-A.

Within AEROPRO Task 8, we have applied the aerosol height retrieval algorithm to O_2 A band observations from GOME-2. Here, we will summarize the main findings from this work package. The combined Technical Notes 8a and 8b describe the work package in detail. GOME-2 has a spectral resolution of about 0.53 nm at the O_2 A band, which is comparable to TROPOMI's anticipated resolution. GOME-2 pixel sizes are, however, much larger than TROPOMI pixels: they are typically 80 km x 40 km (across x along). The general approach is to apply the algorithm in a number of extensive retrieval experiments to GOME-2 observations of a selected set of well-described aerosol events and to subsequently validate retrieval results with ground-based and airborne lidar measurements.

9.2 GOME-2 pixel selection

First, we identified sixteen aerosol scenes that were at least partly cloud-free and for which lidar observations were available around the time of overpass. The aerosol events cover the time period between July 2009 and July 2013. They concern desert dust near the coast of Africa and over the Iberian Peninsula, volcanic ash over Europe, smoke from forest fires in North-America transported across the Atlantic, aerosols over the Aegean Sea, and various boundary layer aerosol and multi-layered aerosol cases over the Netherlands.

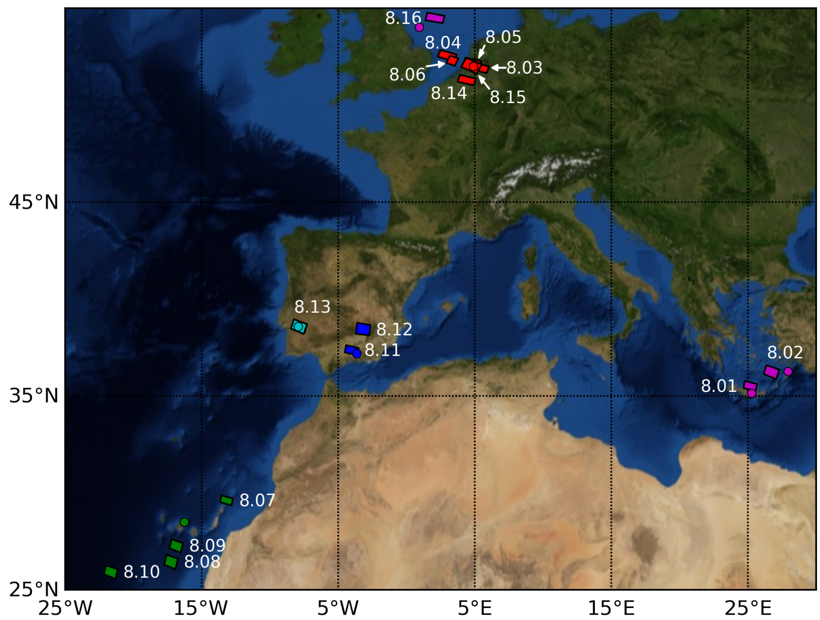

Figure 25: Sixteen GOME-2 pixels (quadrilaterals) and corresponding lidar locations (circles) used in retrieval experiments. The GOME-2 observations are of various strong aerosol events between July 2009 and July 2013. For every observation we collected lidar measurements for validation.

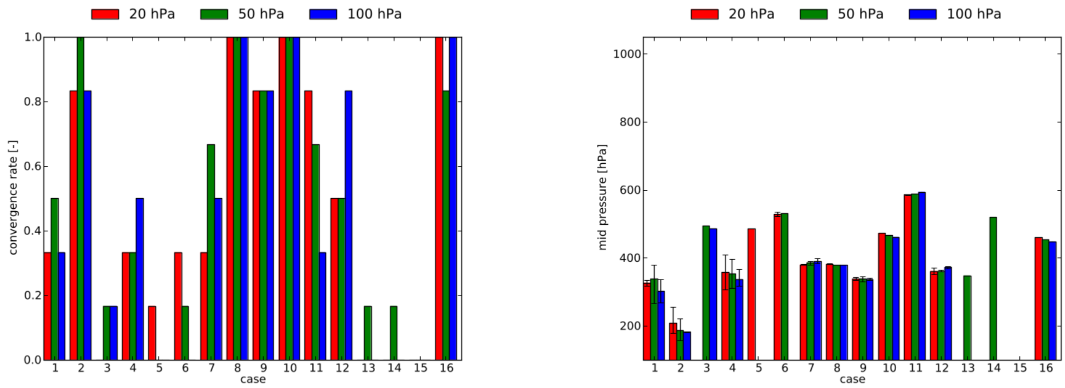

Figure 26: Convergence rate (left panel) and retrieved aerosol mid pressures (right panel) for every aerosol case in the first experiment investigating the effect of the aerosol layer's assumed pressure thickness. Assumed mid pressures are 20 hPa, 50 hPa or 100 hPa. Values for retrieved mid pressure are averages for six runs (initial values). Whiskers here indicate the max-min range of retrieval solutions; often they are barely visible.

Second, we selected the optimal GOME-2 pixel for every scene to be used in retrieval experiments. We made a trade-off between a number of criteria, of which the two most important are spatial collocation with the lidar observation and cloud-free conditions. Often, these criteria could not be fulfilled at the same time. For example, although a lidar observation was available, the GOME-2 pixel collocated with the lidar was not entirely cloud-free (due to the large ground pixel size). Cloud conditions were assessed using FRESCO cloud fractions, a cloud mask from the Advanced Very High Resolution Radiometer (AVHRR), rgb images from the Moderate-Resolution Imaging Spectroradiometer (MODIS) and Polarisation Measurement Devices (PMD) radiance variability. Figure 25 shows the selected GOME-2 pixels (quadrilaterals numbered from 8.01 to 8.16) and the corresponding lidar locations (circles).

9.3 Retrieval experiments

9.3.1 General setup

We made a spectral fit of reflectance between 758 nm and 770 nm and used the elevated layer model (Figure 5A). We assumed a single scattering albedo of 0.95 and a Henyey-Greenstein phase function with asymmetry parameter of 0.7. GOME-2 Level-1b data from processor version 5.3 and meteorological data from ECMWF Reanalysis (ERA) Interim at 0.5° by 0.5° resolution were read. To increase convergence we multiplied the noise error as reported in Level-1b files by two. Furthermore, the oxygen absorption cross section included the three major isotopologues as well as collision-induced absorption and line mixing. The default fit parameters are aerosol mid pressure, aerosol optical thickness and surface albedo (two wavelength nodes).

For every case and every experimental condition, we ran retrieval for six different sets of starting values to test stability of the algorithm. In the following, the convergence rate is defined as the number of converged retrievals divided by six. Here, we will describe three retrieval experiments.

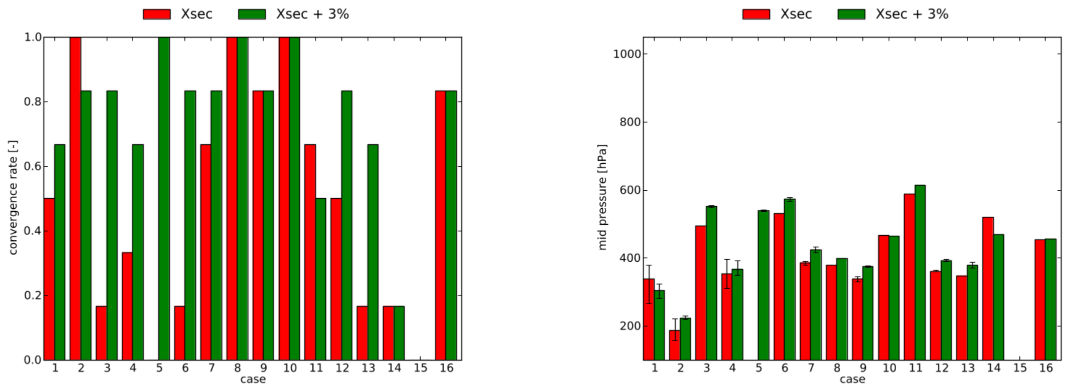

Figure 27: Convergence rate (left panel) and retrieved aerosol mid pressures (right panel) for every aerosol case in the second experiment investigating the effect of an increase of the oxygen absorption cross section by 3% (‘Xsec + 3%’). The baseline experiment against which results are compared (‘Xsec’) is the first experiment (assumed pressure thickness of 50 hPa). Values for retrieved mid pressure are averages for six runs (initial values). Whiskers indicate the max-min range of retrieval solutions.

9.3.2 Varying aerosol layer’s assumed geometric thickness

In the first experiment, we varied the aerosol layer’s geometric thickness for the default retrieval setup. We compare pressure thicknesses of 20 hPa, 50 hPa and 100 hPa. The convergence rate for every case is shown in Figure 26. Also shown are retrieved mid pressures averaged over the six runs. Whiskers indicate the full range (max-min) of retrieval solutions. Note that whiskers are often barely visible because this range is small.

We observe that for some pixels all runs converge, but for other pixels there is no convergence. Also, we see that retrieval solutions are unique: If retrieval converges, it converges to (approximately) the same solution. Retrieved mid pressures are, however, unrealistically low. Finally, there is a small effect of assumed mid pressure, which we will not further discuss here.

9.3.3 Increasing oxygen absorption cross section by 3%

The O_2 A band is often used in trace gas retrieval algorithms to account for atmospheric scattering. Research groups working on CO_2 and CH_4 retrievals using GOSAT have suggested to increase the oxygen absorption cross section by 1-4% [7][65][10][6]. It is suggested that part of this scaling is needed to correct for inaccuracies in current absorption cross section data and part of it is needed to compensate for unknown GOSAT instrument errors. In the second experiment, we investigate the effect on retrieved aerosol pressure of an increase of the oxygen absorption cross section by 3%. This value is in agreement with Butz et al. (2013) [7] and Crisp et al. (2012) [10].

The absorption cross section, including line mixing and collision-induced absorption, is multiplied by 1.03. As a baseline we take the first experiment (pressure thickness of 50 hPa). Convergence rate and retrieved mid pressures are shown in Figure 27.

We observe that overall convergence improves, which suggests that the forward model has improved. We are not aware of anyone having reported oxygen absorption cross section scaling for GOME-2 retrievals. There

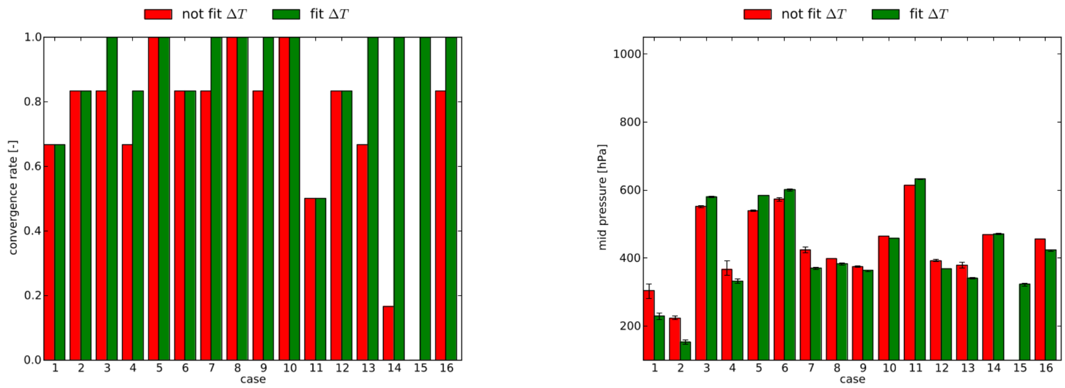

Figure 28: Convergence rate (left panel) and retrieved aerosol mid pressures (right panel) for every aerosol case in the third experiment investigating the effect of including a temperature offset to the *a priori* profile in the state vector ('fit ΔT'). The baseline experiment against which results are compared ('not fit ΔT') is the second experiment. Values for retrieved mid pressure are averages for six runs (initial values). Whiskers indicate the max-min range of retrieval solutions.

is also a strong tendency for retrieved aerosol mid pressure and optical thickness (not shown) to increase: mid pressure changes by about 20 hPa to 50 hPa.

9.3.4 Fitting a temperature offset

In the third experiment, we investigate the effect of also fitting a temperature offset to the a priori temperature profile. A priori profiles are taken from ECMWF fields at 0.5° by 0.5° resolution. Thus, the resolution of meteorological data is comparable or even finer than the GOME-2 ground pixel size. The convergence rate and retrieved mid pressures are shown in Figure 28. As a baseline we take the second experiment.

We observe that the convergence rate further improves. Most cases now converge in five or six out of six runs. Although we have an additional fit parameter, the number of iterations interestingly stays the same (here: ranging from 3 to 11 iterations with an average of 6.1). Apparently, fitting a temperature offset helps to bring the modeled spectrum into much better agreement with the measurement. There is no pronounced effect of fitting a temperature offset on other parameters (small correlations). The retrieved temperature offset, however, is quite large and always negative: it is typically between -5 and -9 K. This means that the entire temperature profile is shifted in retrieval by 5 to 9 K. Such a large shift is unexpected if the temperature offset is supposed to correct for inaccuracies in meteorological data, in which case one would also expect to retrieve random offsets. Perhaps the retrieved temperature offset is related to additional spectroscopic uncertainties.

9.3.5 Residuals

Residuals from the last experiment are shown in Figure 30. These residuals are representative of residuals found in the other experiments. Residuals are defined as the difference between measured and fitted reflectance as a percentage of the measured reflectance. We find residuals up to 7% and we also see that they have a clear systematic shape. Residuals are comparable in magnitude or smaller compared to residuals reported

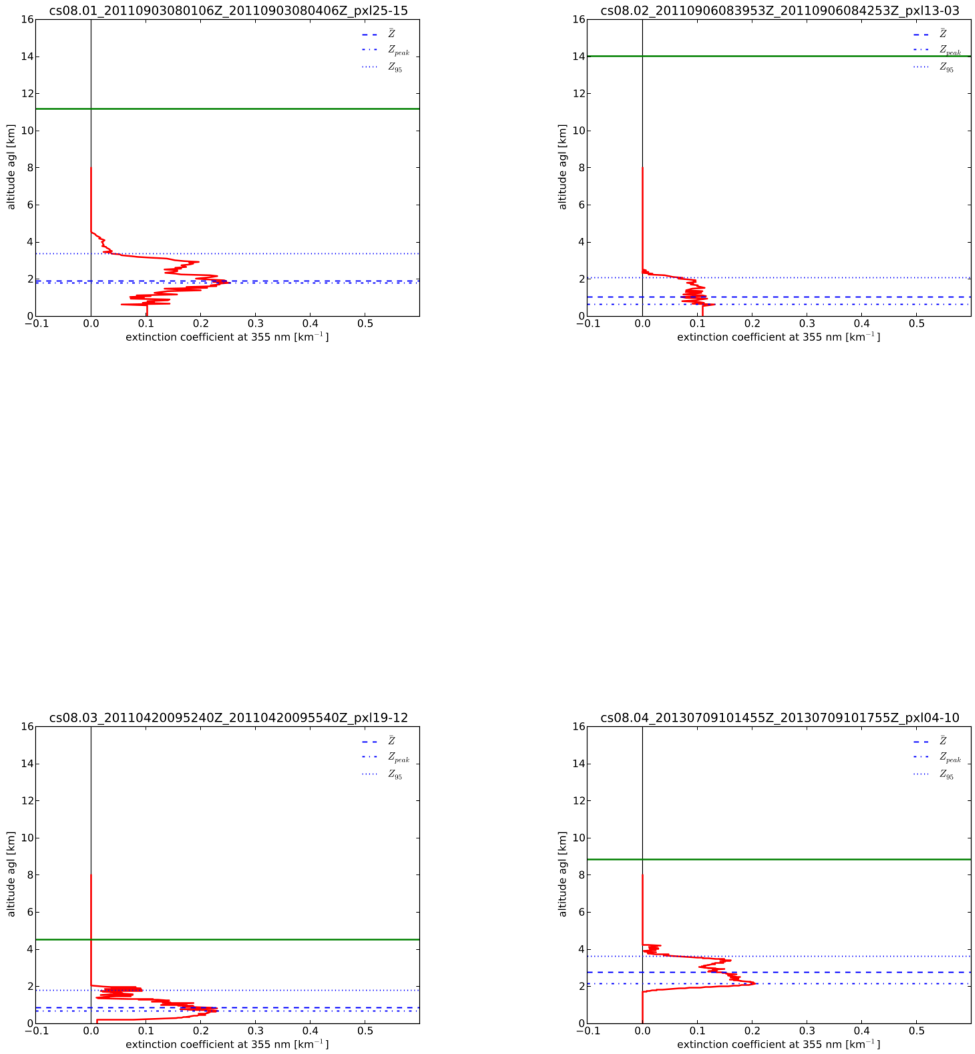

Figure 29: Four example lidar extinction profiles (red line) with corresponding retrieved aerosol heights (green line). Blue dashed lines correspond to various characteristic heights of the lidar profile.

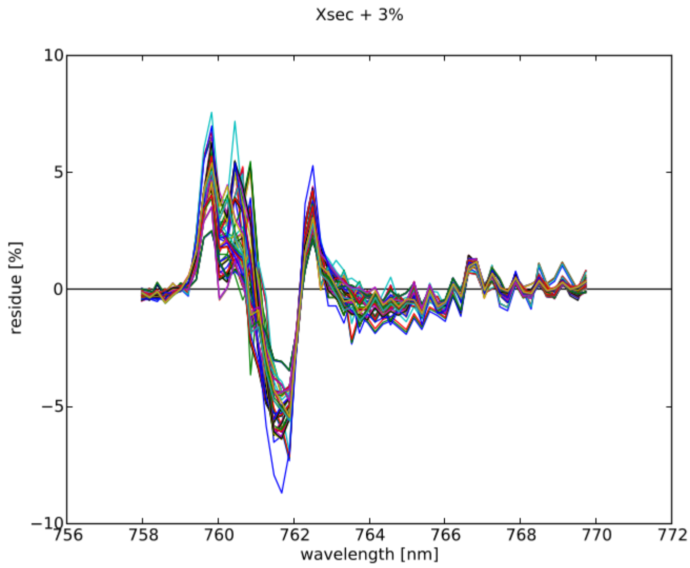

Figure 30: Residuals for every case and every run in the third experiment. Residuals are defined as the difference between measured and fitted reflectance as a percentage of the measured reflectance.

in the literature for similar retrievals from GOME [60] and SCIAMACHY [32]. We also observe comparable spectral features.

9.4 Comparison with lidar observations

As already mentioned, retrieved aerosol mid pressures are unrealistically low (aerosol layer too high in the atmosphere). Note that we have paid particular attention to cloud masking, so we do not expect our results to be explained by cirrus contamination. Figure 29 shows four example lidar profiles and corresponding retrieved heights (in green).

9.5 Retrieval simulation: boundary layer aerosol

To better understand the retrieval results we turn to simulations. In Section 8.8 we have investigated retrieval in case of two scattering layers. More in particular, we have investigated the simultaneous presence of an aerosol layer and a residual cloud layer. There, we found that retrieved height (assuming a single layer in the retrieval) is biased towards the cloud layer and that this bias increases with increasing cloud optical thickness (Figure 22). In case of multilayer profiles, we intuitively expect retrieved height for a single-layer model to be indeed some sort of weighted average of the actual profile. However, extinction profiles that we collected for the GOME-2 retrievals often contain significant boundary layer aerosol. Here, we investigate retrieval in case of the simultaneous presence of an elevated aerosol layer and boundary layer aerosols.

In the simulation, we have elevated aerosols between 500 hPa and 600 hPa and boundary layer aerosols between 910 hPa and the surface. In retrieval we assume a single scattering layer with fixed pressure thickness of 100 hPa. The aerosol is modeled with a single scattering albedo of 1.0 and a Henyey-Greenstein phase function with asymmetry parameter of 0.7. The solar zenith angle is 60° and the viewing direction is nadir.

Figure 31 shows retrieved aerosol pressure as a function of the aerosol optical thickness in the boundary layer for a surface albedo of 0.03. Results are given for three optical thicknesses of the upper aerosol layer in the simulation. Note that on the y-axis we have now indicated the retrieved layer's top pressure. Thus, a retrieved top pressure of 300 hPa means that the layer is between 300 hPa and 400 hPa. If there is no boundary layer aerosol, retrieved (top) pressure is 500 hPa and there is no bias, as expected. Surprisingly, when the optical thickness of boundary layer aerosols increases, retrieved top pressure moves to lower (!) pressures.

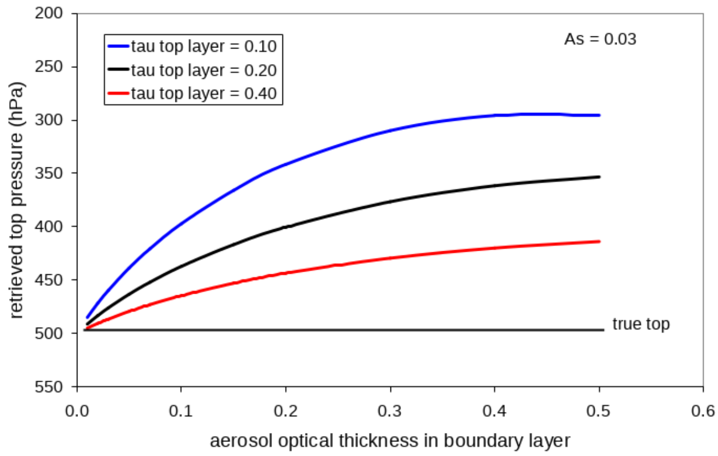

Figure 31: Retrieved aerosol top pressure as function of the aerosol optical thickness in the boundary layer for three values of the optical thickness of the upper (top) aerosol layer. Here the true surface albedo is 0.03.

Figure 32 is the same as Figure 31, but for a surface albedo of 0.20 instead of 0.03. This figure shows that the bias in retrieved pressure of the aerosol layer is larger for the brighter surface. Further, convergence problems arise when the surface albedo is 0.20 and the aerosol optical thicknesses in the boundary layer is large.

Suppose that the goal of the algorithm is to retrieve the height of elevated layers (e.g. volcanic ash). As an aerosol optical thickness (at 760 nm) of 0.05 - 0.10 for the boundary layer is quite common, retrieved aerosol pressure will then often be underestimated by 20 hPa (optically thick upper layer and dark surface) to 150 hPa (optically thin upper layer and bright surface).

Figure 33 shows the residue of the fit when the aerosol optical thickness for the boundary layer and for the elevated layer are 0.10, and the surface albedo is 0.20. Results are shown for different sets of fit parameters. Table 21 gives retrieved values and values for parameters that are not fitted. Only if all three parameters A_s, τ_0 of the elevated layer, and p_{mid} of the elevated layer are fitted do we get a large pressure bias. Note also that the residue is smallest when all three parameters are fitted. Table 22 shows that errors in the three parameters are strongly correlated, especially for the pressure and the aerosol optical thickness of the elevated layer. Hence,

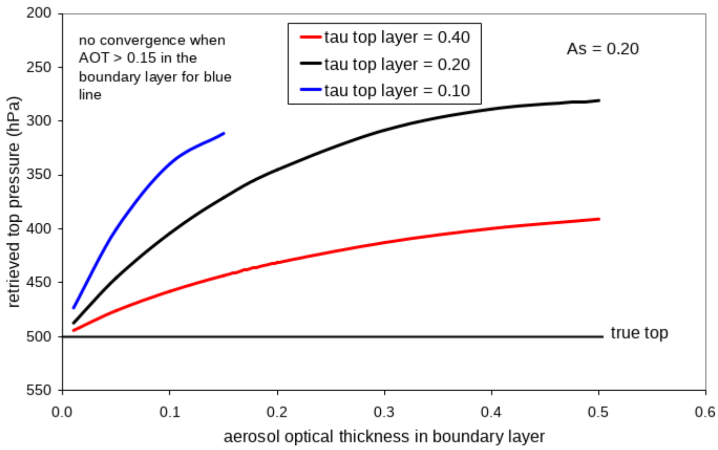

Figure 32: Same as the previous figure, but for a true surface albedo of 0.20 instead of 0.03.

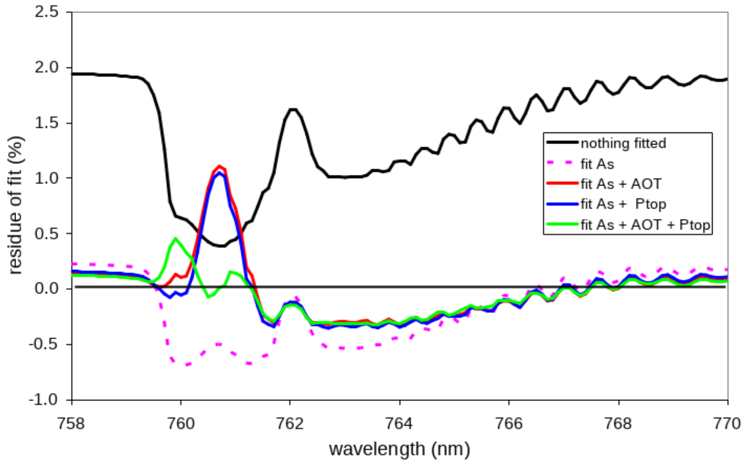

Figure 33: Residue of the fit in percent for different sets of fit parameters. The black curve shows the effect of aerosol in the boundary layer, which increases the reflectance by about 2% in the continuum and 0.4% in the deepest part of the O_2 A band. If only the surface albedo is fitted (dotted line) residues up to ~0.7% occur in the O_2 A band. If the surface albedo is fitted together with the pressure of the aerosol layer (blue line) or the aerosol optical thickness (red line) we get approximately the same residue with a maximum of about 1%. If all three parameters are fitted (bright green line) the residue reduces substantially, but does not vanish.

model errors (here: ignoring aerosol in the boundary layer) can lead to large biases.

We remark that the residue of the fit becomes larger when the optical thickness of the aerosol in the boundary layer increases (not shown). Hence there is some information in the spectrum about the aerosol in the boundary layer.

Table 21: Parameter values for the various sets of fit parameters in the retrieval experiments of Figure 33.

	True values	**fit A_s**	**fit A_s + τ_0**	**fit A_s + p_{top}**	**fit A_s + p_{top} + τ**
A_s	0.2	0.2039	0.2045	0.2041	0.2057
τ_0	0.1	0.1	0.0882	0.1	0.0500
p_{top}	500	500	500	528.89	340.48

Table 22: Correlation matrix (r^2) for the posteriori error when all three parameters are fitted (green line in Figure 33).

	A_s	τ_0	**p_{top}**
A_s	1.00000	-0.97995	0.96972
τ_0	-0.97995	1.00000	-0.99572
p_{top}	0.96972	-0.99572	1.00000

We can now speculate as to the mechanism behind these effects. We assume that a priori values agree with parameters for the upper aerosol layer. In case boundary layer aerosols are present, the surface albedo is increased in the retrieval in order to get agreement outside the absorption band. In the deepest part of the O_2 A band, we do not have agreement because in the retrieval model light transmitted by the elevated aerosol layer has to be reflected by the surface in order to travel back to the instrument, while in the actual atmosphere light can be backscattered by aerosol present in the boundary layer. This leads to too much absorption for the retrieval model in the deepest part of the O_2 A band. To compensate for this absorption the retrieval puts the aerosol layer at lower pressures.

9.6 Conclusion

When we apply the aerosol layer height algorithm to GOME-2 observations we find residuals that are already quite acceptable given that we assume a single elevated layer and the same Henyey-Greenstein aerosol throughout. We also find that retrieval is stable: in the last experiment we have good convergence, find unique solutions and have an acceptable number of iterations. However, retrieved aerosol pressures are unrealistically low. Finally, the results suggest that we may suffer from spectroscopic uncertainties.

Retrieval simulations show that the finding of low aerosol pressures can probably be explained by the presence of boundary layer aerosols. Retrieved height of an elevated aerosol layer is biased in case of significant boundary layer aerosols and interestingly it is biased away from the boundary layer. We hypothesize that this effect is caused by photons scattered by boundary layer aerosols being confused in the retrieval with photons reflected by the surface. To retain the absorption depth, the elevated layer is moved to higher altitudes. Thus, the algorithm needs to be extended to better account for boundary layer aerosols. We anticipate extending DISAMAR so that aerosol properties of two atmospheric layers can be fitted. One layer then represents the elevated aerosol layer and the other represents boundary layer aerosol. A retrieval setup would then be to fit the optical thicknesses of each layer, the mid pressure of the elevated layer and the top pressure of the boundary layer (combination of profile parameterizations A and C in Figure 5). In view of the large correlations, it is doubtful that adding more fit parameters will lead to a stable convergence.

10 Validation

A large-scale global validation of the Aerosol Layer Height product is essential to understand the quality and performance of the sensor and algorithm. Since the altitude of aerosols is difficult to determine from space using passive sensors, validation is best carried out with active aerosol remote sensing, i.e. lidar. First validation of the TROPOMI ALH with CALIOP can be found in [38] and with MISR plume height measurements in [20]. Due to the variable distribution of aerosols in space and time, good collocation is required. Collocated measurements over selected ground-based lidar sites would further help validation. Comparisons with a number of other passive satellite retrievals can also be carried out. Lastly, dedicated validation campaigns can help to further substantiate the validation data set. E.g. the summer campaign of the PANACEA project was carried out in June and August in Greece, providing first validations of the TROPOMI ALH with ground-based lidar [37].

10.1 Validation with lidar measurements

Ground-based lidar measurements provide backscatter profiles and in some cases extinction profiles. These profiles can unambiguously indicate the presence of aerosol and cloud layers. If the optical thickness of the aerosols and clouds is not too high (below about 3 to 4), multiple aerosol and cloud layers can be detected. Information on aerosol properties and aerosol type is sometimes also available, depending on the specific lidar technique, i.e. elastic backscatter versus Raman or High Spectral Resolution Lidar (HSRL).

Aerosol types and distributions vary with weather and climatological regions. Therefore, a number of sites distributed over the globe should be selected to represent climatological regions. For this, existing lidar research networks such as the European Aerosol Research Lidar Network (EARLINET) or the GAW Atmospheric Lidar Observation Network (GALION) may be used as starting point for the selection. Since the lidar networks are designed with long-term observation in mind, the networks are also a suitable source for the long-term validation for the TROPOMI Aerosol Layer Height data product. Data from lidar measurement networks can be used on a case study basis to evaluate specific aerosol episodes or they may be compiled into a larger validation set comprising many validation sites over a longer period of time to allow for a statistical analysis. The ceilometer viewer developed by W. Thomas and coworkers at DWD ([URL04]) shows operational ceilometers and lidars worldwide and is a very useful tool for the selection of validation sites.

Satellite-based lidars include CALIOP onboard Cloud-Aerosol Lidar and Infrared Pathfinder Satellite Observation (CALIPSO, in orbit since 2006), AEOLUS, a Doppler wind lidar launched on 22 August 2018, and the atmospheric lidar as part of the Earth Clouds, Aerosols and Radiation Explorer (EarthCARE) mission (expected launch date 2022). These lidars provide unique validation opportunities as they are in sun-synchronous orbits with equator crossing times in the early afternoon similar to TROPOMI.

10.1.1 First validation with Caliop

A first validation was performed with operational TROPOMI data on 10 No. 2018, shown in Fig. 34. In the top panel the ALH for 10 Nov. 2018 is given, as in Fig. 9. In the bottom panel, the CALIOP 532 nm total attenuated backscatter is shown for the track indicated by the yellow line the top panel. Overplotted are the TROPOMI ALH values for all pixels within 20 km of the CALIPSO track (black/wite dots). It shows that the TROPOMI ALH is generally close to the maximum CALIOP total attenuated backscatter for low altitude maxima. Also, overlying cirrus clouds (like between 32° and 34°) latitude, affect the ALH, increasing the ALH to somewhere the smoke plume and the cirrus clouds. This underlines the need for a very strict clouds screening, and shows the correct sensitivity of the ALH to scatter layers in the atmosphere.

Lidar measurements have a very good vertical resolution but their horizontal coverage is limited. To construct a validation set with statistical significance, lidar measurements from a variety of lidar networks and platforms need first to be collected and collocated with TROPOMI observations. Next, profiles from different types of lidar instruments have to be interpreted in terms of the ALH profile parameter (e.g. height of the assumed single aerosol layer) in a consistent way. This step requires knowledge of instrument sensitivities of both the lidar instrument as well as the TROPOMI spectrometer. It is recommended that future research addresses the question of how to compare lidar profiles with TROPOMI aerosol profile parameters.

10.2 Intercomparison of passive satellite retrievals

A number of other passive satellite retrievals of aerosol height can be used for an intercomparison with ALH. We mention aerosol plume height retrievals over sea from the ratio of reflectances in MERIS channels at

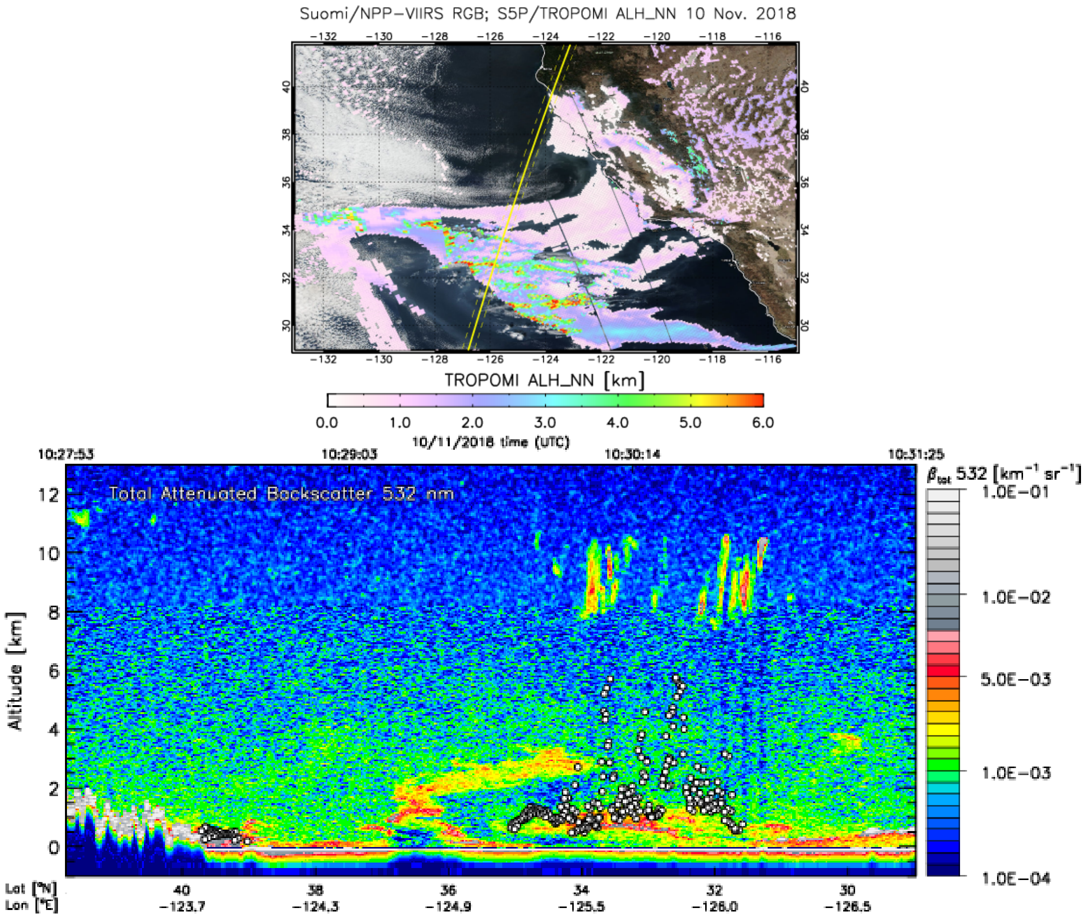

Figure 34: (top) Suomi/NPP VIIRS RGB on 10 Nov. 2018, overlaid with NN ALH. The yellow line depicts the CALIPSO track overpassing that day. The yellow dashed line depict the 20 km range around the CALIPSO track; (bottom) CALIOP Total attenuated backscatter at 532 nm on 10 Nov. 2018 for the track shown by the yellow line in the top panel.

the O_2 A band [16], stereo height retrievals for smoke plumes with clearly discernable sources [29] [28] from the Multi-Angle Imaging Spectroradiometer (MISR), and dust height retrievals from the Infrared Atmospheric Sounding Interferometer's (IASI) hyperspectral thermal infrared measurements [61].

For an internal consistency check of the ALH algorithm, data sets from different satellite platforms can be compared. The ALH algorithm will be applied to GOME-2 and SCIAMACHY in the pre-launch phase as part of TROPOMI algorithm development. In addition, the aerosol profile retrieval concept for Sentinel-4 pre-developed by KNMI continues and builds upon the TROPOMI ALH algorithm. The Sentinel-4 mission is planned for launch in 2021.

10.3 Dedicated validation campaigns

Ground-based stations / networks may need to prepare for dedicated measurements close to overpass times of S5P. A campaign period can be planned in the validation phase after launch.

Airborne lidar systems targeted at specific aerosol episodes (e.g. Saharan dust outbreaks, Asian brown cloud episodes) can be planned in seasons when these phenomena are expected based on existing climatologies. For example, DLR's High Resolution and Long Range Research Aircraft (HALO) will be equipped with a HSRL lidar that provides high quality aerosol profiles. The plane can be commissioned to underfly the satellite track in locations with expected high aerosol loading.

11 Conclusion and outlook

This Algorithm Theoretical Baseline Document describes the TROPOMI Aerosol Layer Height algorithm and product. The ATBD summarizes the current status and implementation of the algorithm and, as such, it provides the basis for further development and refinement of the operational algorithm in the coming time. The forward model, including the atmospheric model and radiative transfer model, as well as the retrieval method and the current state vector composition are described. We have also presented an error analysis illustrating the expected performance of the baseline algorithm.

The algorithm makes a spectral fit of the reflectance at the O_2 A band near 760 nm. Its main fit parameters are aerosol layer pressure and aerosol optical thickness. The baseline algorithm assumes that aerosols are uniformly distributed in a single layer with a fixed pressure thickness and a constant aerosol volume extinction coefficient and aerosol single scattering albedo. The reported pressure is the mid pressure of the layer. Example aerosol cases for which this profile parameterization is particularly suited are free-tropospheric aerosols such as volcanic ash, desert dust and biomass burning aerosols. We have also discussed an alternative profile parameterization that is more appropriate for boundary layer pollution.

The sensitivity analysis shows that when assuming a perfect forward model, precision of retrieved aerosol mid pressure in both ocean and land scenes is usually well below the target requirement of 50 hPa for optical thicknesses at 760 nm above 0.2. This value may tentatively be used as a lower threshold on the optical thickness of the target aerosol plume needed for a reliable retrieval of Aerosol Layer Height.

Retrieved aerosol pressure is robust to a model error in the single scattering albedo. The results suggest that retrieved pressure is also robust to a model error in the phase function, particularly over darker surfaces. Retrieved aerosol optical thickness however deviates from its true value and should be understood in this respect as an effective quantity. Fitting the surface albedo helps to compensate for model errors in aerosol optical properties. In the GOME-2 and SCIAMACHY case studies where Aerosol Layer Height retrievals are performed for realistic profiles, we see however that if the surface albedo is fitted retrieved pressures are biased significantly low (layer too high in the atmosphere) when compared to lidar measurements. We argue that this is caused by the presence of boundary layer aerosols. When fitting the surface albedo, boundary layer aerosol scattering and surface reflection are confused causing the biases in retrieved layer pressure. In the current implementation the surface albedo is therefore not fitted. The results indicate that the retrieved Aerosol Layer Height parameter can then be interpreted as an average aerosol scattering height.

The first verification and validation efforts show a well-behaved ALH product, which produces reliable estimates of fire and dust plume heights. The latest change to the processor, implementing a NN forward model, shows very reliable results, in close agreement with the previous LBL forward model, while the NN allows the retrieval of the TROPOMI ALH in NRT. The ALH over a dark ocean surface is more reliable than over land. Especially over bright surfaces the ALH is dominated by the systematic errors. A first qualitative comparison with CALIOP shows ALH close to the 532 nm total attenuated backscatter.

The following issues should be addressed in the next phase of algorithm development:

- Residual cirrus that is typically undetected by a cloud mask can cause substantial retrieval biases. Effort should be put into developing an accurate cloud mask for both near real-time and offline processing.
- The algorithm needs to be extended to account for boundary layer aerosols. We anticipate extending DISAMAR to simultaneously fit properties of two atmospheric intervals, one representing an elevated layer and on representing the boundary layer.
- The results indicate that particularly over land, retrieval can be unstable or χ^2 can have multiple minima. The extent of this problem for realistic scenarios should be further investigated. A possible solution may be to include the O_2 B band at 685 nm, which is also covered by TROPOMI. Vegetated land surface have a lower albedo at the O_2 B band (it is located to the shorter wavelength end of the red edge). Increasing convergence and dealing with multiple minima in the cost function will be given attention.

  The TROPOMI Aerosol Layer Height product has a number of important applications, notably for aviation safety purposes in near real-time, but also for a range of scientific research themes. The same retrieval technique can be used for the Sentinel-4 and Sentinel-5 missions. Further development of the algorithm is ongoing at KNMI.

12 References

[1] S. A. Ackerman, R. E. Holz, R. Frey, E. W. Eloranta, B. C. Maddux, and M. McGill. Cloud detection with modis. part ii: Validation. *Journal of Atmospheric and Oceanic Technology*, 25(7):1073–1086, 2008.

[2] VV Badayev and MS Malkevich. On the possibility of retrieval of aerosol extinction vertical profile using the satellite observation of reflected radiation in the oxygen band 760 nm. *Proc. Acad. Sci. USSR Sec. Atmos. Oceanic Phys*, 14:10221030, 1978.

[3] H. Bovensmann, J. P. Burrows, M. Buchwitz, J. Frerick, S. Noël, V. V. Rozanov, K. V. Chance, and A. P. H Goede. SCIAMACHY: Mission Objectives and Measurement Modes. *J. Atmos. Sci.*, 56(2):127–150, 1999.

[4] M. Buchwitz, M. Reuter, H. Bovensmann, D. Pillai, J. Heymann, O. Schneising, V. Rozanov, T. Krings, J. P. Burrows, H. Boesch, C. Gerbig, Y. Meijer, and A. Löscher. Carbon monitoring satellite (carbonsat): assessment of atmospheric co_2 and ch_4 retrieval errors by error parameterization. *Atmospheric Measurement Techniques*, 6(12):3477–3500, 2013.

[5] A. Butz, A. Galli, O. Hasekamp, J. Landgraf, P. Tol, and I. Aben. Tropomi aboard sentinel-5 precursor: Prospective performance of ch4 retrievals for aerosol and cirrus loaded atmospheres. *Remote Sensing of Environment*, 120:267 – 276, 2012. The Sentinel Missions - New Opportunities for Science.

[6] A. Butz, S. Guerlet, O. Hasekamp, D. Schepers, A. Galli, I. Aben, C. Frankenberg, J.-M. Hartmann, H. Tran, A. Kuze, G. Keppel-Aleks, G. Toon, D. Wunch, P. Wennberg, N. Deutscher, D. Griffith, R. Macatangay, J. Messerschmidt, J. Notholt, and T. Warneke. Toward accurate co2 and ch4 observations from gosat. *Geophysical Research Letters*, 38(14), 2011.

[7] A. Butz, S. Guerlet, O. P. Hasekamp, A. Kuze, and H. Suto. Using ocean-glint scattered sunlight as a diagnostic tool for satellite remote sensing of greenhouse gases. *Atmospheric Measurement Techniques*, 6(9):2509–2520, 2013.

[8] T. R. Caudill, D. E. Flittner, B. M. Herman, O. Torres, and R. D. McPeters. Evaluation of the pseudo-spherical approximation for backscattered ultraviolet radiances and ozone retrieval. *Journal of Geophysical Research: Atmospheres*, 102(D3):3881–3890, 1997.

[9] Stefano Corradini and Marco Cervino. Aerosol extinction coefficient profile retrieval in the oxygen a-band considering multiple scattering atmosphere. test case: Sciamachy nadir simulated measurements. *Journal of Quantitative Spectroscopy and Radiative Transfer*, 97(3):354 – 380, 2006.

[10] D. Crisp, B. M. Fisher, C. O'Dell, C. Frankenberg, R. Basilio, H. Bösch, L. R. Brown, R. Castano, B. Connor, N. M. Deutscher, A. Eldering, D. Griffith, M. Gunson, A. Kuze, L. Mandrake, J. McDuffie, J. Messerschmidt, C. E. Miller, I. Morino, V. Natraj, J. Notholt, D. M. O'Brien, F. Oyafuso, I. Polonsky, J. Robinson, R. Salawitch, V. Sherlock, M. Smyth, H. Suto, T. E. Taylor, D. R. Thompson, P. O. Wennberg, D. Wunch, and Y. L. Yung. The ACOS CO_2 retrieval algorithm; Part II: Global XCO_2 data characterization. *Atmospheric Measurement Techniques*, 5(4):687–707, 2012.

[11] J. S. Daniel, S. Solomon, H. L. Miller, A. O. Langford, R. W. Portmann, and C. S. Eubank. Retrieving cloud information from passive measurements of solar radiation absorbed by molecular oxygen and o2-o2. *Journal of Geophysical Research: Atmospheres*, 108(D16), 2003.

[12] J.J. Danielson and D.B. Gesch. Global multi-resolution terrain elevation data 2010 (gmted2010), 2011.

[13] JF De Haan, PB Bosma, and JW Hovenier. The adding method for multiple scattering calculations of polarized light. *Astronomy and Astrophysics*, 183:371–391, 1987.

[14] Gerrit de Leeuw, Thomas Holzer-Popp, Suzanne Bevan, William H. Davies, Jacques Descloitres, Roy G. Grainger, Jan Griesfeller, Andreas Heckel, Stefan Kinne, Lars Klüser, Pekka Kolmonen, Pavel Litvinov, Dmytro Martynenko, Peter North, Bertrand Ovigneur, Nicolas Pascal, Caroline Poulsen, Didier Ramon, Michael Schulz, Richard Siddans, Larisa Sogacheva, Didier Tanré, Gareth E. Thomas, Timo H. Virtanen, Wolfgang von Hoyningen Huene, Marco Vountas, and Simon Pinnock. Evaluation of seven european aerosol optical depth retrieval algorithms for climate analysis. *Remote Sensing of Environment*, 162:295 – 315, 2015.

[15] Oleg Dubovik, Brent Holben, Thomas F Eck, Alexander Smirnov, Yoram J Kaufman, Michael D King, Didier Tanré, and Ilya Slutsker. Variability of absorption and optical properties of key aerosol types observed in worldwide locations. *Journal of the atmospheric sciences*, 59(3):590–608, 2002.

[16] Philippe Dubuisson, Robert Frouin, David Dessailly, Lucile Duforêt, Jean Francois Léon, Kenneth Voss, and David Antoine. Estimating the altitude of aerosol plumes over the ocean from reflectance ratio measurements in the o2 a-band. *Remote Sensing of Environment*, 113(9):1899–1911, 9 2009.

[17] C Frankenberg, A Butz, and GC Toon. Disentangling chlorophyll fluorescence from atmospheric scattering effects in o2 a-band spectra of reflected sun-light. *Geophysical Research Letters*, 38(3), 2011.

[18] Christian Frankenberg, Joshua B. Fisher, John Worden, Grayson Badgley, Sassan S. Saatchi, Jung-Eun Lee, Geoffrey C. Toon, André Butz, Martin Jung, Akihiko Kuze, and Tatsuya Yokota. New global observations of the terrestrial carbon cycle from gosat: Patterns of plant fluorescence with gross primary productivity. *Geophysical Research Letters*, 38(17), 2011.

[19] Marco Gabella, Vlatcheslav Kisselev, and Giovanni Perona. Retrieval of aerosol profile variations from reflected radiation in the oxygen absorption a band. *Applied optics*, 38(15):3190–3195, 1999.

[20] D. Griffin, C. Sioris, J. Chen, N. Dickson, A. Kovachik, M. de Graaf, S. Nanda, J. P. Veefkind, E. Dammers, C. A. McLinden, and P. Maker. The 2018 fire season in north america as seen by tropomi: aerosol layer height validation and evaluation of model-derived plume heights. *Atmos. Chem. Phys.*, 19, 2019.

[21] Luis Guanter, Christian Frankenberg, Anu Dudhia, Philip E. Lewis, Jos'E g'Omez Dans, Akihiko Kuze, Hiroshi Suto, and Roy G. Grainger. Retrieval and global assessment of terrestrial chlorophyll fluorescence from gosat space measurements. *Remote Sensing of Environment*, 121:236 – 251, 2012.

[22] O. Hasekamp and R. Siddans. Chapter 8: Aerosols. in: Camelot task 3 report – retrieval simulations, j.p. veefkind (ed.). *RP-CAM-KNMI-033, issue 1*, 30 November 2009.

[23] Otto Hasekamp, Andre Galli, Haili Hu, Paul Tol, Jochen Landgraf, and Andre Butz. Algorithm theoretical baseline document for sentinel-5 precursor methane retrieval. Technical report, SRON, 2015.

[24] A. Hollstein, R. Lindstrot, and J. Fischer. Retrieval of aerosol vertical profile from top of atmosphere and high spectral resolution radiance measurements in the o2 a band. *Technical note within the ESA project FLUSS.*, 2012.

[25] Joop W Hovenier, Cornelis VM van der Mee, and Helmut Domke. *Transfer of polarized light in planetary atmospheres: basic concepts and practical methods*, volume 318. Springer Science & Business Media, 2014.

[26] Paul Ingmann, Ben Veihelmann, Jörg Langen, Daniel Lamarre, Hendrik Stark, and Grégory Bazalgette Courrèges-Lacoste. Requirements for the gmes atmosphere service and esa's implementation concept: Sentinels-4/-5 and -5p. *Remote Sensing of Environment*, 120:58 – 69, 2012. The Sentinel Missions - New Opportunities for Science.

[27] J. Joiner, Y. Yoshida, A. P. Vasilkov, Y. Yoshida, L. A. Corp, and E. M. Middleton. First observations of global and seasonal terrestrial chlorophyll fluorescence from space. *Biogeosciences*, 8(3):637–651, 2011.

[28] R. A. Kahn and J. Limbacher. Eyjafjallajökull volcano plume particle-type characterization from space-based multi-angle imaging. *Atmospheric Chemistry and Physics*, 12(20):9459–9477, 2012.

[29] Ralph A. Kahn, Yang Chen, David L. Nelson, Fok-Yan Leung, Qinbin Li, David J. Diner, and Jennifer A. Logan. Wildfire smoke injection heights: Two perspectives from space. *Geophysical Research Letters*, 35(4), 2008.

[30] R. B. A. Koelemeijer, P. Stammes, J. W. Hovenier, and J. F. de Haan. A fast method for retrieval of cloud parameters using oxygen A-band measurements from GOME. *J. Geophys. Res.*, 106(D04):3475–3490, 2001.

[31] RBA Koelemeijer, JF De Haan, and P Stammes. A database of spectral surface reflectivity in the range 335–772 nm derived from 5.5 years of gome observations. *Journal of Geophysical Research: Atmospheres*, 108(D2), 2003.

[32] Alexander A Kokhanovsky and Vladimir V Rozanov. The determination of dust cloud altitudes from a satellite using hyperspectral measurements in the gaseous absorption band. *International Journal of Remote Sensing*, 31(10):2729–2744, 2010.

[33] GAA Koppers, J Jansson, and DP Murtagh. Aerosol optical thickness retrieval from gome data in the oxygen a-band. *ESA SP*, pages 693–696, 1997.

[34] Akihiko Kuze, Hiroshi Suto, Masakatsu Nakajima, and Takashi Hamazaki. Thermal and near infrared sensor for carbon observation fourier-transform spectrometer on the greenhouse gases observing satellite for greenhouse gases monitoring. *Appl. Opt.*, 48(35):6716–6733, Dec 2009.

[35] Jochen Landgraf, Otto P Hasekamp, Michael A Box, and Thomas Trautmann. A linearized radiative transfer model for ozone profile retrieval using the analytical forward-adjoint perturbation theory approach. *Journal of Geophysical Research. D. Atmospheres*, 106:27, 2001.

[36] L. Lelli, A. Kokhanovsky, V. Rozanov, M. Jaeger, and J. Burrows. Retrieval of aerosol layer height in the oxygen a-band: case studies using synthetic and multiple remote sensing data. *EGU General Assembly 27 April – 2 May 2014, EGU2014-4092-2*, 2014.

[37] K. Michailidis, N. Siomos, D Balis, M. E. Koukouli, K. A Voudouri, O. Tuinder, G. Tilstra, P. Wang, M. de Graaf, and J. P. Veefkind. Validation of tropomi's/s5p and gome-2/metop aerosol height products using the elevated height obtained from thessaloniki lidar station during panacea campaign, 2019.

[38] S. Nanda, M. de Graaf, J. P. Veefkind, M. Sneep, M. ter Linden, J. Sun, and P. F. Levelt. Validating tropomi aerosol layer height retrievals with caliop data. *Atmos. Meas. Tech. Disc.*, 19(19), 2019.

[39] Hovakim Nazaryan, M. Patrick McCormick, and W. Paul Menzel. Global characterization of cirrus clouds using calipso data. *Journal of Geophysical Research: Atmospheres*, 113(D16), 2008.

[40] C. W. O'Dell, B. Connor, H. Bösch, D. O'Brien, C. Frankenberg, R. Castano, M. Christi, D. Eldering, B. Fisher, M. Gunson, J. McDuffie, C. E. Miller, V. Natraj, F. Oyafuso, I. Polonsky, M. Smyth, T. Taylor, G. C. Toon, P. O. Wennberg, and D. Wunch. The acos co_2 retrieval algorithm – part 1: Description and validation against synthetic observations. *Atmospheric Measurement Techniques*, 5(1):99–121, 2012.

[41] M. J. M. Penning de Vries, S. Beirle, and T. Wagner. Uv aerosol indices from sciamachy: introducing the scattering index (sci). *Atmospheric Chemistry and Physics*, 9(24):9555–9567, 2009.

[42] C. Popp, P. Wang, D. Brunner, P. Stammes, Y. Zhou, and M. Grzegorski. Meris albedo climatology for fresco+ O_2 a-band cloud retrieval. *Atmos. Meas. Tech.*, 4:463–483, 2011.

[43] M. Reuter, M. Buchwitz, O. Schneising, J. Heymann, H. Bovensmann, and J. P. Burrows. A method for improved sciamachy co_2 retrieval in the presence of optically thin clouds. *Atmospheric Measurement Techniques*, 3(1):209–232, 2010.

[44] Clive D Rodgers. *Inverse methods for atmospheric sounding: theory and practice*, volume 2. World scientific, 2000.

[45] Vladimir V. Rozanov and Alexander A. Kokhanovsky. Semianalytical cloud retrieval algorithm as applied to the cloud top altitude and the cloud geometrical thickness determination from top-of-atmosphere reflectance measurements in the oxygen a band. *Journal of Geophysical Research: Atmospheres*, 109(D5), 2004.

[46] David A. Salstein, Rui M. Ponte, and Karen Cady-Pereira. Uncertainties in atmospheric surface pressure fields from global analyses. *Journal of Geophysical Research: Atmospheres*, 113(D14), 2008.

[47] A. F. J. Sanders and J. F. de Haan. Retrieval of aerosol parameters from the oxygen A band in the presence of chlorophyll fluorescence. *Atmospheric Measurement Techniques*, 6(10):2725–2740, October 2013.

[48] A. F. J. Sanders, J. F. de Haan, M. Sneep, A. Apituley, P. Stammes, M. O. Vieitez, L. G. Tilstra, O. N. E. Tuinder, C. E. Koning, and J. P. Veefkind. Evaluation of the operational aerosol layer height retrieval algorithm for sentinel-5 precursor: application to o_2 a band observations from gome-2a. *Atmospheric Measurement Techniques Discussions*, 8(6):6045–6118, 2015.

[49] AFJ Sanders, JF de Haan, M Sneep, A Apituley, P Stammes, MO Vieitez, LG Tilstra, CE Koning, and JP Veefkind. Evaluation of the operational aerosol layer height retrieval algorithm for sentinel-5 precursor: application to o 2 a band observations from gome-2a. *Atmospheric Measurement Techniques*, 8(11):4947–4977, 2015.

[50] A.F.J. Sanders, O. Vieitez, and P. Stammes. Aeropro technical note tn3: Theoretical baseline description of the aerosol profile retrieval algorithm concept. *ESA ITT AO/1-7017/11/NL/MP, version 1.0,*, 14 March 2013.

[51] S Sanghavi, JV Martonchik, J Landgraf, and U Platt. Retrieval of the optical depth and vertical distribution of particulate scatterers in the atmosphere using o 2 a-and b-band sciamachy observations over kanpur: a case study. *Atmospheric Measurement Techniques*, 5(5):1099–1119, 2012.

[52] F. C. Seidel and C. Popp. Critical surface albedo and its implications to aerosol remote sensing. *Atmospheric Measurement Techniques*, 5(7):1653–1665, 2012.

[53] R. Siddans, B.G. Latter, and B.J. Kerridge. Study to consolidate the uvs mission requirements for the oxygen a-band. *EUMETSAT Contract No. EUM/CO/05/1411/SAT, version 1.2*, 24 May 2007.

[54] Christopher E. Sioris and Wayne F. J. Evans. Impact of rotational raman scattering in the o2a band. *Geophysical Research Letters*, 27(24):4085–4088, 2000.

[55] Maarten Sneep. Analysis of the transistion to the small pixel operational settings on nrti data. Technical report, KNMI, 2019.

[56] L. G. Tilstra, O. N. E. Tuinder, P. Wang, and P. Stammes. Surface reflectivity climatologies from uv to nir determined from earth observations by gome-2 and sciamachy. *Journal of Geophysical Research: Atmospheres*, 122(7):4084–4111, 2017.

[57] H. Tran, C. Boulet, and J.-M. Hartmann. Line mixing and collision-induced absorption by oxygen in the a band: Laboratory measurements, model, and tools for atmospheric spectra computations. *J. Geophys. Res.*, 111(D15), August 2006.

[58] H. Tran and J.-M. Hartmann. An improved O2 A band absorption model and its consequences for retrievals of photon paths and surface pressures. *J. Geophys. Res.*, 113(D18):D18104, September 2008.

[59] B. van Diedenhoven, O. P. Hasekamp, and I. Aben. Surface pressure retrieval from SCIAMACHY measurements in the O₂ A Band: validation of the measurements and sensitivity on aerosols. *Atmospheric Chemistry and Physics*, 5(8):2109–2120, August 2005.

[60] B. van Diedenhoven, O. P. Hasekamp, and J. Landgraf. Retrieval of cloud parameters from satellite-based reflectance measurements in the ultraviolet and the oxygen A-band. *J. Geophys. Res.*, 112(D15208), 2007.

[61] S. Vandenbussche, S. Kochenova, A. C. Vandaele, N. Kumps, and M. De Mazière. Retrieval of desert dust aerosol vertical profiles from iasi measurements in the tir atmospheric window. *Atmospheric Measurement Techniques*, 6(10):2577–2591, 2013.

[62] A. Vasilkov, J. Joiner, and R. Spurr. Note on rotational-raman scattering in the o_2 a- and b-bands. *Atmospheric Measurement Techniques*, 6(4):981–990, 2013.

[63] J. P. Veefkind, I. Aben, K. McMullan, H. Förster, J. de Vries, G. Otter, J. Claas, H. J. Eskes, J. F. de Haan, Q. Kleipool, M. van Weele, O. Hasekamp, R. Hoogeveen, J. Landgraf, R. Snel, P. Tol, P. Ingmann, R. Voors, B. Kruizinga, R. Vink, H. Visser, and P. F. Levelt. TROPOMI on the ESA Sentinel-5 Precursor: A GMES mission for global observations of the atmospheric composition for climate, air quality and ozone layer applications. *Remote Sensing of Environment*, 120:70–83, May 2012.

[64] P. Wang, O. N. E. Tuinder, L. G. Tilstra, M. de Graaf, and P. Stammes. Interpretation of fresco cloud retrievals in case of absorbing aerosol events. *Atmospheric Chemistry and Physics*, 12(19):9057–9077, 2012.

[65] Y. Yoshida, N. Kikuchi, I. Morino, O. Uchino, S. Oshchepkov, A. Bril, T. Saeki, N. Schutgens, G. C. Toon, D. Wunch, C. M. Roehl, P. O. Wennberg, D. W. T. Griffith, N. M. Deutscher, T. Warneke, J. Notholt, J. Robinson, V. Sherlock, B. Connor, M. Rettinger, R. Sussmann, P. Ahonen, P. Heikkinen, E. Kyrö, J. Mendonca, K. Strong, F. Hase, S. Dohe, and T. Yokota. Improvement of the retrieval algorithm for gosat swir xco_2 and xch_4 and their validation using tccon data. *Atmospheric Measurement Techniques*, 6(6):1533–1547, 2013.

[66] Y. Yoshida, Y. Ota, N. Eguchi, N. Kikuchi, K. Nobuta, H. Tran, I. Morino, and T. Yokota. Retrieval algorithm for co_2 and ch_4 column abundances from short-wavelength infrared spectral observations by the greenhouse gases observing satellite. *Atmospheric Measurement Techniques*, 4(4):717–734, 2011.

[67] Y. Zhou, D. Brunner, K. F. Boersma, R. Dirksen, and P. Wang. An improved tropospheric no_2 retrieval for omi observations in the vicinity of mountainous terrain. *Atmospheric Measurement Techniques*, 2(2):401–416, 2009.